2018

Dopaminergic Modulation Shapes Sensorimotor Processing in the Drosophila Mushroom Body

Raphael Cohn

DOPAMINERGIC MODULATION SHAPES SENSORIMOTOR PROCESSING IN THE *DROSOPHILA* MUSHROOM BODY

A Thesis Presented to the Faculty of

The Rockefeller University

in Partial Fulfillment of the Requirements for

the degree of Doctor of Philosophy

by

Raphael Cohn

June 2018

DOPAMINERGIC MODULATION SHAPES SENSORIMOTOR PROCESSING IN THE *DROSOPHILA* MUSHROOM BODY

Raphael Cohn, Ph.D.

The Rockefeller University 2018

To survive in a complex and dynamic environment, animals must adapt their behavior based on their current needs and prior experiences. This flexibility is often mediated by neuromodulation within neural circuits that link sensory representations to alternative behavioral responses depending on contextual cues and learned associations. In *Drosophila*, the mushroom body is a prominent neural structure essential for olfactory learning. Dopaminergic neurons convey salient information about reward and punishment to the mushroom body in order to adjust synaptic connectivity between Kenyon cells, the neurons representing olfactory stimuli, and the mushroom body output neurons that ultimately influence behavior. However, we still lack a mechanistic understanding of how the dopaminergic neurons represent the moment-to-moment experience of a fly and drive changes in this sensory-to-motor transformation. Furthermore, very little is known about how the output neuron pathways lead to the execution of appropriate odor-related behaviors.

We took advantage of the mushroom body's modular circuit organization to investigate how the dopaminergic neuron population encodes different contextual cues. *In vivo* functional imaging of the dopaminergic neurons reveals that they represent both external reinforcement stimuli, like sugar rewards or punitive electric shock, as well as the fly's motor state, through coordinated and partially antagonistic activity patterns across the population. This multiplexing of motor and reward signals by the dopaminergic neurons parallels the dual roles of dopaminergic inputs to the vertebrate basal ganglia, thus demonstrating a conserved link between these distantly related neural circuits. We proceed to demonstrate that this dopaminergic signal in the mushroom body modifies neurotransmission with synaptic specificity and temporal precision to coordinately regulate the propagation of sensory signals through the output neurons.

To explore how these output pathways ultimately influence olfactory navigation we have developed a closed loop olfactory paradigm in which we can monitor and manipulate the mushroom body output neurons as a fly navigates in a virtual olfactory environment. We have begun to probe the mushroom body circuitry in the context of olfactory navigation. These preliminary investigations have led to the identification of putative pathways for linking mushroom body output with the circuits that implement odor-tracking behavior and the characterization of the complex sensorimotor representations in the dopaminergic network. Our work reveals that the *Drosophila* dopaminergic system modulates mushroom body output at both acute and enduring timescales to guide immediate behaviors and learned responses.

To Chava, my partner in life,

for making this possible through your love, support, help, and patience.

To Anna,

for teaching me what it's all about.

ACKNOWLEDGEMENTS

I would like to start by acknowledging the people who contributed directly to the work presented here. Ianessa Morantte did the NMJ immunostaining and RNAi experiments. Ari Zolin collected most of the images for the single-cell KC labeling with PA-GFP and has been the main driver behind the project looking at DAN activity in the closed loop system. Annie Handler did the experiments showing bidirectional plasticity that emerges from backward pairing of KC and DAN activation and the representative example of odor-specific depression from forward pairing. Anoj Ilanges performed many of the odor tracking and optogenetic experiments in the closed loop system. Rich Pang calculated the filters connecting behavioral parameters with DAN activity. Nilay Yapici did much of the analysis and made the original figure describing functional imaging of the SEZ interneurons. Jackson Rogow and Ianessa Morantte performed the *trans*-TANGO imaging. Donovan Ventimiglia, Tim Ryan, Ari Zolin, Eliezer Pickholtz, and Josh Salvi gave technical advice for different parts of this project. Mustafa Talay, Gilad Barnea, Karla Kaun, Kristin Scaplen, and Yoshi Aso are part of an ongoing collaboration using *trans*-TANGO to look at circuits downstream of the mushroom body. Rich Pang and Adrienne Fairhall are part of an ongoing collaboration working to analyze and make sense of the behavior-related DAN activity. Nilay Yapici and Leslie Vosshall were great teammates on a short and sweet collaboration looking at activity in interneurons in the SEZ. Many people gave us feedback on our original manuscript, which forms a part of this thesis. Those include Leslie Vosshall, Cori Bargmann, Richard Axel, Larry Abbott, Sandeep Datta, Barbara Noro, Daisuke Hattori, Meg Younger, and many members of the Ruta Lab.

Developing the closed loop olfactory system has been a fun and exciting project for me and would not have been possible without assistance and input from many sources. Most importantly, Jim Petrillo and the Rockefeller Precision Fabrication Facility were instrumental in the design and assembly of the closed loop systems. Funding for the project was generously provided by a Kavli Neural Systems Institute pilot grant. Along the way, I had other help with troubleshooting and figuring out how to make use of the system from Adam Samulak, Anoj Ilanges, Ari Zolin, Annie Handler, and Max Seppo. Richard Moore, who developed the FicTrac software, was very responsive and helpful with troubleshooting. Gaby Maimon, Cheng Lyu, Jonathan Green, Jonathan Hirokawa, and other members of the Maimon Lab gave a lot of advice about how to set up a closed loop system, shared reagents and taught me about the central complex.

I am lucky to have had the opportunity to work with a wonderful group of intelligent, engaging scientists and people over the past several years in the Ruta Lab. I'd especially like to acknowledge Eva Luderowski, who helped get the lab started and Ianessa Morantte for continuing to keep the lab running smoothly. Over the past couple of years it has been a great pleasure to see projects continue to grow and take off in different directions. I've been fortunate to work closely with Ari Zolin, who was brave enough to dive into the complex patterns of activity in the DANs, and with Annie Handler, who has done an excellent job of exploring the mechanisms underlying

bidirectional plasicity at KC-MBON synapses. Scientific discussions with everyone in the lab over the years, in lab meetings and informal discussions, have contributed greatly to my growth as a scientist, and I'd especially like to thank Josie Clowney, Laura Seeholzer, Rory Coleman, and Joel Butterwick for those.

Most of all, I am incredibly grateful to Vanessa Ruta for being my advisor and mentor. In addition to being a scientific inspiration, Vanessa has also been unbelievably generous with her time, energy and support. Her insights and ideas have been instrumental in every step of my PhD, and I've relied on her pep talks to get through more bumps in the road than I care to recall. All of us who have had the privilege of being part of the Ruta Lab from near its beginning know that it's a very special place to do science. Vanessa pushes all of us to become the best scientists we can be, and we have all benefited from her care and attention.

There are so many individuals at Rockefeller and elsewhere who have contributed to my scientific and personal growth during my PhD. I'd like to thank Winrich Freiwald and Cori Bargmann for their support and input as members of my thesis committee over the years. I'd also like to thank John Tuthill for agreeing to serve as my external thesis examiner. The monthly BSVMRKYZ meetings have been a great chance to get to know colleagues and to learn about the exciting science going on in different labs, and I've greatly enjoyed them. The Rockefeller Dean's Office has been amazingly helpful in so many ways, and I'd like to especially recognize Cris Rosario, Emily Harms, Stephanie Fernandez, Sid Strickland, Marta Delgado and Kristen Cullen for all that they do. I learned so much by being a part of the Summer Neuroscience Program, and I'd like to thank the students who taught me more than I taught them, and my co-directors: Deanna Belsky, Laura Seeholzer, Aylesse Sordillo and Bennett Ferris. I'd also like to thank Filippo Mancia and Giuliano Sciara for giving me my first lab experience and getting me hooked.

Support and creative outlets outside of the lab have been instrumental in my ability to succeed in the lab. Thank you to Liz Campbell for keeping me (and Chava) sane with exercise classes and to all of the wonderful teachers at the CFC for taking such good care of Anna. I'd like to thank Marc Tessier-Lavigne, Alex Kogan and Tim O'Connor for working with me to designate space for an art studio on the Rockefeller campus. I owe much to my friends, in and out of Rockefeller, for support and advice over the years. I'd like to especially acknowledge Ted Scovell for great chats about science and life over the tennis net, Jon Weiner for always being there and for being a great sounding board for ideas and thoughts and Josefina del Marmol for calling me out when I need it.

Finally I want to thank my family, by blood and by marriage, for their unending support, willingness to listen to obscure thoughts about flies, to read rough drafts and sit through practice talks. I appreciate all of you, and my life is so full because of you.

And thank you to Chava, who manages to do it all – helping and encouraging me, while working her way into and through medical school, and, of course, being a great mom to Anna. I could not have made it without you.

TABLE OF CONTENTS

Chapter 4

Chapter 5

Chapter 6

Chapter 7

LIST OF FIGURES

LIST OF TABLES

LIST OF ABBREVIATIONS

AL – Antennal Lobe

CS – Conditioned Stimulus

CX – Central Complex

DAN – Dopaminergic Neuron

EB – Ellipsoid Body

FSB – Fan Shaped Body

GECI – Genetically Encoded Ca^{2+} Indicators

KC – Kenyon Cell

LH – Lateral Horn

LTD – Long Term Depression

LTP – Long Term Potentiation

MB – Mushroom Body

MBON – Mushroom Body Output Neuron

NMJ – Neuromuscular Junction

OR – Olfactory Receptors

ORCO – Olfactory Receptor Co-Receptor (also known as OR83B)

OSN – Olfactory Sensory Neurons

PB – Protocerebral Bridge

PN – (olfactory) Projection Neuron

R##*## – Janelia Flylight Collection Identifier

RPE – Reward Prediction Error

STDP – Spike Timing Dependent Plasticity

syt-GCaMP – Synaptotagmin1–GCaMP fusion

UAS – Upstream Activating Sequence

US – Unconditioned Stimulus

VTA – Ventral Tegmental Area

Chapter 1

Introduction

Neuromodulation of Neural Circuit Function

Earlier this year, the Grey Art Gallery at NYU put on an exhibition of drawings by the father of modern neuroscience, Ramón y Cajal[1]. In exquisite sketches of stained neural tissue, Cajal captured the intricacy and diversity of neurons in the brains of different animals. With remarkable intuition, Cajal correctly inferred much about how the nervous system functions based primarily on these snapshots of neuronal anatomy. Building on this foundation with new technologies and methodologies, neuroanatomists continue to paint an increasingly detailed atlas of neural tracts and synaptic connections. The hope is that constructing a connectome – a complete description of the connections between the neurons in a neural structure – will help us to understand how these circuits work[2].

While anatomical studies will continue to shed light on the function of neural circuits, connectomics alone will not be sufficient to understand how our brains work. Circuit diagrams are only part of the story. To truly understand the workings of the brain we need to examine the functional relationships between the components of each circuit. Here we are presented with an additional hurdle: these functional relationships are dynamic. There are a host of mechanisms by which circuits change on timescales ranging from seconds to lifetimes[3,4]. Synapses are grown and pruned. Neurons become more or less excitable. Many of these changes are mediated by neuromodulators, molecular signals used by the brain to adjust neural circuit function to serve the needs of its owner. The flexibility endowed by neuromodulation allows us to adapt to changing environments, adjust our behaviors based on internal states such as hunger or arousal, and, importantly, learn from our experiences.

Given the importance of neuromodulation, it is not surprising that many disorders that result from dysfunctional regulation of brain states, such as depression and addiction, involve neuromodulators, such as dopamine and serotonin[5,6]. Interestingly, these same modulators are also implicated in movement disorders[7,8], pointing to a diversity of roles that we will return to. Dissecting how neuromodulators appropriately tune neural circuits for any given situation is therefore essential not just to explain how the brain works, but to help develop treatments for a range of neurophysiological diseases. However, as anatomists continue to reveal, the dense web of

interconnections between neurons in even a miniscule volume of brain tissue is incredibly complex. Addressing not just how these circuits function, but also how their functions can be modulated is thus a daunting challenge.

The capacity of neuromodulators to dynamically reconfigure the functional properties of anatomically static neuronal circuits is essential for many of the nervous system's most remarkable capabilities. The flexibility of neural circuits allows for sensory processing and behavioral outcomes to be modulated based on changes in the external environment as well as the internal state of the animal. For instance, in the relatively simple stomatogastric ganglion of crustaceans, neuromodulators can modify many different properties of rhythmic circuit outputs[4]. In peripheral sensory circuits, modulators can change the gain of sensory processing based on inputs from other sensory modalities[9], satiety state[10] or behavioral state[11]. But modulation is especially important in the complex circuits that underlie the cognitive abilities of many different species. Neuromodulators are often essential for circuits that make decisions by combining information from multiple modalities, including sensory pathways and internal states[12–14]. With the capacity to affect changes that persist over a range of time scales, neuromodulators are also primary drivers of the circuit plasticity that underlies learning and memory[15,16].

While neuromodulators have many important functions, understanding how they affect circuit function remains a distinct challenge. Significant insights have been made by investigating the modulation of relatively simple circuits. For instance, serotonin-mediated synaptic facilitation has been shown to be responsible for sensitization of the gill-withdrawal reflex in *Aplysia*[17]. The same molecule can modulate a chemosensory circuit to alter odorant responses in the nematode, *C. elegans*[18]. While these systems have been valuable for describing mechanisms of neuromodulation and its effects on circuit function and behavior, it is unclear how far such findings can be generalized to more complex circuits. In particular, how are neural circuits modified so that the same, high dimensional, sensory representation can be alternately linked to different behavioral outputs, thereby imparting meaning to arbitrary sensory stimuli?

Dopaminergic Signaling in Higher Brain Centers

Investigations across several model systems have established the critical role of dopamine, a ubiquitous neuromodulator, in the neural circuits that endow animals with the ability to adjust their responses to sensory stimuli based on learned experience. The function of dopaminergic circuits in the vertebrate brain have been most heavily studied in the striatum, though dopaminergic projections to the prefrontal cortex have also been shown to play critical roles in cognitive functions[19,20]. Like the MB, the striatum receives convergent input from dopaminergic neurons (DANs) and from sensory circuits that

project from the thalamus and cortical regions, while striatal outputs are thought to contribute to action selection and execution[21,22]. In a remarkable case of neurobiological fulfillment of a prediction made by psychological modeling, dopaminergic projections from the ventral tegmental area (VTA) to the striatum of non-human primates were found to represent the presence of unexpected rewards. This neural representation of the difference between the expected and received reward is known as the reward prediction error (RPE) and was inferred to be an essential component of circuits that implement learned associations[23]. The ability to more selectively target specific dopaminergic populations using the genetic tools available in rodents has begun to elucidate more detailed properties of the RPE, while also allowing for inferences regarding the neuronal computations that give rise to these error signals[24]. Recent studies have also identified dopaminergic RPE representations in circuits that are responsible for other types of learning. For instance, a dopaminergic RPE signal in the zebra finch encodes the accuracy of song syllables produced by an adolescent bird in comparison with the tutor song it is intending to imitate[25]. Thus, dopaminergic neurons appear to play the role of the 'critic'[26] in the implementation of a range of learning paradigms.

The relative simplicity of this proposed role of dopaminergic signaling, however, conceals many layers of complexity and controversies. For one, RPEs are not the only signals present in striatal DANs. While many DANs respond to unexpected rewards, others respond to aversive stimuli[27–29]. Furthermore, it has long been known that DANs

also encode movement-related signals, and perturbation of dopamine signaling, such as occurs in Parkinson's disease, leads to disruption of motor control[8]. One prevalent model held that movement-related signals might be encoded in the tonic activity of the DANs, while the more acute, phasic, activity was responsible for reward-related signals[30]. However, as the tools to record from identifiable subpopulations of DANs have improved, the accuracy of this model has come into question. Some studies have indicated that distinct subsets of striatum-projecting DANs encode reward signals and actions, respectively[31–33]. Still, others have suggested that the same DANs might encode action initiation during early phases of the learning process, but later come to represent reward expectation[34] or that reward signaling is gated by the initiation of motivated movement[35]. The dual role of dopamine in representing motor-related signals and unexpected rewards is an interestingly conserved feature of this neuromodulator that we will explore further in subsequent chapters. Nonetheless, the anatomic and functional heterogeneity of DANs in the basal ganglia and the intricate wiring of their target neuropils[29,36–38], has made it difficult for the field to coalesce around a single model for the role of these modulatory circuits.

This picture is further complicated by the fact that dopamine can act over long distances, by diffusing through the extracellular space, and locally at select synaptic sites[39]. Dopamine also binds to multiple receptors that each couple to distinct intracellular signaling cascades, enabling this single neuromodulator to have diverse effects on synaptic function and communication. For instance, within the basal ganglia,

activation of the D1 or D2 dopamine receptors can lead to either an increase, or a decrease in intracellular cAMP, respectively[20,40,41]. Consequently, even if a consensus were to emerge regarding the types of signals encoded in the DANs of the striatum, how dopaminergic pathways sculpt synaptic connections to precisely shape circuit function remains unclear.

The Mushroom Body

The insect mushroom body (MB) is, in many ways, an ideal substrate for investigating how dopamine modifies neural circuits that underlie learned and context-dependent processing of arbitrary sensory stimuli. The MB was first identified in 1850 by the French biologist Félix Dujardin[42]. A forerunner of Cajal, Dujardin similarly used careful anatomical observations and comparative studies to hypothesize that the MB was the seat of free will or intelligent control across diverse insect species[43]. In the decades since its discovery, the MB has been shown to play roles in many aspects of insect behavior, including locomotion[44,45], sleep[46–49], multimodal sensory processing[50,51] and multiple types of conditioning[52,53]. Functional investigations of the MB in honeybees and locusts have given insight into both the general and specific roles it plays in different insects[54–59] while comparative studies of the MB have continued to shed light on how this structure is involved in complex invertebrate behavior[43,60,61]. For instance, recent investigations suggest that MBs may be present in specific crustaceans that

exhibit relatively sophisticated behaviors[62,63]. There may even be a common evolutionary origin for the MB and the vertebrate cortex[64]. Interestingly, as the anatomy of the MB has been dissected at increasing levels of detail, similarities with evolutionarily distant brain structures have emerged, suggesting convergent evolution of this particular circuit architecture. In particular, the MB circuitry bears a striking resemblance to that of the cerebellum and cerebellum-like structures[65], suggesting that this organization is ideally suited for adaptive filtering of sensorimotor pathways.

Over the course of the 20th century, as *Drosophila melanogaster* grew into a powerful genetic model organism, the tools to investigate the specific functions of the MB have flourished. A major milestone in the study of fly behavior came in the lab of Seymour Benzer in the 1970's where it was shown that flies were capable of forming associative memories[66]. Subsequent studies leveraged the powerful *Drosophila* genetic toolkit and ablation studies to highlight the central role played by the MB in associative learning[66–70] and to identify many of the genes that are required for normal memory functioning[71–76]. These genetic studies pointed to the importance of dopaminergic modulation for olfactory associative learning and identified many genes downstream of dopamine receptors that have since been shown to play conserved roles in memory from *Aplysia* to mammals[77,78].

In the years since associative learning was first demonstrated in *Drosophila* the tools for studying learning and memory in the fly have continued to improve[79,80]. Increasingly detailed analyses of memory performance using different training protocols have identified multiple phases of both aversive and appetitive memory that are dependent on the MB, revealing that this same circuit architecture can support both transient and persistent memories[81–92]. The adoption of the Gal4/UAS system[93,94] and the development of a steady stream of tools for the manipulation and recording of specific neuronal subpopulations in the *Drosophila* brain[79] have facilitated the detailed dissection of the mechanisms underlying learning and memory in the MB. These investigations have demonstrated the necessity and sufficiency of particular neuronal populations within the MB for formation and retrieval of different phases of memory[95–102]. In parallel, functional imaging experiments have begun to reveal potential changes in activity in parts of the MB as the result of learning[95,97,103–105].The identification of such engrams–changes in the brain that occur through learning–has long been recognized as a fundamental goal in understanding how information is stored within the brain[106,107].

Together, these modern neurogenetic tools have further strengthened the case for using the MB as a model for studying the circuit mechanisms underlying flexible sensorimotor processing. A large body of research on the early stages of olfactory processing have provided a detailed framework for understanding how olfactory stimuli are processed before arriving at the Kenyon cells (KCs), which serve as the input layer of the MB[108,109]. These investigations have revealed that this sensory information is

conveyed to the MB in a format that is especially well suited to the assignment of value to arbitrary sensory inputs[110–113]. In the spirit of Cajal, detailed anatomical studies of the MB revealed a circuit architecture that is highly suggestive of how this learning center might function[114,115]. Deploying thermogenetic, chemogenetic and optogenetic tools, together with functional Ca^{2+} imaging has identified different dopaminergic neurons (DANs) innervating the MB that are necessary for the formation, but not retrieval, of olfactory associations[116]. Finally, in the past ten years, Gal4 lines labeling the output neurons of the MB have been developed and used to show the necessity and sufficiency of these output pathways to induce specific biases to the fly's behaviors[100,117–119]. These investigations have led to a broad model of the MB's role in learning: Any given odor is represented by the activation of a sparse subset of KCs. Distinct subsets of DANs encode either rewarding or punishing stimuli and modify KC to mushroom body output neuron (MBON) communication so that the MBON responses to the olfactory conditioned stimulus (CS) is changed after the learning experience. This modified pattern of MBON activity is then presumed to effectuate the altered behavior that is induced through learning.

Investigating Dopaminergic Modulation of the Mushroom Body

While this model provides a general framework for thinking about the function of the MB in olfactory learning, the precise mechanisms by which dopamine reshapes MB

signaling to generate flexible odor responses remain unclear. In recent years, it has become increasingly apparent that the same MB circuitry that underlies the formation of olfactory associations is also involved in other forms of context-dependent modulation of olfactory behaviors[120–128]. In hindsight, it may not be surprising that the same circuit architecture necessary for associative learning, where there is a convergence of sensory information with modulatory reinforcement cues, is also ideally suited to modulate ongoing behavior based on relevant contextual information. However, outside of their roles relaying rewarding and punishing reinforcement signals, we have a very minimal understanding of what features of the environment are relayed by the DANs. Even less is known about how ongoing DAN activity might modulate the MB circuit or the fly's behavior. Furthermore, while general models for learning-dependent plasticity in the MB have been proposed, there has not yet been a satisfying functional demonstration of the synaptic modulation that occurs during learning and how such changes alter the output of the MB. Finally, while the MBONs have been shown to bias the fly's behavior towards or away from specific odors, little is known about the downstream targets of the MBONs, or how the population of MBONs actually influences such circuits in order to lead to the appropriate behaviors.

In my thesis work described here, we took advantage of the *Drosophila* genetic toolkit and the MB's orderly anatomic organization to elucidate how dopaminergic pathways instruct synaptic and circuit plasticity in this structure.

In Chapter 2, I describe the background information relevant for understanding our investigations of the MB circuit. In particular, I give an overview of what is known about the *Drosophila* olfactory processing pathway and how this gives rise to the sparse encoding of odor stimuli within the MB. This is followed by a more detailed description of the MB anatomy that has allowed us to probe the plasticity mechanisms within it.

In Chapter 3, I describe our development of a presynaptically localized Ca^{2+} indicator, syt-GCaMP, designed to reveal spatial patterns of dopaminergic modulation within the MB. I then detail a series of experiments in which we used syt-GCaMP to visualize spatiotemporal patterns of activity in the population of DANs innervating the MB. These investigations revealed that coordinated patterns of DAN activity represent both salient external cues as well as internally generated behavioral states. Furthermore, I explore how network interactions between DANs and MBONs may contribute to these patterns of DAN activity.

In Chapter 4, I describe how we again made use of syt-GCaMP to search for local modulation of KC presynaptic Ca^{2+}. These experiments revealed that presynaptic Ca^{2+} is asymmetrically distributed along the length of the KC axons, suggesting the possibility of local modulation of individual synapses. Further perturbations using

genetic manipulations of dopaminergic pathways and activation of DANs demonstrated that dopamine is indeed responsible for dynamically modulating the Ca^{2+} levels at each KC synapse.

Chapter 5 expands upon this demonstration of dopaminergic modulation in the MB lobes by investigating the effects of this modulatory signal on KC-MBON synapses. These experiments revealed that the DANs bi-directionally modify KC-MBON synaptic efficacy with exquisite spatial and temporal precision. In particular, we demonstrated that a fictive learning paradigm, in which DANs are activated following KC odor stimulation, leads to robust synaptic depression. In contrast, unpaired or backward-paired DAN activation leads to synaptic potentiation. These experiments provide a plausible mechanism for the role of dopaminergic modulation in the formation of olfactory associations, while revealing additional forms of plasticity within the MB circuit.

Finally, in Chapter 6, I report the development of a closed loop apparatus in which a head-fixed fly can perform realistic odor-tracking behavior. This virtual olfactory arena allowed us to begin to explore the neural circuits downstream of the MB that are responsible for implementing odor valence-guided behavior. In particular, we identified a putative locus for the convergence of odor-valence information with directional cues in the fan shaped body (FSB). Furthermore, we used this system to demonstrate that the

population of DANs encodes detailed behavioral and sensory parameters while the fly is engaged in naturalistic walking and exploration of a virtual environment.

Chapter 2

The *Drosophila* Mushroom Body and Flexible Odor Processing

The remarkable ability of the animal nervous system to flexibly generate a wide array of responses to a given sensory stimulus allows for a level of behavioral complexity and adaptability that far exceeds what can be encoded in the genome. Understanding how the relatively stable neural circuitry of the brain can generate such diversity remains a fundamental question in neuroscience. The neural circuits underlying this flexibility will necessarily mediate the convergence of sensory information with contextual signals. In this way, the same sensory input can be linked to alternate output circuits, leading to different behaviors that are contingent upon changing circumstances or previously learned associations.

There are many possible mechanisms through which circuit function can be modulated, including changes in synaptic connectivity or strength, adjustments to cell-intrinsic properties such as membrane excitability[20], or even modification of plasticity rules[129,130]. Some of these changes can be mediated by intrinsic activity within a given circuit, and many different stimulation protocols have been found to induce various

forms of long term potentiation (LTP) or depression (LTD) at specific synapses[131]. For instance, spike-timing dependent plasticity (STDP) allows for the adjustment of synaptic strength between two neurons that is contingent upon the relative timing of action potentials in each synaptic partner[132]. While these modes of plasticity do not require the input of an external teaching signal, their implementations generally rely upon patterns of activity that occur over millisecond timescales, making it difficult to understand how they might account for sensory and behavioral associations that occur over longer periods of time. Alternatively, functional alterations in neural circuits often rely upon heterosynaptic input from neuromodulators, such as dopamine[3,4]. Since learning and other context-dependent modulation can often persist over a wide range of timescales, circuit plasticity may involve a variety of different molecular mechanisms, from local modifications in signaling pathways at individual synapses to global changes in transcription. Thus, it is desirable to study mechanisms of neuronal plasticity in the context of the behavioral modifications they underlie, thereby linking circuit physiology with the relevant impacts on animal survival.

My thesis work has focused on the *Drosophila* MB, studying how neuromodulation acts on a neural circuit to adjust the behavioral responses to arbitrary sensory stimuli. The MB has a well-established role in olfactory learning and memory[66–70] that has been dissected using the powerful genetic toolkit of *Drosophila* from the level of molecular mechanisms through behavioral studies of various stages and types of memory[133,134]. These investigations have revealed a fundamental role for dopaminergic

modulation in mediating the plasticity necessary for forming learned associations[116]. The MB has also been shown to play a role in other context-dependent behaviors[127,135,136], suggesting that the multimodal convergence necessary for forming associations also underlies the ongoing modulation of behavior based on the current circumstances. Furthermore, recent studies have provided a detailed understanding of how odors are represented in this structure[110,137], while high resolution anatomical dissection of MB circuitry has suggested an elegant relationship between form and function[114,115]. This unique anatomical organization has made the MB particularly well-suited for functional investigation of circuit plasticity with the tools of modern functional neuroscience.

Drosophila **Olfactory Circuitry: Sensory Neurons to Kenyon Cells**

Early Olfactory Processing

In order to probe the mechanisms by which a neural circuit can flexibly link a sensory input to a range of behavioral outcomes, it is essential that we have a thorough understanding of how sensory stimuli are represented at the input layer to such a circuit. Fortunately, the first stages of olfactory processing in *Drosophila*, up to and including how odor stimuli are represented in the MB, have been extensively studied[108,109]. Our understanding of olfactory representations in the MB is aided by the fact that odor

sensation at the periphery arrives at the KCs through a shallow circuit with only two intervening synapses. Odorants are initially sensed in the fly antennae by binding to olfactory receptors (ORs) in the dendrites of olfactory sensory neurons (OSNs) that are housed in sensory sensilla (Figure 2.1A). Each OSN expresses just one out of the approximately 60 ORs in the fly genome together with a highly conserved olfactory receptor co-receptor (ORCO, also known as OR83b) that is required for proper trafficking and function of the ORs[138–140]. In each OSN, the OR-ORCO pair is thought to form a heteromeric ion channel that opens in response to odorant binding, with odorant-selectivity determined by the specific OR expressed in each OSN[141]. The necessity of ORCO expression for proper function of the entire set of ORs has made the ORCO gene a powerful tool for wholesale manipulation of the olfactory sensory pathway in flies[138] and other insects[142–144]. In addition to the OR pathways, there are two other known chemosensory pathways in insects, which work through a family of ionotropic receptors[145,146] and gustatory receptors[147], respectively[148].

All OSNs that express the same OR project axons from the antennae to innervate a specific target glomerulus in the antennal lobe (AL, Figure 2.1A). Within the AL glomeruli, OSNs synapse onto approximately 150 olfactory Projection Neurons (PNs) along with a number of local interneurons. Local circuit interactions in the AL perform several important functions for incoming odor signals, including gain control and normalization[149–155], thereby enhancing signal to noise and pattern separation. While our focus will be on the essential role of MB plasticity in flexible olfactory processing,

Figure 2.1, The *Drosophila* Olfactory Processing Pathway. A, Schematic of early olfactory processing circuitry in *Drosophila.* Olfactory Sensory Neurons (OSN, cyan) dendrites detect odorant molecules in the Antennae (An). OSNs synapse onto olfactory projection neurons (PN, red) in antennal lobe (AL) glomeruli. PNs project to the lateral horn (LH) and the calyx (Ca) of the mushroom bodies, where they synapse onto the claw-like dendrites of Kenyon cells (KC, green). Inset shows an individual PN axonal bouton in the calyx ensheathed by the claw-like dendrites of several KCs. **B,** Adapted from Wang et al.[156] Combinatorial encoding of odor identity in the antennal lobe glomeruli. Heatmap shows GCaMP fluorescence in the PN dendrites in the antennal lobe in response to a panel of monomolecular odorants revealing distinct patterns of glomerular activity in response to each odor. **C,** Courtesy of Vanessa Ruta.[110] The claw-like dendrite of a single KC labeled using photoactivatable GFP (green) ensheaths the axonal bouton of a single PN labeled by dye-filling with Texas Red Dextran (red) in the MB calyx.

Figure 2.1

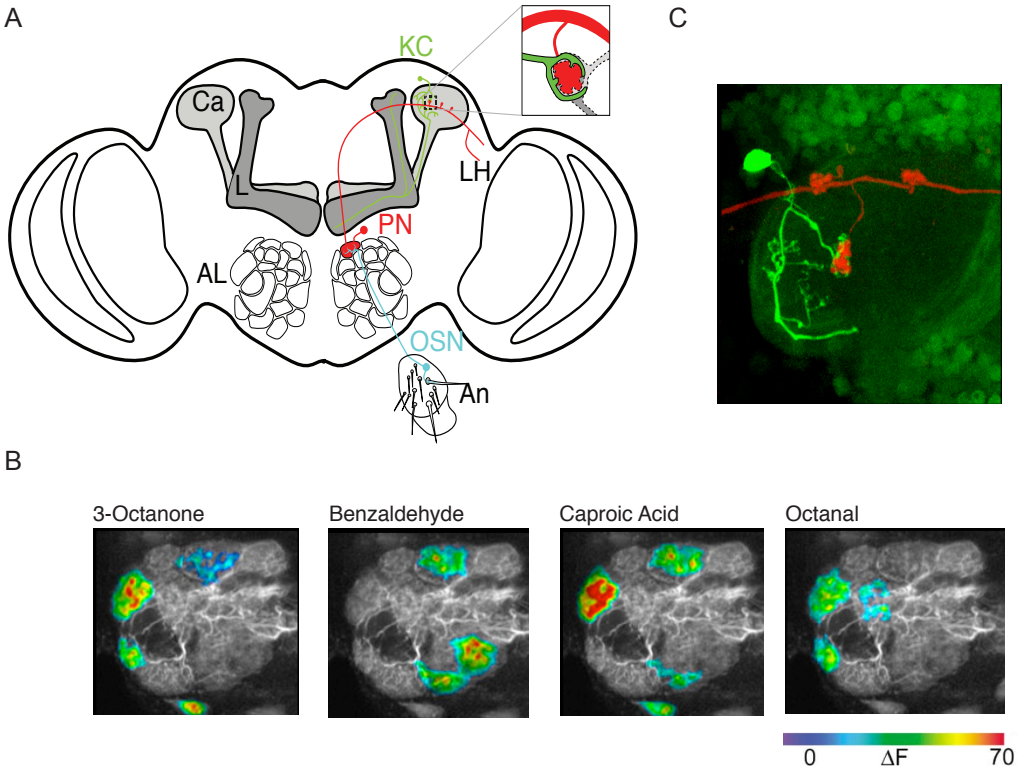
A
KC
Ca
L
LH
PN
AL
OSN
An
C
B
3-Octanone
Benzaldehyde
Caproic Acid
Octanal
0
ΔF
70

certain forms of context- and learning-dependent modulation have been proposed to also occur in earlier stages of the olfactory processing pathway[10,157–160].

Most ORs tend to be fairly promiscuous and broadly-tuned to odorants[161], meaning that any given odor will lead to varying levels of activity throughout the population of OSNs, resulting in a combinatorial pattern of activity across the antennal lobe glomeruli (Figure 2.1B)[156]. This odor representation is then relayed via the PNs to two main targets in the protocerebrum: the lateral horn (LH) and the calyx of the MB (Figure 2.1A). Historically, the LH has been thought to mediate innate behaviors, such as attraction to food odors and responses to pheromones[162–164], while the MB has long been known to be essential for learned olfactory associations[69]. However, recent studies have begun to reveal unexpected interactions downstream of the LH and MB that suggest the MB may also play a prominent role in innate or context-dependent behaviors[162,165]. In accord with the proposed role of the LH circuitry in mediating responses to odors with innate meaning, it has been suggested that PN synaptic targets in the LH are stereotyped across individuals and anatomically organized according to the innate valence or meaning of particular odorant mixtures[163,164,166–172]. In contrast to the hard-wired olfactory circuits of the LH, odor stimuli should be represented in the MB in a form that is amenable to the assignment of meaning to arbitrary olfactory cues through experience.

In the MB calyx, PNs form large axonal boutons that synapse onto the claw-like dendrites of the KCs (Figure 2.1A,C)[110,173–175]. While the PN projections to the LH seem to obey a spatial and synaptic organization that is thought to result in segregated pathways for odors with different behavioral relevance, each KC appears to sample randomly from, on average, 7 of the PN boutons in the MB calyx[110,111]. This stochastic connectivity, together with non-linear integration of PN inputs by each individual KC[176,177] and global inhibitory feedback through a large GABAergic neuron[178–183] allows for any specific olfactory stimulus to elicit activity in a small and unique subset of the ~2000 KCs (Figure 2.2A)[137,184–187]. Computational modeling has suggested that this type of sparse sensory representation is ideally suited to generate the greatest coding capacity, allowing for distinct representations of a large number of arbitrary sensory inputs[113,188–191]. Modeling studies have also suggested that the specific connectivity parameters in the MB and related circuit architectures, like the cerebellum, are optimized for the sparse, high-dimensional encoding of sensory stimuli that is amenable to the formation of associative memories[112].

While the *Drosophila* KCs receive predominantly olfactory information, there are a smaller number of inputs from other sensory modalities such as vision and gustation[192–194]. In other insects that rely more on non-olfactory sensory information the

Figure 2.2, Sparse Odor Coding in Kenyon Cells. A, Courtesy of Vanessa Ruta. Sparse encoding of odor identity in the KCs. Heatmap shows GCaMP fluorescence in the KC soma in response to a panel of monomolecular odorants. **B,** Anatomy of three main classes of KCs shown in schematics (left) and single-KC labeling using photoactivatable GFP (right, courtesy of Ari Zolin). Dorsal(D)-Ventral(V) and Medial(M)-Lateral(L) dimensions are indicated below.

Figure 2.2

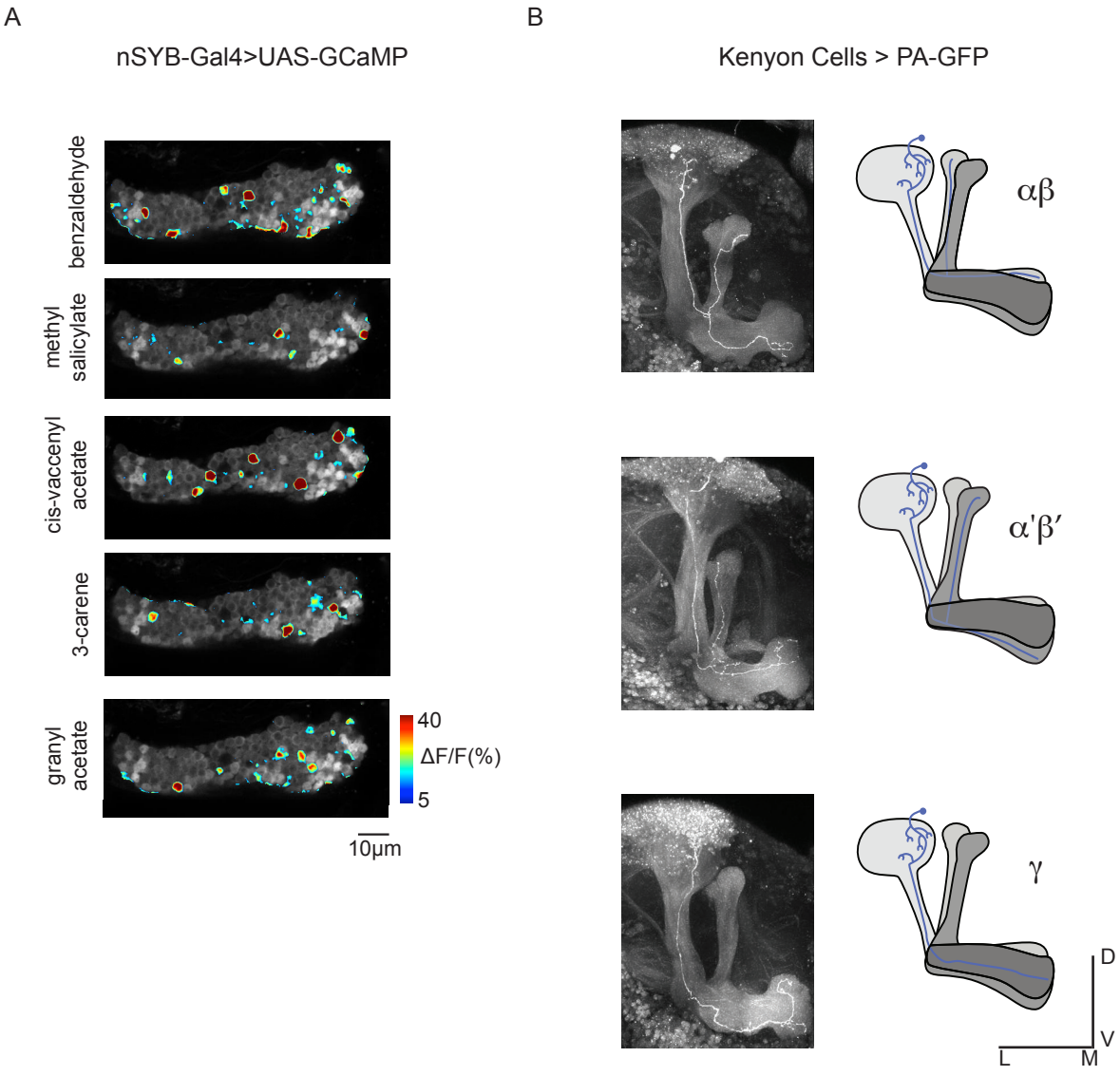
A
nSYB-Gal4>UAS-GCaMP
benzaldehyde
methyl salicylate
cis-vaccenyl acetate
3-carene
granyl acetate
40
ΔF/F(%)
5
10μm
B
Kenyon Cells > PA-GFP
αβ
α'β'
γ
D
V
L
M

share of KC synaptic input from these other modalities can be much larger[50,192]. This suggests that the general architecture of the MB is not specifically optimized for olfactory processing, but rather represents a circuit organization that is suited for the implementation of general purpose learning and context-dependent behavioral flexibility[195,196].

Convergent Evolution of Olfactory Processing Circuitry

The functional architecture of the early olfactory processing circuitry in flies and other insects bears a striking resemblance to mammalian olfactory circuits. In mammals, each OSN class likewise expresses a single OR (though in the case of mammals these are GPCRs while the insect ORs are a distinct gene family) and converge on a single glomerulus in the olfactory bulb[197]. From the olfactory bulb, there is a similar bifurcation of downstream pathways through the amygdala, thought to underlie innate odor responses[198], and the piriform cortex[199–201], thought to mediate learned olfactory associations. Interestingly, the piriform cortex, like the MB, is heavily targeted by neuromodulatory inputs, including DANs, suggesting that there, too, heterosynaptic modulation of olfactory processing shapes odor responses and associations[202,203]. It has been proposed that the remarkable convergence in the organization of odor processing circuits might have evolved because of the unique properties of olfactory space. Unlike other modalities, such as vision or audition,

olfactory space is determined by the shape of odorant molecules, without obvious features that are relevant to odor source or identity. The multilayered feature detection present in other sensory processing pathways is therefore absent in olfactory systems, which instead rely on shallow circuits that encode odor identity with distributed, combinatorial patterns of activity in sensory channels defined by a large class of receptor molecules with different binding affinities for a range of molecular shapes[204]. The striking resemblance between these distantly related olfactory circuits suggests the possibility that understanding the principles of circuit mechanisms and modulation in the *Drosophila* olfactory system will provide fundamental insight into how neural circuits achieve the functional flexibility in sensory processing that is necessary for survival.

Mushroom Body Anatomy Underlying Flexible Sensorimotor Processing

Kenyon Cell Anatomy and Classes

Approximately 2,000 KCs make up the intrinsic neurons of the MB and propagate their odor responses along fasciculated parallel axon fibers through the pedunculus and into the MB's output lobes. In *Drosophila*, the KC axons form five such output lobes: the α and α' lobes project dorsally while the β, β' and γ lobes project medially. KCs can be assigned into one of three broad classes based on which lobes their axons target. The

αβ and α'β' KC axons bifurcate into the α/β and α'/β' lobes, respectively, while γ KCs project a single axon into the medial γ lobe (Figure 2.2B). Neuronal recordings have suggested that the different KC classes possess distinct physiological properties[205], while behavioral genetic experiments have demonstrated that each class may underlie distinct phases and forms of memory[81–88].

In this work, we have focused primarily on the γ KCs for several reasons. The γ KCs have been shown to be essential during the initial phases of memory formation and for short term olfactory associations[206–208] suggesting it should be possible to functionally characterize learning-dependent γ lobe plasticity over timescales accessible in a relatively short-lived experimental preparation. Furthermore, the γ KC axons transect the largest number of contiguous compartments within a single, medial lobe, while the other classes of KCs bifurcate to form two perpendicular lobe structures (vertical lobes and medial lobes) (Figure 2.2B). The compartments traversed by the γ KC axons include sub-circuits that have been implicated in both appetitive and avoidance learning[209–211]. Thus, focusing on the γ lobe allowed us to visualize all γ lobe compartments in a single imaging plane (Figure 2.3), maximizing our ability to simultaneously investigate local modulation in compartments with different functions in learning.

Figure 2.3, Compartmentalized Architecture of the Mushroom Body. A, Schematic of mushroom body anatomy focusing on the γ lobe (left). Each γ Kenyon cell (KC, blue) receives olfactory input in the calyx and projects a single axon into the γ lobe (dashed line). KCs form *en passant* synapses with mushroom body output neurons (MBONs, green) and receive modulatory input from dopaminergic neurons (DANs, magenta) within discrete anatomic compartments (shown for γ2–γ5). Composite image showing compartmentalized innervation of the γ5 compartment by DANs (magenta), the γ5 MBONs (green) together with a single KC highlighted with photoactivatable GFP (cyan, right). **B,** A single γ KC axon photolabeled with PA-GFP (cyan) projects across the complete length of the lobe (dashed line). **C,** Segregated dendritic innervation of MBONs (green) is revealed by expression of GFP in pairs of MBONs in each panel using MBON-specific drivers. **D,** Compartmentalized axonal projections of DANs photolabeled with PA-GFP (magenta) in alternating compartments. PA-GFP is expressed under the TH and DDC promoters.

Figure 2.3

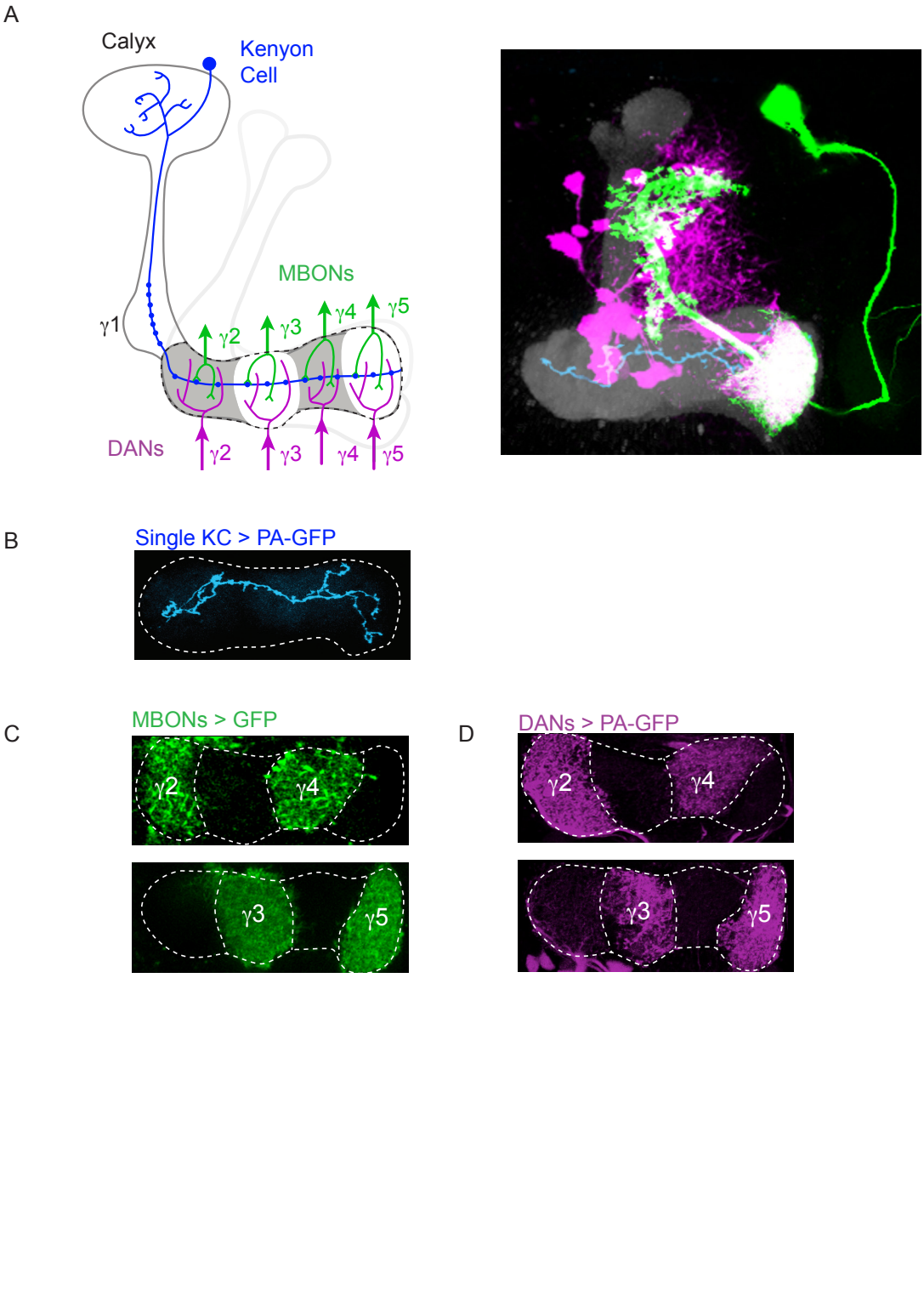
A
Calyx
Kenyon Cell
MBONs
γ1
γ2
γ3
γ4
γ5
DANs
γ2
γ3
γ4
γ5
B
Single KC > PA-GFP
C
MBONs > GFP
γ2
γ4
γ3
γ5
D
DANs > PA-GFP
γ2
γ4
γ3
γ5

Within the MB lobes, the KC axons intersect with the processes of a number of MB extrinsic neurons. These include some neurons, such as octopaminergic neurons, the Dorsal Paired Medial (DPM) neurons, and the Anterior Paired Lateral (APL) neurons with broad innervation patterns throughout all or part of the lobes[114,115]. Here, however, we focus on two sets of extrinsic neurons, the MBONs and DANs whose innervation patterns in the MB define discrete compartments that tile along the length of the lobes (Figure 2.3), and which have been shown to play distinct roles in olfactory learning.

Mushroom Body Output Neurons

The MBONs are the primary synaptic targets of the KCs and must therefore translate KC odor representations into adaptive behavioral responses[114,115,118,212]. The γ KCs synapse onto MBONs in five distinct compartments, γ1-γ5 (Figure 2.3A,C). The KC-MBON synapses are thought to be primarily excitatory, cholinergic synapses[213], however KCs may also release neuropeptides such as sNPF[214,215]. The ensemble of MBONs converges onto a small number of target neuropil where their concerted activity has been proposed to bias an animal's olfactory preferences[100,117–119,212]. Most relevant for our studies, thermogenetic blockade or optogenetic activation of specific MBONs has been shown to lead the fly to express either approach or avoidance behavior, depending on which MBON is activated[118,216]. Similar optogenetic experiments also demonstrated roles for individual MBONs in contributing to sleep-related behavior, as

well as various types of conditioning[118]. While these studies have clearly demonstrated that MBONs can influence the fly's actions, little is known about the circuits downstream of the MBONs or how their combined activity actually implements any given effect on behavior. We will return to this question in chapter 6.

Dopaminergic Neurons

The mushroom body lobes are also innervated by DANs (Figure 2.3D)[114,115,217], which are thought to convey the contextual signals that impart meaning to an odor[88,210,217–220]. Rewarding and punishing experiences have been shown to activate distinct subsets of MB DANs[88,210,221], each of which projects axons into just one or two of the lobe compartments (Figure 2.3A,D), mirroring the segregated innervation pattern of the MBONs. This anatomic arrangement suggests that DANs may convey positive and negative contextual information to each compartmentalized segment along a KC axon, potentially facilitating independent tuning of neurotransmission to each MBON in different circumstances.

The idea that dopaminergic modulation of KC-MBON communication is responsible for the plasticity underlying learned associations is supported by the necessity of dopaminergic signaling pathways specifically in KCs. The DopR1 (also

known as DUMB, Dop1R1 or dDA1) dopamine receptor was shown to be required in the KCs for the formation of both aversive and appetitive memories[222]. Interestingly, another receptor, DopR2 (also known as DAMB or Dop1R2) was shown to be required for active forgetting of previously learned associations[223]. Thus, it appears likely that dopaminergic signaling in the MB works through distinct downstream signaling pathways leading to different types of plasticity within the MB. While this body of research clearly indicates the importance of dopaminergic modulation in MB-mediated learning, the specific mechanisms of plasticity remain unclear. This is, in part, because, as in mammals, dopamine can act through multiple receptors with different downstream effectors[20,224,225]. Several studies have demonstrated either increases[100] or decreases[117,119,226] in specific MBON responses to trained odors. Furthermore, while cAMP signaling has been implicated as an important driver of KC plasticity[75,227–229], whether and how dopaminergic release might induce such plasticity has not been thoroughly investigated.

Mushroom Body Anatomy Suggests a Logic for Learned Associations

The distinct anatomical features of the MB circuitry evoke clear predictions about how it might function to flexibly impart olfactory stimuli with meaning based on experience. The parallel axons of the KCs, carrying sparsely encoded odor representations are poised to form independent connections with each MBON in distinct

anatomical compartments. The input from similarly compartmentalized modulatory signals in the DANs strongly suggests the possibility that behavioral modification could occur through independent tuning of synapses between odor-specific KCs and the post-synaptic MBONs innervating each compartment[216]. It is interesting to note the striking similarity of many of these features with the architecture of the cerebellum and cerebellum-like structures[65]. At the input layer to each circuit, the intrinsic neurons (KCs in the MB and granule cells in the cerebellum) extend a small number of claw-like dendritic structures, each of which ensheaths the large axonal bouton of an incoming sensory signal. In both circuits, it is thought that non-linear integration of these synaptic inputs[176,177,230–232], together with global inhibitory feedback[178,181,182,233] leads to sparse activity of these neurons, allowing them to distinctly encode a large number of sensory inputs[113,188]. Recent computational studies have suggested that the particular parameters in each system (such as the number of neurons in each layer and fraction of connected neurons) are optimized for the task of forming flexible sensory associations[112]. In both the MB and cerebellum, there is a large expansion in the number of cells representing sensory stimuli, which then converge onto a much smaller set of output neurons. This type of 'fan-out-fan-in' circuitry is thought to be ideal for the translation of a large sensory coding space into the smaller space of sensory valence, which is more appropriate for the execution of a limited repertoire of behaviors[234,235]. To achieve this convergence, both sets of intrinsic neurons extend fasciculated parallel axonal process which synapse onto perpendicularly arrayed output neurons (MBONs and Purkinje cells, respectively). These output synapses are the targets of

heterosynaptic plasticity induced by DANs in the case of the MB and by climbing fibers in the cerebellum[236]. Finally, the parallels even extend to the feedback loops that are thought to lie downstream of the output neurons and influence the modulatory feedback in each circuit[114,237]. This remarkable convergence in neuroanatomy and functional organization suggests that this circuit architecture is optimized for the types of adaptive filtering and sensorimotor flexibility that these circuits are thought the implement. Related structural parameters have also been identified in other intelligent animals with complex brains[234,235,238]. To shed light on how this neural circuit architecture implements flexible sensorimotor processing, we set out to design tools and protocols that would allow us to probe the plasticity and functional properties of the MB circuitry with synaptic resolution.

Chapter 3

Synaptic Ca^{2+} Imaging Reveals Population-Encoding of Context in DANs

Dopaminergic modulation of neural circuits is ubiquitous across the animal kingdom and has been implicated in a range of neurological diseases, from depression and addiction to Parkinson's disease. In the mammalian nervous system dopaminergic signaling has been identified as an essential component in conveying the rewarding signals that reinforce actions that lead to positive outcomes[20]. Investigations of these dopaminergic systems have suggested that they may relay the RPE signal that plays a prominent role in many supervised learning models[23,239]. While there is considerable evidence to support the idea that DANs in the striatum encode RPE, there is still extensive debate about what other signals might be encoded in subsets of the these neurons, such as motivational or movement-related representations[240]. Investigations into the role of dopaminergic signaling in *Drosophila* have revealed many conserved functions for this neuromodulator, including prominent roles in signaling the rewarding and punishing signals that lead to memory formation within the MB[241]. Interestingly, dopamine is also important for *Drosophila* motivation and movement[242,243]. Thus, dopaminergic modulation appears to be a common thread linking the neural circuitry underlying locomotor control and learned associations in very distantly related species.

Recent investigations into the role of dopaminergic signaling in the basal ganglia have benefited greatly from the ability to selectively record and manipulate distinct DAN populations based on differences in their anatomic projections or activity profiles [29,32,33,244]. These advances have led to the understanding that different regions within the striatum may receive distinct dopaminergic signals and play diverse roles in shaping behavior[29,31,32]. Different types of reinforcement-related signals have also been recorded in identified zones in the striatum, known as striasomes, when compared with the surrounding matrix[245]. In order to investigate similar regional specializations in the MB, the non-overlapping, compartmentalized innervation of DANs suggests that it should be possible to simultaneously visualize and distinguish between synaptic sites of different DANs. Optical recording methods using genetically encoded Ca^{2+} indicators (GECIs) should therefore allow for the measurement of activity throughout the DAN population. GECIs have undergone continual improvements in sensitivity over the past decade[246], and the ability to measure intracellular Ca^{2+} influx as a proxy for neural activity[247] has become a mainstay of modern neuroscience. In this chapter we describe the development of a presynaptically localized Ca^{2+} sensor, syt-GCaMP, that allowed us to simultaneously record from DANs across multiple compartments of the MB.

However, intracellular Ca^{2+} is also a common target of molecular signaling cascades and neuromodulation[20,248–250]. This suggests that monitoring Ca^{2+} levels at presynaptic sites might tell us not only about the spiking activity of a neuron, but also provide insight into functional modulation at individual synapses. The anatomic

organization of the MB lobes raises the possibility that compartmentalized dopaminergic release might serve to locally modulate signaling within each segment of the KC axons. This model suggests that the ability to simultaneously monitor the functional properties of synapses within each compartment with high resolution would provide a powerful means to interrogate the mechanisms of plasticity underlying MB circuit flexibility. In Chapter 4, we will use syt-GCaMP to investigate this compartmentalized modulation of KC presynaptic Ca^{2+}.

An Optical Sensor of Presynaptic Activity

Localization of activity reporters to subcellular compartments, especially synapses, has been achieved in several experimental systems and shown to afford the ability to resolve anatomical and functional properties that are not apparent with pan-cellular cytoplasmic expression[247,251–254]. We therefore targeted the latest generation of GECIs[246] to presynaptic sites in *Drosophila* neurons, allowing us to monitor local Ca^{2+} levels at each synapse and potentially serve as a readout of synapse-specific modulation. We anticipated that localizing GCaMP expression to presynaptic sites might result in weaker fluorescence signals compared to cytoplasmic GCaMP. We consequently decided to use GCaMP6s (rather than 6f or 6m) because it generates the highest signal to noise ratio in response to Ca^{2+} binding[246]. Following the strategy adopted by Ventimiglia et al.[255], we designed constructs in which GCaMP6s was

tethered, via a C-terminal 3xGS linker, to either of two different synaptically localized proteins (Figure 3.2A): synaptogyrin, a modulator of synaptic vesicle biogenesis, chosen because of its abundance at *Drosophila* presynaptic sites[256], and synaptotagmin, because it is known to bind to presynaptic Ca^{2+} as a mediator of synaptic vesicle fusion[257]. In order to assess whether these fusion constructs localized GCaMP to presynaptic terminals, we initially drove their expression in the majority of KCs under the control of OK107-Gal4[258]. This preliminary experiment revealed that synaptotagmin-GCaMP (syt-GCaMP) provided significantly better synaptic localization when compared with synaptogyrin-GCaMP. We therefore focused on syt-GCaMP as a reporter of presynaptic Ca^{2+}.

To further confirm and characterize the presynaptic localization of this reporter, we co-expressed syt-GCaMP and tdTomato in a small subset of PNs under the control of MZ19-Gal4[259]. PNs have been extensively studied and are known to have distinct presynaptic sites in antennal lobe glomeruli, the calyx of the MB and the LH, connected by long axons lacking presynaptic machinery (Figure 3.1B-C)[109]. PNs are therefore useful to validate presynaptic targeting, since there should be clear differences between presynaptic zones and non-synaptic axonal tracts. Basal syt-GCaMP fluorescence in PNs was largely restricted to the known presynaptic sites while tdTomato was equivalently distributed throughout the neurons (Figure 3.1E). We then assessed whether functional imaging of syt-GCaMP during activation of the PNs would provide a synaptically localized readout of Ca^{2+} influx. We activated the dendrites of MZ-19

Figure 3.1, A Synaptically Localized Ca^{2+} Indicator. A, Schematic of the syt-GCaMP construct (left) showing protein domains of synaptotagmin (blue) and GCaMP6s (green), including membrane-spanning portion of synaptotagmin (TM) and a GS-repeat linker (yellow). Schematic of syt-GCaMP orientation placing the sensor outside the lumen of a synaptic vesicle (right). **B,** Schematic of antennal lobe projection neurons (PNs are red, presynaptic sites in green) labeled by MZ19-Gal4. PNs receive excitatory input and synapse onto interneurons in the antennal lobe glomeruli (including DA1). They project axons into the mushroom body calyx, where they form *en passant* synaptic boutons and then terminate in the lateral horn (LH). **C,** MZ19+ neurons are labeled red with the red fluorophore, tdTomato, and their synapses labeled green with GFP-tagged presynaptic protein, bruchpilot (brp), expressed from the endogenous promoter through recombination in flies of genotype UAS-tdTomato, brp > stop > GFP; MZ19-Gal4/UAS-FLP Recombinase. Presynaptic sites are visible in the antennal lobe glomeruli, mushroom body calyx and lateral horn. **D,** Peak syt-GCaMP fluorescence evoked by DA1 glomerular stimulation with acetylcholine and **E,** basal fluorescence of syt-GCaMP expressed in MZ19+ neurons (inset shows magnified boutons in calyx) indicating presynaptic localization that closely resembles the presynaptic sites identified by brp-GFP labeling in **B**. Note the absence of syt-GCaMP labeling on the shaft of PN axons that lack presynaptic sites. Green scales represent fluorescence intensity (A.U.) in same units for **D-E**. **F,** Immunostaining of larval NMJ with syt-GCaMP expressed in motorneurons using VGlut-Gal4. α-GFP staining (green) shows co-localization of syt-GCaMP with presynaptic cysteine string protein (CSP, left, red) and active zone protein bruchpilot (BRP, right, red). α-HRP staining (blue) labels motorneurons and highlights axon shaft.

Figure 3.1

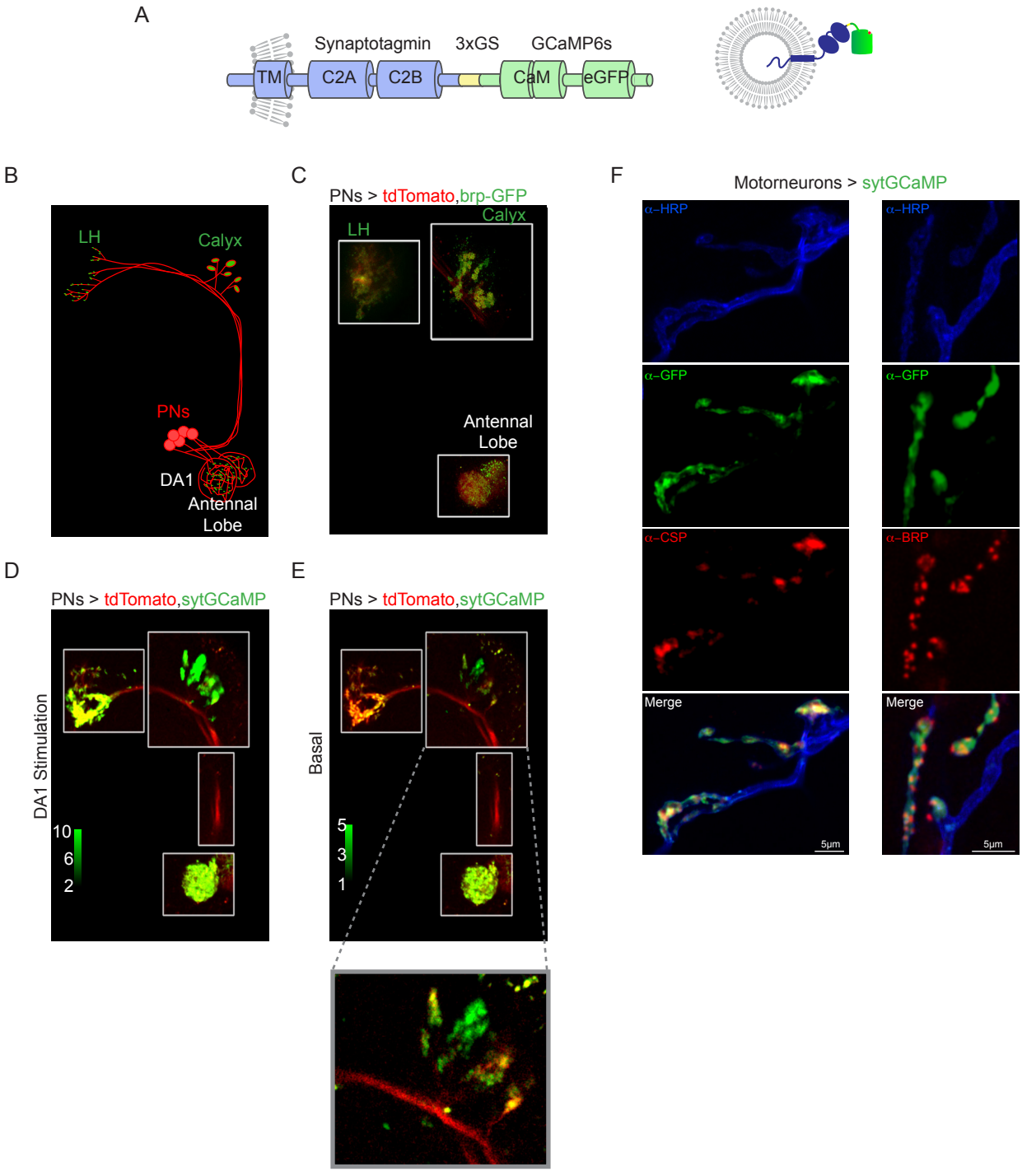
A
Synaptotagmin
3xGS
GCaMP6s
TM
C2A
C2B
CaM
eGFP
B
LH
Calyx
PNs
DA1
Antennal
Lobe
C
PNs > tdTomato,brp-GFP
LH
Calyx
Antennal
Lobe
F
Motorneurons > sytGCaMP
α-HRP
α-GFP
α-CSP
α-BRP
Merge
5μm
D
PNs > tdTomato,sytGCaMP
DA1 Stimulation
10
6
2
E
PNs > tdTomato,sytGCaMP
Basal
5
3
1

labeled PNs in the DA1 glomerulus with iontophoresis of acetylcholine, an excitatory neurotransmitter, and recorded the fluorescence of syt-GCaMP in the DA1 glomerulus, along the PN axonal tract, in the MB calyx and in the LH. PN activation led to robust increases in fluorescence that were highly localized to PN presynaptic sites and largely absent from axonal tracts (Figure 3.1D), suggesting that syt-GCaMP effectively localizes to presynaptic sites.

In order to further corroborate the synaptic targeting of syt-GCaMP we expressed it in motor neurons using VGlut-Gal4. The *Drosophila* neuromuscular junction (NMJ) is a well-studied system for understanding the development and plasticity of synaptic structures and therefore has well-established protocols for the identification of presynaptic markers[260]. We performed immunohistochemistry of the NMJ in order to visualize the motor neuron synapses and found that syt-GCaMP co-localized with other presynaptic proteins–bruchpilot (BRP) and cysteine string protein (CSP) (Figure 3.1F). Thus, we conclude that syt-GCaMP provides an effective means to monitor presynaptic Ca^{2+} in *Drosophila* neurons. We therefore proceeded to utilize this tool to investigate the population activity of the DANs in the MB lobes.

Coordinated Dopaminergic Neuron Activity Encodes Rewards and Punishments

Dopaminergic signaling pathways are prominent features of the MB circuitry[261,262] and play an essential role in the fly's ability to learn olfactory associations[222]. Until fairly recently, it was thought that the DANs innervating the *Drosophila* MB were only required for the learning of aversive associations, while octopamine was implicated as the reinforcer of appetitive associations[263]. However, as the tools for investigating the MB circuitry have improved, it has become clear that the TH-Gal4 line[264] that was thought to label all DANs was actually only expressed in a subset. Identification of additional DAN clusters (such as those labeled in the DDC-Gal4 line) revealed that DANs are actually responsible for both appetitive and aversive learning signals[116,219]. Subsequently, subpopulations of DANs have been shown to be responsible for conveying the neural signals that represent particular types of positive and negative reinforcement[209,210,220,221,265–268].

While the DANs have been shown to relay a diverse array of sensory stimuli that are used in conditioning paradigms (most frequently punitive electric shock and sugar rewards), recent anatomical studies have suggested that MBONs and DANs both project to a small number of convergence zones in the *Drosophila* protocerebrum[114]. This convergent architecture suggests that rather than independently relaying feed-forward sensory signals, the different DAN classes might form part of an interconnected

network with the MBONs. We therefore asked whether imaging the entire population of MB DANs in response to salient sensory stimuli would shed light on the role of this circuit in representing relevant contextual information.

We utilized the presynaptic localization of syt-GCaMP to monitor the activity of the DAN population and gain insight into the patterns of dopamine release across the MB lobes in different contexts. We combined the tyrosine hydroxylase (TH) and dopa-decarboxylase (DDC) promoters to drive expression of syt-GCaMP in the DANs innervating most compartments of the MB lobes (Figure 3.2A). We found that syt-GCaMP greatly enhanced our ability to visualize and resolve the borders between the individual MB compartments compared with soluble GCaMP6s (Figure 3.2B-C). Volumetric imaging of the DANs in the MB lobes *in vivo* revealed patterns of activity throughout the DAN population, suggesting that activity between DANs innervating different compartments may be coordinated (Figure 3.2D). As described above, we subsequently focused on DANs of the γ2-γ5 compartments, as their axon terminals could be monitored in a single optical imaging plane, allowing us to simultaneously record, with high temporal resolution, the synaptic responses of this subpopulation to positive and negative reinforcement stimuli.

We found that while sugar-feeding activated the γ4 and γ5 DANs, in accord with previous reports and their behavioral role in driving the formation of appetitive olfactory

Figure 3.2, Imaging Population Activity of Mushroom Body Dopaminergic Neurons. A, Schematic of γ-lobe DANs labeled by combining TH and DDC promoters. **B,** Max-Z projection of basal fluorescence in the MB lobes for flies in which the combined TH-Gal4 and DDC-Gal4 promoters drive expression of syt-GCaMP or **C,** soluble GCaMP6s. Same imaging settings were used for both preparations highlighting the improved ability to resolve the DAN innervation of the different γ-lobe (outlined in magenta) compartments when using syt-GCaMP. **D,** Spontaneous activity simultaneously recorded using syt-GCaMP expressed using TH-DDC-Gal4 in 13 MB compartments using volumetric imaging of the MB lobes *in vivo*. Fluorescence for each compartment is internally normalized for display purposes. Compartments are ordered by average correlation between compartment activity among a cohort of flies.

Figure 3.2

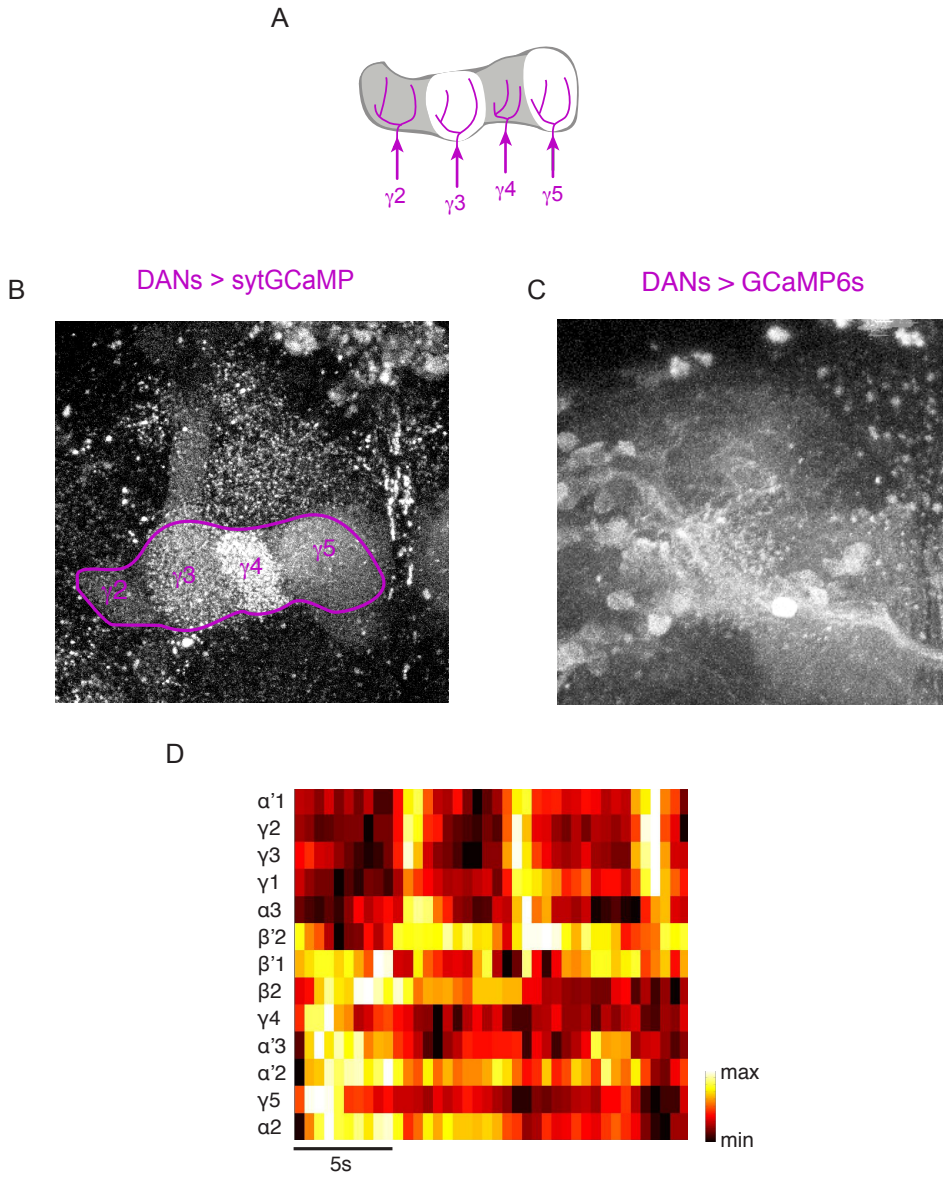
A
γ2
γ3
γ4
γ5
B
DANs > sytGCaMP
γ2
γ3
γ4
γ5
C
DANs > GCaMP6s
D
α'1
γ2
γ3
γ1
α3
β'2
β'1
β2
γ4
α'3
α'2
γ5
α2
5s
max
min

associations[88,210,221], ingestion of a sugar reward also inhibited γ2 and γ3 DAN activity (Figure 3.3A-B, Table 3.1). Conversely, the DAN innervating the γ2 compartment has been shown to respond to electric shock and contribute to aversive olfactory conditioning[192,209,217,218,220]. We confirmed that a brief electric shock applied to the fly's abdomen activated the γ2 DAN, but found that it also activated the γ3 DANs and inhibited the γ4 and γ5 DANs (Figure 3.3C, Table 3.1). Thus, the DANs of each compartment represent reinforcement stimuli through either excitation or inhibition, analogous to the bidirectional signaling observed in mammalian midbrain DANs in response to positive and negative contextual cues[27,29,36,239,269]. The reciprocal patterns of DAN activity evoked by these appetitive and aversive stimuli suggest that mushroom body reinforcement pathways may act cooperatively to regulate olfactory processing through coordinated patterns of dopamine release across all compartments.

Dopaminergic Population Activity Represents Ongoing Motor State

In our DAN population-imaging experiments we noticed that even in the absence of overt stimulation DANs exhibited significant fluctuations in their basal activity (Figure 3.2D). Video monitoring of a tethered animal during DAN imaging revealed that these fluctuations are, in fact, highly correlated with a fly's motor output (Figure 3.3D-E, Table

Figure 3.3, DAN Network Activity Reflects Both External Sensory Stimuli and Internal Behavioral State. A, syt-GCaMP was expressed in DANs of all γ-lobe compartments, driven by the combination of TH and DDC promoters. **B and C,** Schematic of stimulus (top) with representative heatmap ($\Delta F/F_0$) and normalized intensity trace of DAN syt-GCaMP response to the stimulus (**B,** sucrose; **C,** shock) below. (Bottom) Stimulus-triggered averages ± SEM for DANs of each compartment are shown. (B, n = 10 traces in nine flies; C, n = 21 traces in 11 flies). Fluorescence in other lobes is masked for clarity. Black scale bar indicates 1 s throughout figures unless otherwise noted. **D,** Representative normalized fluorescence traces of γ lobe DANs aligned to fly's motion (top). Dashed lines delineate start and end of a single representative bout of flailing. Cross-correlations between motion trace and activity in DANs of each compartment are shown (bottom, n = 12 traces in six flies). **E,** Schematic and still image from video showing the fly in flailing (right) and quiescent (left) behavioral states (top). Representative heatmap ($\Delta F/F_0$) of DAN activity in response to start and stop of flailing (middle). Average DAN fluorescence ± SEM in each compartment aligned to the start and stop of flailing (bottom, n = 14 traces in six flies). See also Table 3.1.

Figure 3.3

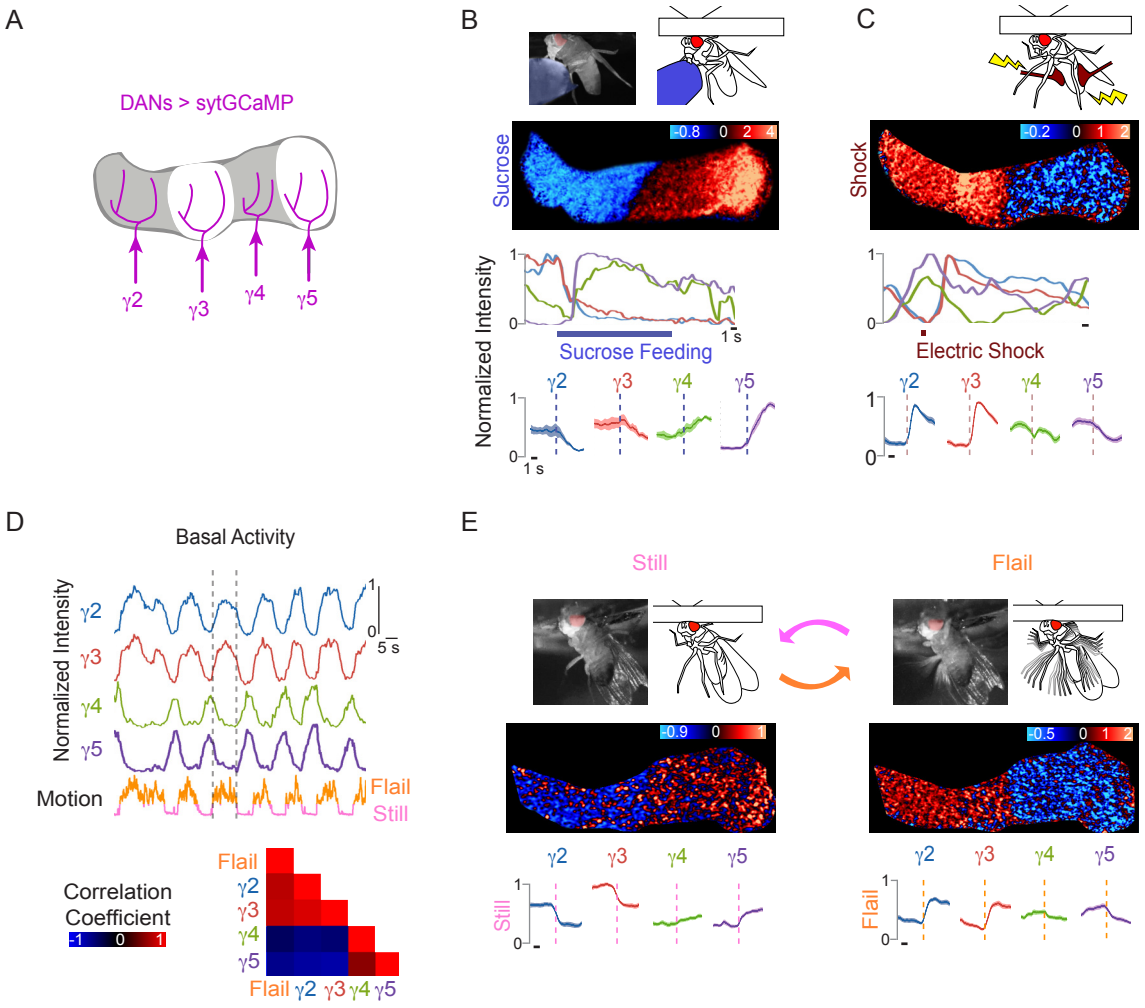
A
DANs > sytGCaMP
γ2
γ3
γ4
γ5
B
Sucrose
-0.8 0 2 4
Normalized Intensity
1
0
1 s
Sucrose Feeding
γ2 γ3 γ4 γ5
C
Shock
-0.2 0 1 2
Electric Shock
D
Basal Activity
Normalized Intensity
5 s
Motion
Flail
Still
Correlation Coefficient
-1 0 1
E
Still
Flail
-0.9 0 1
-0.5 0 1 2

Table 3.1

Statistical Measures of Induced Changes in DAN Fluorescence

	γ2 DANs	γ3 DANs	γ4 DANs	γ5 DANs
Sugar	0.020684751	0.038021709	0.035413261	4.16266E-05
Shock	8.5723E-05	2.20578E-07	0.008606605	0.000795113
Flail	1.21501E-11	2.568E-10	0.044450088	5.11192E-06
Still	8.37411E-12	5.51872E-12	0.036962279	6.16218E-07
58E02-DANs> P2X2	1.07325E-09	0.61686413	3.94375E-07	1.56546E-08
γ2 DAN>P2X2	0.009663704	6.87552E-09	2.06957E-06	6.71104E-06
γ3 DAN>P2X2	0.000321854	0.000103841	1.19609E-05	3.48101E-07
γ4 DAN>P2X2	0.000161199	0.001572201	6.61172E-06	1.29759E-05
γ5 DAN>P2X2	0.013657448	6.42053E-05	3.52496E-05	0.000246935

p-values from paired T-tests comparing fluorescence intensities in DANs of each compartment before and after each stimulus shown in Figures 3.3 and 3.5.

3.1). Tethered animals generally alternated between two distinct behavioral states—quiescence and rapid, uncoordinated kicking or "flailing" that resembles escape behavior. Leg kicking was strongly correlated with high γ2/γ3 and low γ4/γ5 DAN activity, similar to the pattern evoked by electric shock. In contrast, quiescence elicited the reciprocal DAN activity pattern, resembling the response to sugar-feeding, although somewhat smaller in magnitude (Figure 3.4A). Thus, different behavioral states induce distinct patterns of bidirectional activity across the DAN population. It is interesting to note that a previous study found that flies are incapable of walking and eating at the same time, raising the possibility that the DAN response to sugar may be, at least partially, induced by the state of stillness that necessarily accompanies ingestion[270]. Similarly, it is possible that the DAN representation of electric shock is a result of the flailing behavior that shock elicits (Figure 3.3).

Interestingly, the strict correlations exhibited by DANs during tethered behavior were altered when the same fly walked on a freely rotating ball (Figure 3.4B). For example, γ4 and γ5 DANs were no longer strictly synchronized during walking and γ4 DANs instead became transiently entrained to either γ3 or γ5 DAN activity. Odor stimuli, likewise, disrupted the baseline correlations between DANs (Figure 3.4C). These observations imply that the functional relationships between specific DANs are not absolute but rather an emergent property, depending on both salient external sensory signals and a fly's internal state. Dopaminergic signaling has been shown to be sufficient to alter subsequent behavioral responses[12,128,271] suggesting that the ongoing

Figure 3.4, DAN Network Interactions Depend on Context. A, Representative raw fluorescence traces of γ lobe DANs expressing syt-GCaMP in the same fly without any external stimulus (left) and in response to sugar ingestion (right) show that sugar-induced responses of DANs are qualitatively similar, but quantitatively greater than baseline, motor correlated activity. Average sugar-induced responses were 2.2 (±0.35)-fold greater in the γ4 DAN and 4.8 (±0.8)-fold greater in the γ5 DAN compared to the amplitude of spontaneous fluctuations in the same flies (n = 9). **B,** Normalized basal intensity traces of γ lobe DANs expressing syt-GCaMP for the same fly when walking on a freely rotating ball (top left) and when taken off of the ball and transitioning between quiescence and flailing behavioral states (top right). The correlations between all compartments are altered in these different behavioral contexts. Note for example that activity in γ3 and γ4 DANs, generally anti-correlated when the fly is dangling, become transiently correlated when the fly walks on a ball. Tethered, dangling flies exhibit a very consistent pattern of DAN correlations (compare individual and average for all flies, n = 12 traces in 6 flies, bottom), in accord with the notion that it underlies the consistent modulation of mushroom body processing we observe in Figure 4.3C. **C,** Odor stimuli evoke responses in the DANs that alter basal correlations between dopaminergic compartments in a tethered animal. Representative traces of DANs show that odor (here isobutyl acetate) evokes increases in DANs of all 4 compartments, resulting in altered correlations between them. Note for example that odor evokes an increase in the correlation between γ2 and γ4 DANs, which basally are strictly anticorrelated in a tethered and dangling animal (bottom, correlation trace is running correlation of ten imaging frames aligned to center frame. Correlation scale same as in **B**.

Figure 3.4

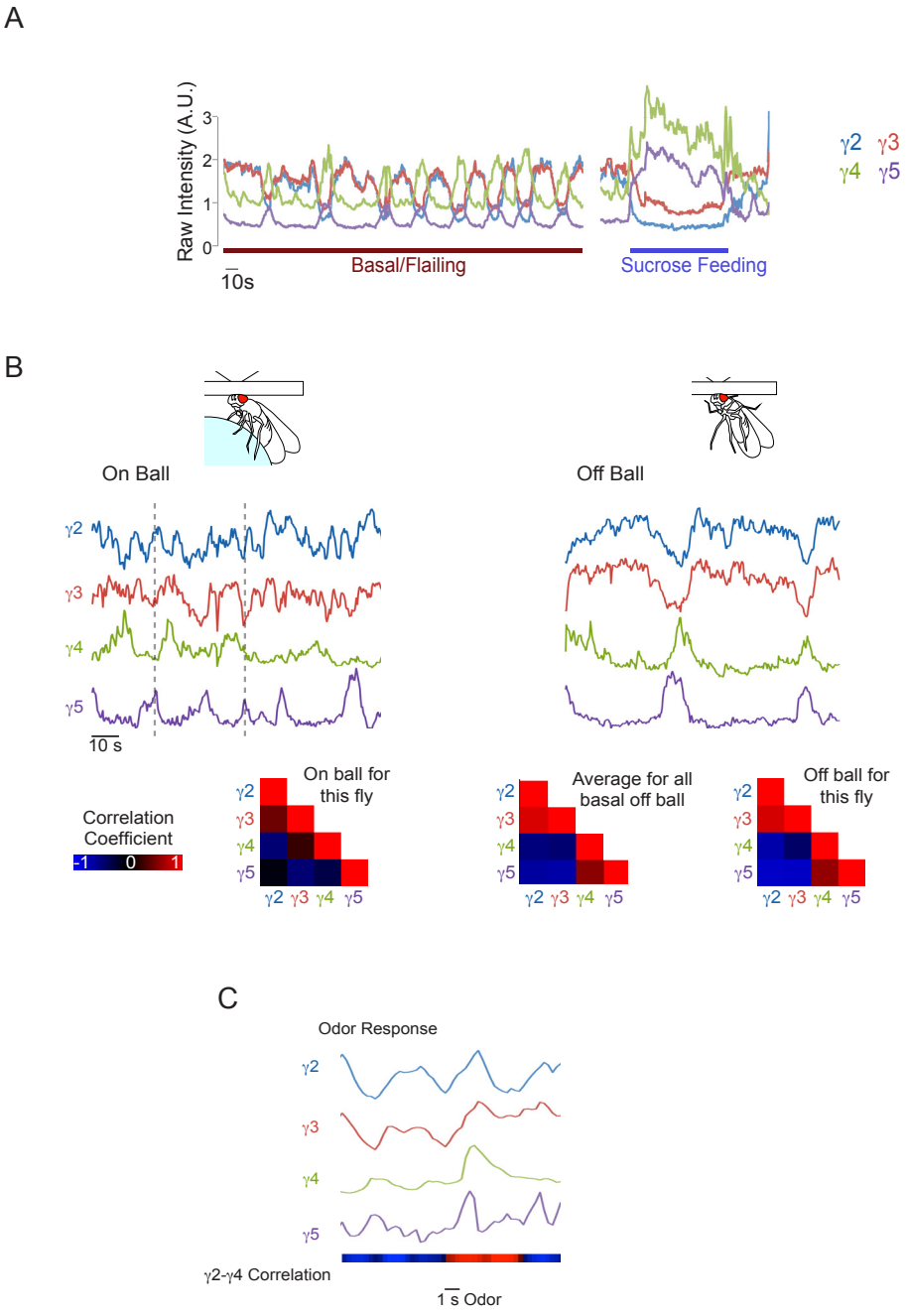
A
Raw Intensity (A.U.)
3
2
1
0
γ2 γ3
γ4 γ5
10s
Basal/Flailing
Sucrose Feeding
B
On Ball
Off Ball
γ2
γ3
γ4
γ5
10 s
Correlation Coefficient
-1 0 1
On ball for this fly
Average for all basal off ball
Off ball for this fly
γ2 γ3 γ4 γ5
C
Odor Response
γ2-γ4 Correlation
1 s Odor

activity representations of internal state in the DAN population might influence the fly's reactions to ensuing events.

Several other studies have recently reported similar 'spontaneous' or oscillatory DAN activity that likely reflects the same types of locomotor-states that we observe in our preparations. These studies have proposed that this ongoing DAN activity may play a role in both gating the formation of certain types of long term memory[272] and in a 'forgetting' signal that is necessary for erasing memories[223,273,274]. Thus, rather than simply representing rewards and punishments, the combinatorial patterns of DAN activity encode a range of internal states and external cues and may help guide the fly's behavioral choices[275]. Studies of mammalian dopaminergic systems have also shown that in addition to RPE, dopaminergic populations likely represent and influence aspects of locomotion and action selection[33,276,277]. How do these coordinated patterns of DAN activity emerge in order to convey multimodal sensorimotor signals to the appropriate targets? By making use of the genetically identifiable DAN classes in the *Drosophila* MB together with targeted recording and manipulation of these neurons we were able to begin to address this question.

Functional Communication Between Compartments Coordinates DAN Activity

The coordinated patterns of DAN activity could arise solely through common inputs from feedforward sensory and motor pathways or through network interactions with other parts of the MB circuitry. Anatomic evidence has suggested that there may be synaptic connectivity between the different MBONs and DANs[114,278]. We therefore asked whether the correlated, partially antagonistic activity patterns we observe across DANs of the γ lobe are shaped by circuit interactions between compartments. We first used the R58E02 promoter fragment[210,279] to selectively express the ATP-gated P2X2 channel in a subset of DANs, including those innervating the γ4 and γ5 compartments, and stimulated them by local application of ATP to their dendrites[280]. Activation of R58E02+ DANs evoked robust inhibition of the γ2 DAN (Figure 3.5A, Table 3.1). The γ3 DANs were also frequently inhibited, but occasionally activated due to variable labeling of this compartment by the R58E02 promoter. Therefore, excitation of a subset of DANs is sufficient to suppress those targeting other compartments, yielding a bidirectional pattern of activity similar to that evoked by a sugar reward (Figure 3.3B). This result suggests that direct or indirect functional communication between DANs may underlie their concerted representation of reinforcement signals, distributed across the compartments of a lobe.

Figure 3.5, Functional Communication between Compartments Coordinates DAN Network Activity. A-E, DAN syt-GCaMP activity patterns evoked by activation of P2X2 expressed in the **A,** R58E02+ DANs innervating γ4-5, **B,** γ2 MBON, **C,** γ3 MBON, **D,** γ4 MBON, and **E,** γ5 MBON. syt-GCaMP was expressed in DANs of all γ-lobe compartments using the TH and DDC promoters. Schematic of stimulus (top left), representative heatmap (bottom left, ΔF/F0), normalized intensity trace for representative experiment shown (top right), and stimulus-triggered averages ± SEM for DANs of each compartment (bottom right) are shown. ATP stimulation is shown as pink bar(**A**, n=8; **B**,n=8; **C**,n=8; **D**,n=8; **E**, n = 12). See also Table 3.1.

Figure 3.5

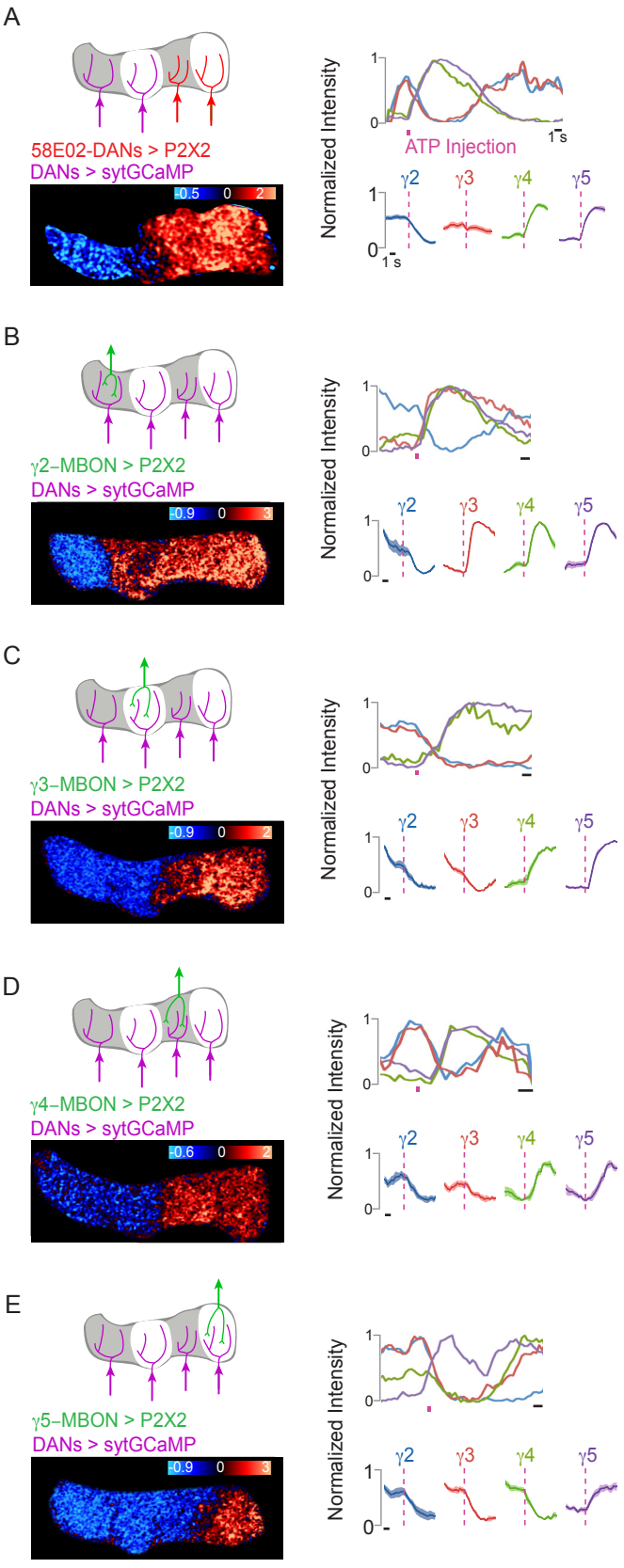
A
58E02-DANs > P2X2
DANs > sytGCaMP
-0.5 0 2
Normalized Intensity
1
0
1 s
ATP Injection
γ2 γ3 γ4 γ5
B
γ2–MBON > P2X2
DANs > sytGCaMP
-0.9 0 3
C
γ3–MBON > P2X2
DANs > sytGCaMP
-0.9 0 2
D
γ4–MBON > P2X2
DANs > sytGCaMP
-0.6 0 2
E
γ5–MBON > P2X2
DANs > sytGCaMP
-0.9 0 3

To investigate whether feedback from MBONs may contribute to the functional coordination between DANs, we expressed P2X2 in each MBON of the γ lobe and examined how stimulation of individual output pathways influences the activity pattern of the DAN population. Activation of each MBON triggered either excitation or inhibition in the DANs of every compartment imaged (Figures 3.5B-E, Table 3.1), similar to the distributed patterns of dopaminergic activity evoked by physiological reinforcement experiences. The bidirectional nature of DAN activity elicited by excitation of single MBONs indicates that multisynaptic interactions likely link extrinsic neurons innervating different lobe compartments. Thus, MBONs and DANs comprise a complex interconnected network, providing a potential substrate for the diverse functional relationships between DANs that emerge in different sensory and behavioral contexts (Figure 3.3).

Interestingly, a recent study demonstrated that suppression of the γ3 DAN is sufficient to induce reward learning[281], which can also be induced by activation of the R58E02+ DAN population[210]. We speculate that this learning may be mediated by the reciprocal functional relationship between the R58E02+ DANs and the γ3 DAN that we observe (Figure 3.5A). Similarly, suppression of the γ1 MBON leads to aversive learning[282], likely through the sort of feedback connections from MBONs to DANs described here (Figure 3.5B-E). These results suggest that learning in the MB is achieved not simply by autonomous activation of specific DANs, but rather by a coordinated, bidirectional pattern of activity throughout the DAN population. Subsequent

studies have revealed additional functional roles for the recurrent connectivity between MBONs and DANs, including the generation of behaviorally relevant persistent activity[283], context-dependent control of learning[284] and the ability to re-evaluate previously learned associations[285]. Together, these data suggest that DANs do not act autonomously to convey the valence of a reinforcement stimulus to just a single compartment. Rather, the DAN population functions as a dynamic ensemble, integrating information about environmental stimuli and internal state to convey the moment-by-moment experience of the fly to all compartments of the lobe.

A Conserved Dual Function of Dopaminergic Circuits

Several decades of research on the mechanisms of learning in the *Drosophila* MB have revealed a role for dopaminergic signaling in reinforcement learning that is evolutionarily conserved from flies to humans. Phasic activity of DANs in the striatum has long been thought to represent the reward signals that are responsible for updating an animal's behaviors based on learning[24,286]. Recent efforts have begun to describe how the DANs might calculate the RPE necessary for reinforcement learning[287,288]. However, there is considerable complexity to this circuitry, and it appears that some inputs to DANs already contain an RPE representation, further confounding our ability to understand the emergence of this signal[24]. Exploiting the accessibility of distinct dopaminergic populations in the MB and genetic control of specific neurons within the

MB circuits, we have begun to describe the source of their coordinated representations of rewards and punishments as emergent properties of an interconnected network. Further dissecting the computations performed by the interactions within this network will be an interesting topic for future investigations.

The dopaminergic circuits in the basal ganglia are also known to be required for normal action initiation[8,243,289], and recent experimental approaches have strengthened the suggestion that subsets of midbrain DANs represent and invigorate animal movement[31–33]. The unexpected finding that the MB DANs also relay motor signals further strengthens this parallel. The coupling of reinforcement signals and locomotor representations in the same neuromodulatory system across such distantly related phyla suggests an inherent connection between these dual roles of dopamine. Many different conceptual models have been proposed and revised in order to reconcile these two signaling modes of DANs in the striatum. For instance, the action-invigorating function of DANs has been incorporated into 'actor-critic' algorithms of reinforcement learning, suggesting that the dopaminergic signal is responsible for binding action to reward[290,291]. Alternative models that have recently found experimental support include the idea that the DAN activity represents the initiation of movement that leads to reward, rather than the reward itself[34,291], or that dopamine is involved in arousing a behavioral response to salient sensory inputs[31,292,293]. The focus of these models is generally to try to understand the algorithmic function of the dopaminergic signals in underlying adaptive sensorimotor processing. However, very little is known about how these

proposed functions of striatal DANs are actually implemented by the modulatory effects of the dopamine they release on downstream circuits. Because of the difficulty of studying circuit plasticity *in vivo,* nearly all studies of the neurophysiological functions of dopamine release in the striatum have either looked at the effects of dopaminergic perturbations on behavior, or taken place in in brain slices, where it is difficult to connect specific observations with behavior[21,24]. Taking advantage of the compartmentalized DAN innervation of the MB lobes and their well-defined roles in fly behavior, we therefore decided to probe the precise targets and mechanisms of dopaminergic modulation in the MB. These investigations form the basis for Chapters 4 and 5.

Chapter 4

Kenyon Cell Presynaptic Ca^{2+} is Modulated by Dopaminergic Neurons

The coordinated and partially antagonistic patterns of activity in the DANs (Figures 3.3-3.5) that tile along the length of the KC axons suggest the possibility that different segments of the KC axons might be independently modulated by the dopaminergic signals resulting from reinforcing stimuli and locomotor state. Intraneuronal functional differences between synapses have been described in a number of other systems[294–296] and should provide increased computational capacity by allowing a neuron to differentially signal to different postsynaptic partners[297–299]. We therefore asked whether we might be able to monitor functional differences at the synapses along the γ KC axons using syt-GCaMP. Differential modulation of KC synapses along the length of the lobe would allow for the same activated KC to lead to different MBON activation depending on the context in which it is experienced and previously learned associations. In order to assess whether syt-GCaMP could be used to monitor the synapses at different points along KC axons we expressed syt-GCaMP in all KCs using a selective promoter and focally stimulated the calyx with the excitatory neurotransmitter acetylcholine to activate an individual neuron in a brain explant

Figure 4.1, syt-GCaMP Highlights Presynaptic Activity Along KC Axons. Iontophoresis of acetylcholine into the mushroom body calyx was titrated to excite a single KC, as revealed by a sole activated process running through the pedunculus, shown in schematic form in **A,** and syt-GCaMP response along the axon captured by volumetric imaging in **B**. Note that in a brain explant, we observe a relatively uniform syt-GCaMP signal at individual presynaptic sites along the entire length of the KC axon. **C,** Co-expression of tdTomato and synaptotagmin-GFP in a subset of γ KCs under VT043657-Gal4 shows the distribution of presynaptic sites along the entire length of a KC axon. Dashed line outlines the γ lobe. **D,** Comparison of soluble GCaMP6s and syt-GCaMP response in KCs to minimal stimulation through acetylcholine iontophoresis into the mushroom body calyx. Note the individual presynaptic puncta clearly defined in the syt-GCaMP signal compared to the more continuous GCaMP6s signal along the KC axons in the pedunculus.

Figure 4.1

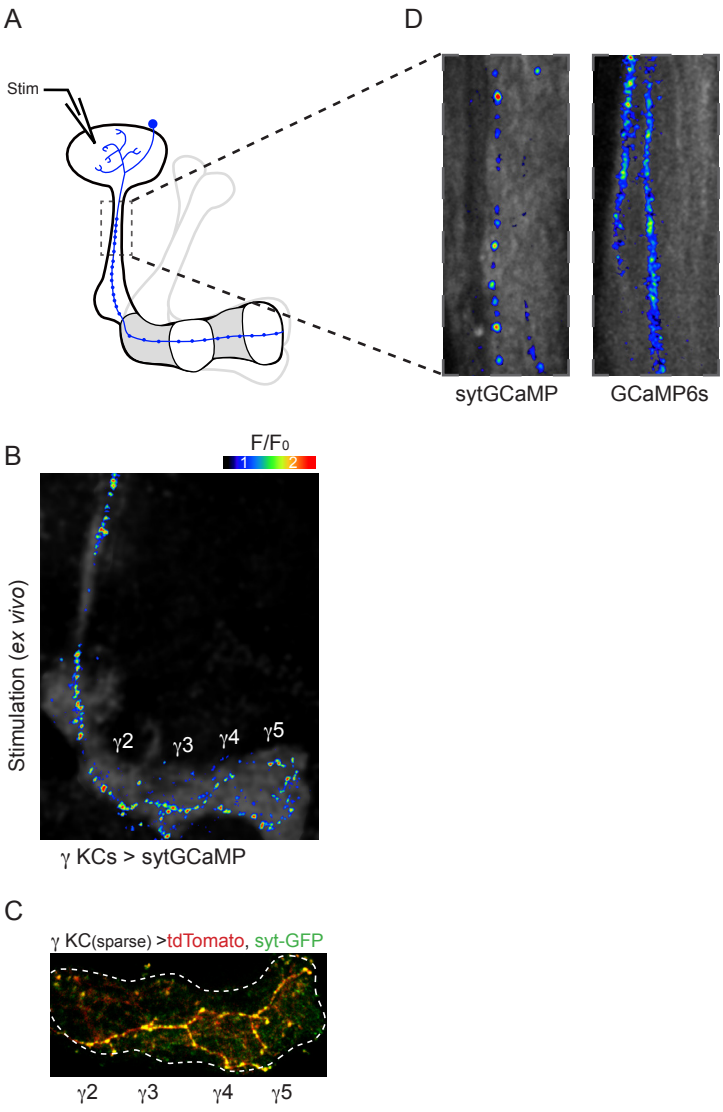
A
Stim
D
sytGCaMP
GCaMP6s
B
F/F0
1
2
Stimulation (ex vivo)
γ2
γ3
γ4
γ5
γ KCs > sytGCaMP
C
γ KC(sparse) >tdTomato, syt-GFP
γ2
γ3
γ4
γ5

(Figure 4.1A). We performed volumetric two-photon imaging to capture the fluorescently tagged synapses of the KC's full axonal arbor as it ramifies through multiple imaging planes within the γ lobe. Stimulation of a single KC evoked robust fluorescence increases at punctate loci distributed along the length of its axon (Figure 4.1B), consistent with syt-GCaMP's synaptic localization and anatomic evidence that KCs form output synapses in all compartments of the γ lobe (Figure 4.1C). This punctate pattern was not apparent when using soluble GCaMP6s in place of syt-GCaMP under the same experimental conditions (Figure 4.1D), highlighting the presynaptic localization of syt-GCaMP. Thus syt-GCaMP facilitates the detection of Ca^{2+} influx at individual synaptic sites, providing a technical strategy to resolve differences in presynaptic function and modulation across the compartments of the lobe[248].

Compartmentalized Synaptic Domains Along Kenyon Cell Axons

We expressed syt-GCaMP in the γ KCs (Figure 4.2A,E) and used volumetric two-photon imaging to monitor the odor-evoked responses of the entire complement of synapses within the γ lobe of a living tethered fly. Unexpectedly, we observed that the distribution of odor-evoked presynaptic Ca^{2+} *in vivo* was highly non-uniform and displayed a modular pattern along the length of the lobe that was apparent in each of the 12-18 imaging planes (Figure 4.2B-C), despite the fact that labeled synaptic sites

Figure 4.2, Compartmentalized Ca^{2+} Domains along KC Axons *In Vivo.* A, Schematic (left) and representative basal fluorescence of syt-GCaMP expressed in γ KCs labeled with approximate compartmental borders (right). **B,** Volumetric 2-photon resonant scanning imaging of γ KCs expressing syt-GCaMP under R16A06-Gal4 in response to an odor stimulus. Schematic of imaging strategy (top-left inset). At each time point, data was collected at 12-18 Z-planes encompassing the entire γ lobe. Peak fluorescence of the 12 individual Z-planes and maximum Z projection (top-right). Compartmental differences in Ca^{2+} distribution are apparent in every imaging plane and the maximum-Z projection. **C,** Normalized intensity profile plot of syt-GCaMP fluorescence along the length of the lobe for each imaging plane (gray) and of the maximum-Z projection (white) for the representative images shown in **B,** indicate that every imaging plane displays a very similar Ca^{2+} distribution. (Only the 9 planes in which the entire length of the lobe is visible are included.) Odor used was isobutyl acetate, however, a similar distribution of presynaptic Ca^{2+} was seen for all odor stimuli, see Figure 4.5B. **D,** Immunolabeling of GFP tagged synaptic protein bruchpilot (brp) expressed in γ KCs under the R16A06-Gal4 promoter with α-GFP staining reveals an equivalent distribution throughout the compartments of the lobe. **E,** Expression of syt-GCaMP under R16A06-Gal4 shows homogeneous and specific labeling of γ KCs by this driver line (left). All KCs express DsRed and allow us to define the different mushroom body lobes as indicated (right). Image was taken in a brain explant.

Figure 4.2

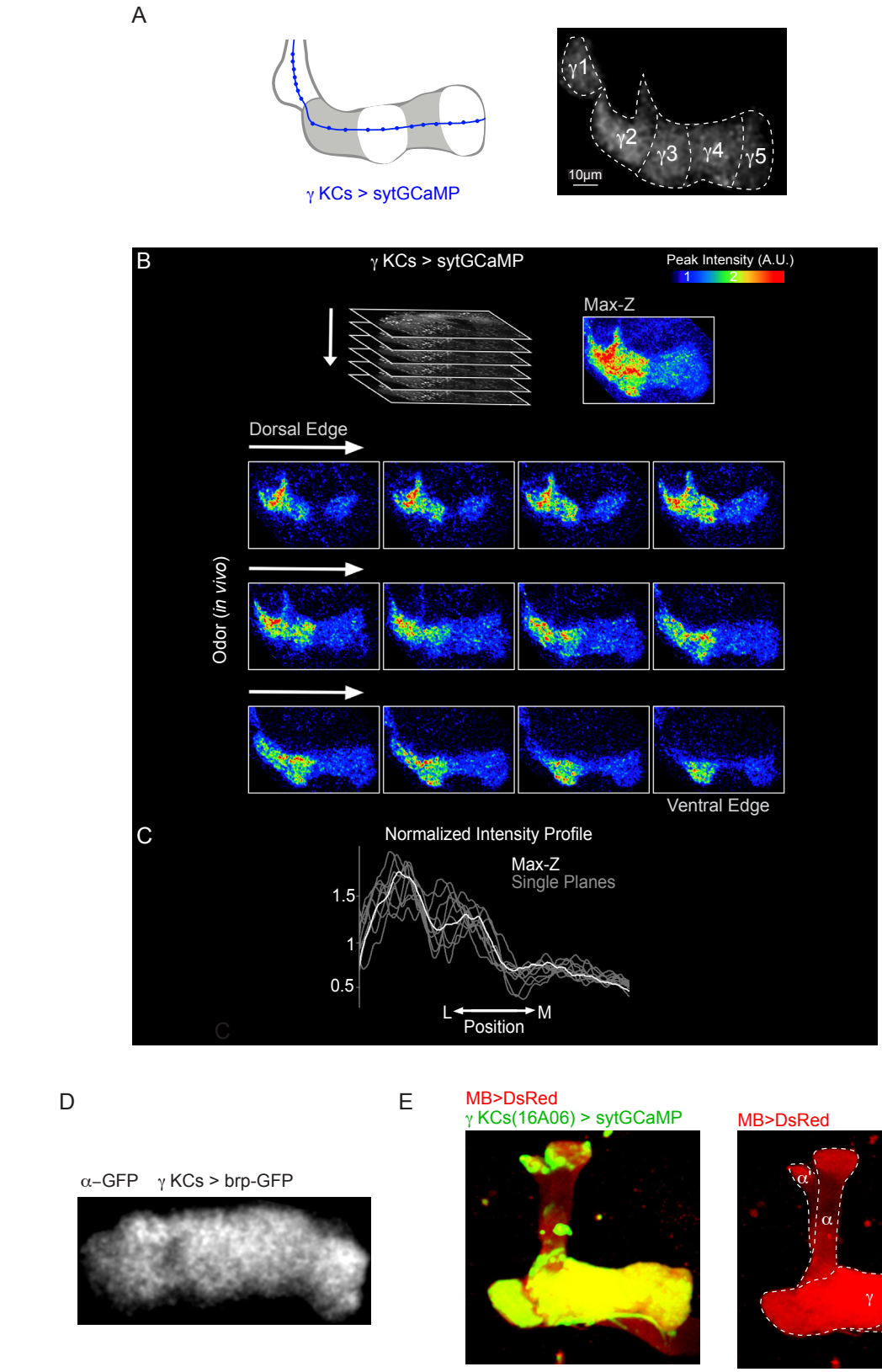
A
γ KCs > sytGCaMP
γ1
γ2
γ3
γ4
γ5
10μm
B
γ KCs > sytGCaMP
Peak Intensity (A.U.)
1
2
Max-Z
Dorsal Edge
Odor (in vivo)
Ventral Edge
C
Normalized Intensity Profile
Max-Z
Single Planes
1.5
1
0.5
L
M
Position
D
α–GFP
γ KCs > brp-GFP
E
MB>DsRed
γ KCs(16A06) > sytGCaMP
MB>DsRed
α
α
γ

(Figure 4.2D)[300] and the syt-GCaMP protein (Figure 4.2E) were equivalently distributed along the length of the lobe.

Alignment of syt-GCaMP responses with the segregated projections of MBONs and DANs in the γ lobe indicated that the discrete Ca^{2+} domains apparent in KC axons map to the different compartments of the lobe (Figure 4.3A). To confirm this, we imaged KC synaptic Ca^{2+} in animals that also express tdTomato in a subset of DANs and observed that the sharp borders separating regions of high and low synaptic Ca^{2+} activity align to the compartmental boundaries (Figure 4.3B). Thus in a tethered animal, the odor-evoked synaptic responses of KCs were significantly more robust in the γ2 and γ3 compartments relative to those in the γ4 compartment, with even weaker responses apparent in the γ5 compartment (Figure 4.3C). The distribution of presynaptic Ca^{2+} in KC axons therefore adheres to the modular architecture of the lobes, demonstrating that the anatomic compartments represent functionally distinct units.

Asymmetric presynaptic Ca^{2+} domains could arise from differences in KC innervation along the γ lobe or from functional variation along individual KC axons. Single cell labeling of more than 80 γ KCs confirmed that they invariantly traverse the entire lobe (Figure 4.4A) and are thus poised to carry the same odor signals to each compartment. However, functional synaptic heterogeneity was evident along sparsely labeled γ KC axons[301] co-expressing syt-GCaMP and a red fluorophore to delineate

Figure 4.3, KC Ca^{2+} Distribution Reflects the Compartmental Organization of the MB Lobes. A, Registration strategy used to define compartmental borders. Fluorescent reporters were expressed in MBONs and DANs (bottom, n = 10, 1 representative example is shown) and labeling by extrinsic neuron innervation was used to define the average position of compartmental borders along the longitudinal axis of the γ lobe. The average border positions between compartments are indicated by dashed vertical lines. The SEM of the border positions are indicated between compartment names. To generate an average value of syt-GCaMP intensity for each compartment (termed the compartment average in **C-D**) the intensity values for the center 50% of each compartment were averaged (red area, see methods for details). The representative image and dot/box plot from **C** is shown. **B,** tdTomato expressed in γ4 and γ5 DANs using R58E02-LexA (top, middle). Compartmentalized KC syt-GCaMP responses in the same fly shows synaptic Ca^{2+} domains have sharp boundaries that align to the border between γ3 and γ4 compartments. **C,** Maximum-intensity Z-projection of all 15 imaging planes sampled through the γ lobe in the example shown in Figure 4.2B (top). Average normalized odor-evoked profile of syt-GCaMP fluorescence intensity along the γ lobe (gray line, n = 21 flies) and peak intensity for each compartment (black dots, n = 21) with mean ± SEM in red (middle). Odor-evoked time courses were imaged in each compartment for representative experiment shown above (bottom, blue lines indicate 1-s odor stimulus). **D,** Representative image of syt-GCaMP signal in γ KCs in response to direct stimulation of KCs by acetylcholine iontophoresis into the mushroom body calyx in a brain explant (top). Normalized intensity profiles for *ex vivo* stimulation across a range of iontophoretic voltages (1–10 V) with average profile for each voltage in a different colored line (n = 6, voltage coloring as in Figure 4.6). Stimulation-evoked time courses were imaged in each compartment for representative experiment shown above (bottom, blue lines indicate stimulation). **E,** Odor response in a sparse subset of γ KCs expressing syt-GCaMP (heatmap, top) and tdTomato (grayscale, middle). Odor-evoked time courses were measured at individual synaptic boutons (bottom). All KC heatmaps in this figure represent peak fluorescence. Values marked with different lowercase letters represent significant differences ($p < 0.05$ by t-test with correction for multiple comparisons).

Figure 4.3

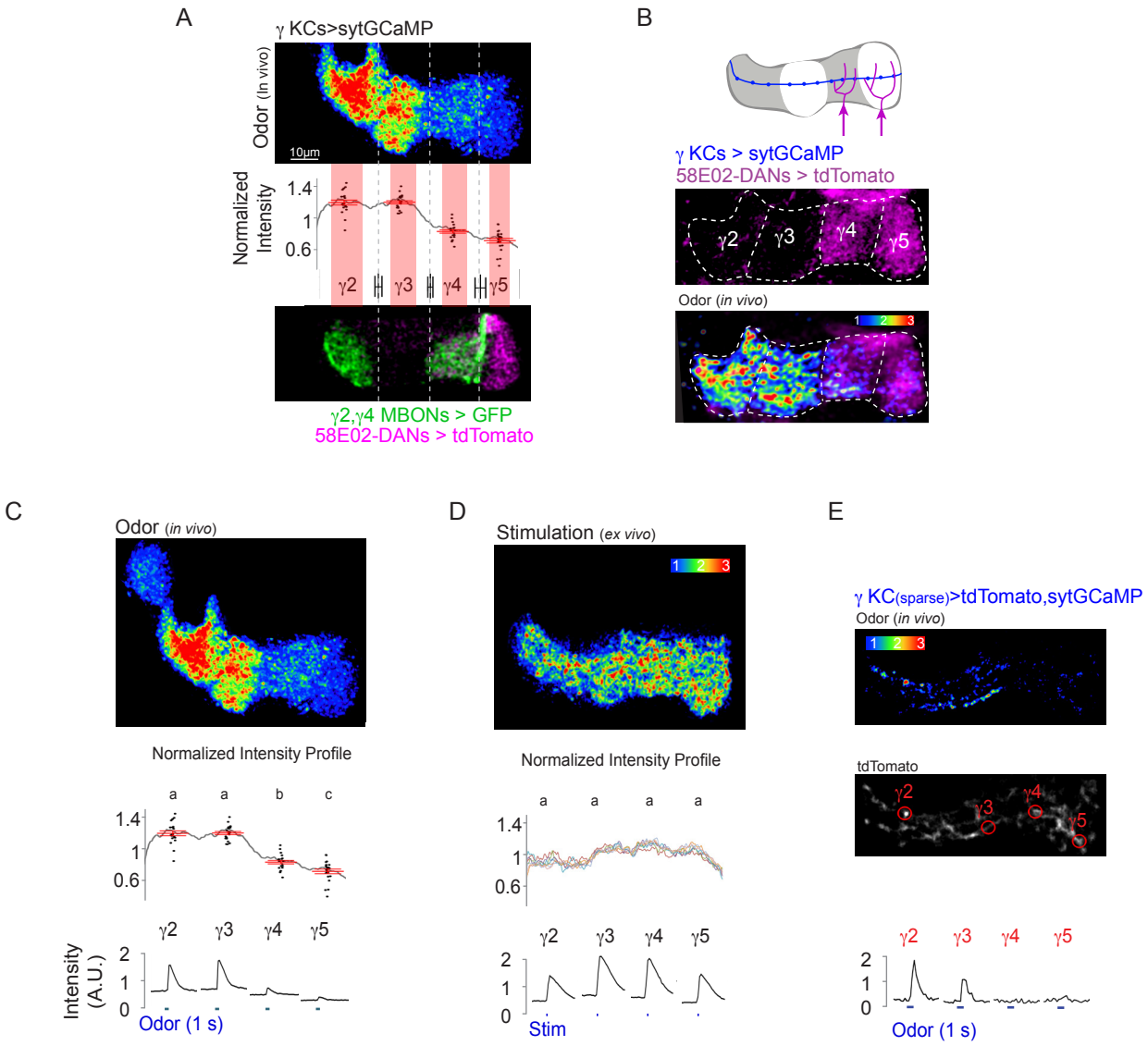
A
γ KCs>sytGCaMP
Odor (In vivo)
10μm
Normalized Intensity
1.4
1
0.6
γ2
γ3
γ4
γ5
γ2,γ4 MBONs > GFP
58E02-DANs > tdTomato
B
γ KCs > sytGCaMP
58E02-DANs > tdTomato
γ2
γ3
γ4
γ5
Odor (in vivo)
1
2
3
C
Odor (in vivo)
Normalized Intensity Profile
a
a
b
c
1.4
1
0.6
γ2
γ3
γ4
γ5
Intensity (A.U.)
2
1
0
Odor (1 s)
D
Stimulation (ex vivo)
1
2
3
Normalized Intensity Profile
a
a
a
a
1.4
1
0.6
γ2
γ3
γ4
γ5
2
1
0
Stim
E
γ KC(sparse)>tdTomato,sytGCaMP
Odor (in vivo)
1
2
3
tdTomato
γ2
γ3
γ4
γ5
γ2
γ3
γ4
γ5
2
1
0
Odor (1 s)

Figure 4.4, Asymmetric Ca^{2+} Signals Along Individual KC Axons. A, Single KC labeling by PA-GFP expressed under the MB247 promoter demonstrates that γ KCs (n = 82, 16 shown) project their axons across the entire lobe, traversing all compartments (imaging courtesy of Ari Zolin). **B,** Volumetric imaging of sparsely labeled γ KCs co-expressing syt-GCaMP and tdTomato confirms compartmentalized presynaptic Ca^{2+} differences along single KC axons that traverse the full length of the lobe. Representative images for the same example shown in Figure 4.3E with tdTomato used to anatomically label axons (grayscale, top of each image), peak odor-evoked syt-GCaMP fluorescence (heatmap, middle of each image) and peak syt-GCaMP fluorescence normalized by tdTomato signal within each pixel (heatmap, bottom of each image). Maximum intensity Z projection (top-left), normalized intensity profiles (top-center) and each of the 12 optical planes from dorsal to ventral edge. Note that while the tdTomato signal is uniform along the length of the lobe, the syt-GCaMP signal is asymmetric and resembles the modular pattern apparent when imaging the total γ KC population. Odor used was benzaldehyde, however, a similar distribution of presynaptic Ca^{2+} was seen for all odor stimuli, see Figure 4.5B.

Figure 4.4

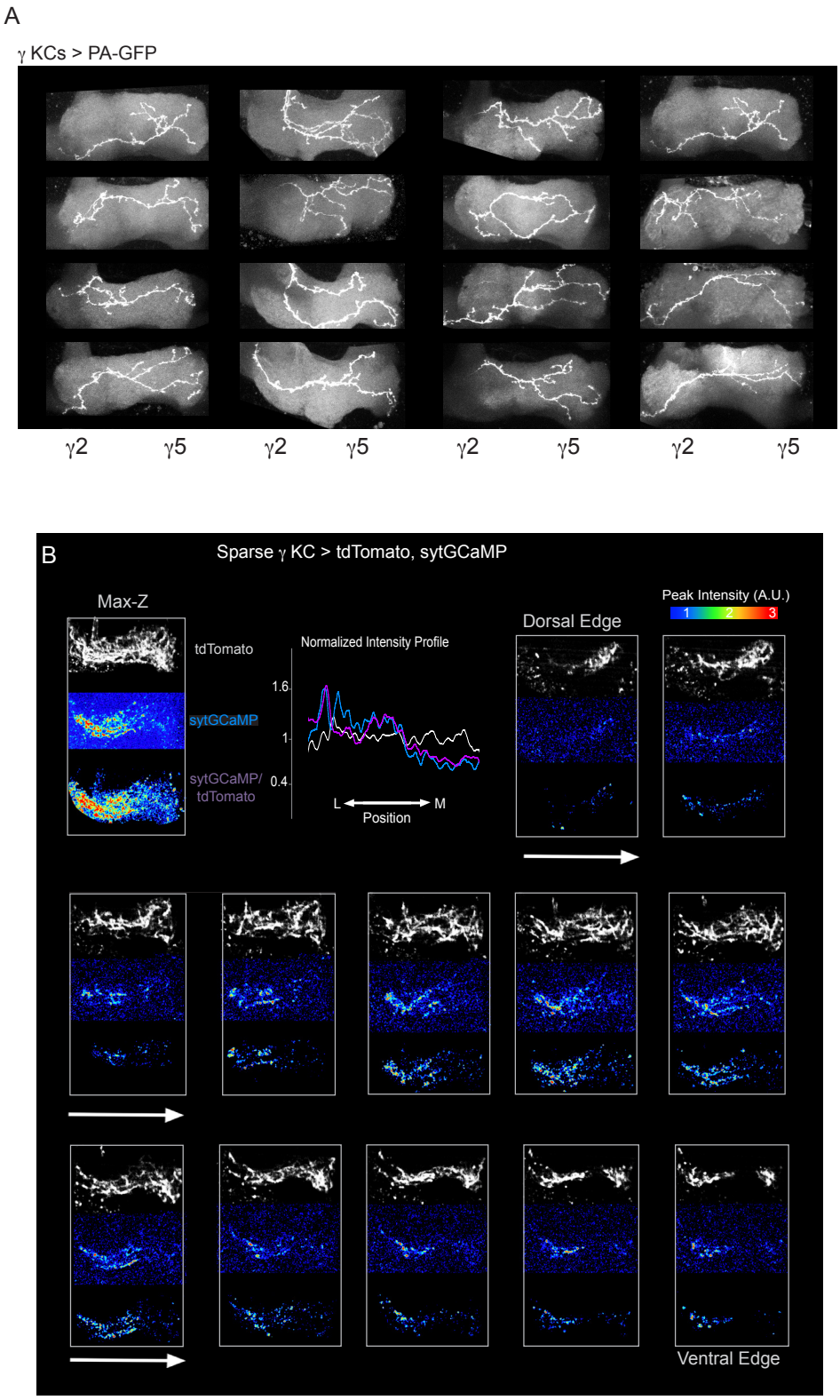
A
γ KCs > PA-GFP
γ2
γ5
γ2
γ5
γ2
γ5
γ2
γ5
B
Sparse γ KC > tdTomato, sytGCaMP
Max-Z
tdTomato
sytGCaMP
sytGCaMP/
tdTomato
Normalized Intensity Profile
1.6
1
0.4
L
M
Position
Dorsal Edge
Peak Intensity (A.U.)
1
2
3
Ventral Edge

their projections to the distal tip of the lobe (Figures 4.3E, 4.4B). We observed that synaptic boutons decorating the same KC axons exhibited differential responses to odor, with more robust activity evoked in the individual synapses in the γ2 and γ3 compartments relative to those in the γ4 and γ5 compartments. Although we did not routinely image the γ1 compartment, presynaptic Ca^{2+} was often lower there in comparison to more distal portions of the lobe (Figure 4.3C), indicating it is unlikely that action potentials simply fail to propagate along the narrow KC axons. Together, these data suggest that the synapses along individual KC axons are functionally distinct, such that the same olfactory signal is differentially represented by each axonal segment of a neuron.

Interestingly, the asymmetry in presynaptic Ca^{2+} was often present basally, prior to odor stimulation (Figure 4.5A) suggesting persistent differences in synaptic function along KC axons that could influence how all incoming odor stimuli are processed. Consistent with this idea, the same modular pattern of presynaptic Ca^{2+} was evoked in response to every odor tested and over a range of odor concentrations (Figures 4.5B). Moreover, KC classes innervating other lobes also exhibit modular syt-GCaMP signals (Figure 4.5C), suggesting that compartmentalized synaptic Ca^{2+} is a general feature of odor representations in the mushroom body lobes. We compared the KC Ca^{2+} distributions in the γ lobe in response to KC stimulation by acetylcholine iontophoresis *in vivo* and *in vitro*. Interestingly, the asymmetry present *in vivo* is not apparent in a brain explant (Figure 4.3D, 4.6A-E), suggesting that this pattern of modulation is maintained

Figure 4.5, Compartmentalized Ca^{2+} is Independent of Odor Identity or an Animal's Satiety State. A, Compartmentalized KC Ca^{2+} is also apparent in the basal state (top), prior to odor stimulation but becomes more apparent in odor-evoked responses (bottom). Note the heatmaps represent different intensity scales and there is a significant increase in syt-GCaMP fluorescence evoked by an odor stimulus. **B,** The distribution of presynaptic Ca^{2+} along KCs was independent of odorant identity or satiety state. Normalized intensity profiles of peak fluorescence shown for isobutyl acetate, trans-3-hexen-1-ol, ethyl acetate, and apple cider vinegar at a range of concentrations (top, n = 4). Average normalized intensity profile of odor-evoked γ KC syt-GCaMP fluorescence in sated flies (black, n = 21) and in flies that were food-deprived for 20-26 hr (red, n = 9) reveals no apparent difference in presynaptic Ca^{2+} distribution along the γ lobe (bottom). **C,** Schematic of compartmentalized anatomic organization in the α' and β' lobes (top). Odor-evoked presynaptic Ca^{2+} signal in α'β' KCs visualized by expressing syt-GCaMP under the R35B12-Gal4 driver (bottom) reveals compartmentalized signals similar to those observed in γ KCs. Image is a maximum intensity projection of peak odor-evoked fluorescence from volumetric imaging of the lobe.

Figure 4.5

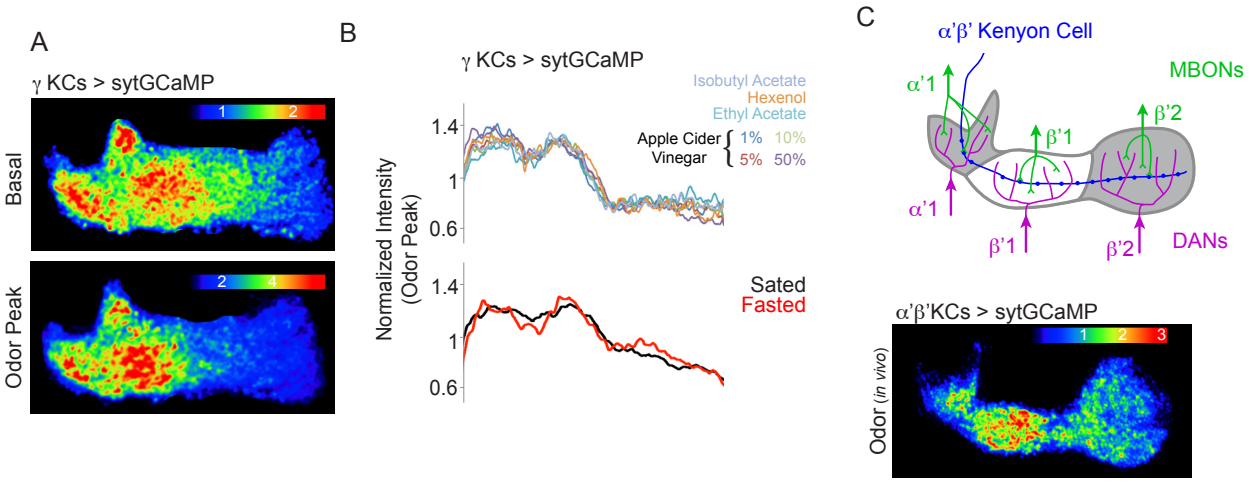
A
γ KCs > sytGCaMP
Basal
1
2
Odor Peak
2
4
B
γ KCs > sytGCaMP
Isobutyl Acetate
Hexenol
Ethyl Acetate
Apple Cider Vinegar
1%
10%
5%
50%
Normalized Intensity (Odor Peak)
1.4
1
0.6
Sated
Fasted
C
α'β' Kenyon Cell
MBONs
α'1
β'1
β'2
DANs
α'β'KCs > sytGCaMP
Odor (in vivo)
1
2
3

Figure 4.6, Compartmentalized Ca^{2+} Requires Ongoing *In Vivo* Modulation. A, Representative images of peak syt-GCaMP signal in γ KCs in response to direct stimulation of KCs by iontophoresis of acetylcholine on their dendrites in the mushroom body calyx in a brain explant. A range of iontophoretic voltages was used, as indicated. **B,** Normalized intensity profiles for experiment shown in **A**. The color of the line in the profile plot indicates the iontophoretic voltage used as shown in **A**. Each trace is the average of two stimulations at the indicated voltage for n = 6 mushroom bodies. Statistical analysis done using values averaged from traces at all voltages used. Values marked with different lowercase letters represent significant differences with $p < 0.05$ by t test with correction for multiple comparisons. **C,** Representative images for same stimulation protocol as in **A** in a tethered fly *in vivo*. **D,** Same as **B**, but for *in vivo* data in **C**, n = 6 mushroom bodies. **E,** Peak odor-evoked intensity in a living fly across a range of odor concentrations (isobutyl acetate). **F,** Integrated normalized basal DAN activity in tethered flies in each compartment (n = 6 flies). Normalized intensities for each compartment were summed over entire recordings and each data point represents the sum for that compartment over the total sum for all four compartments in that fly.

Figure 4.6

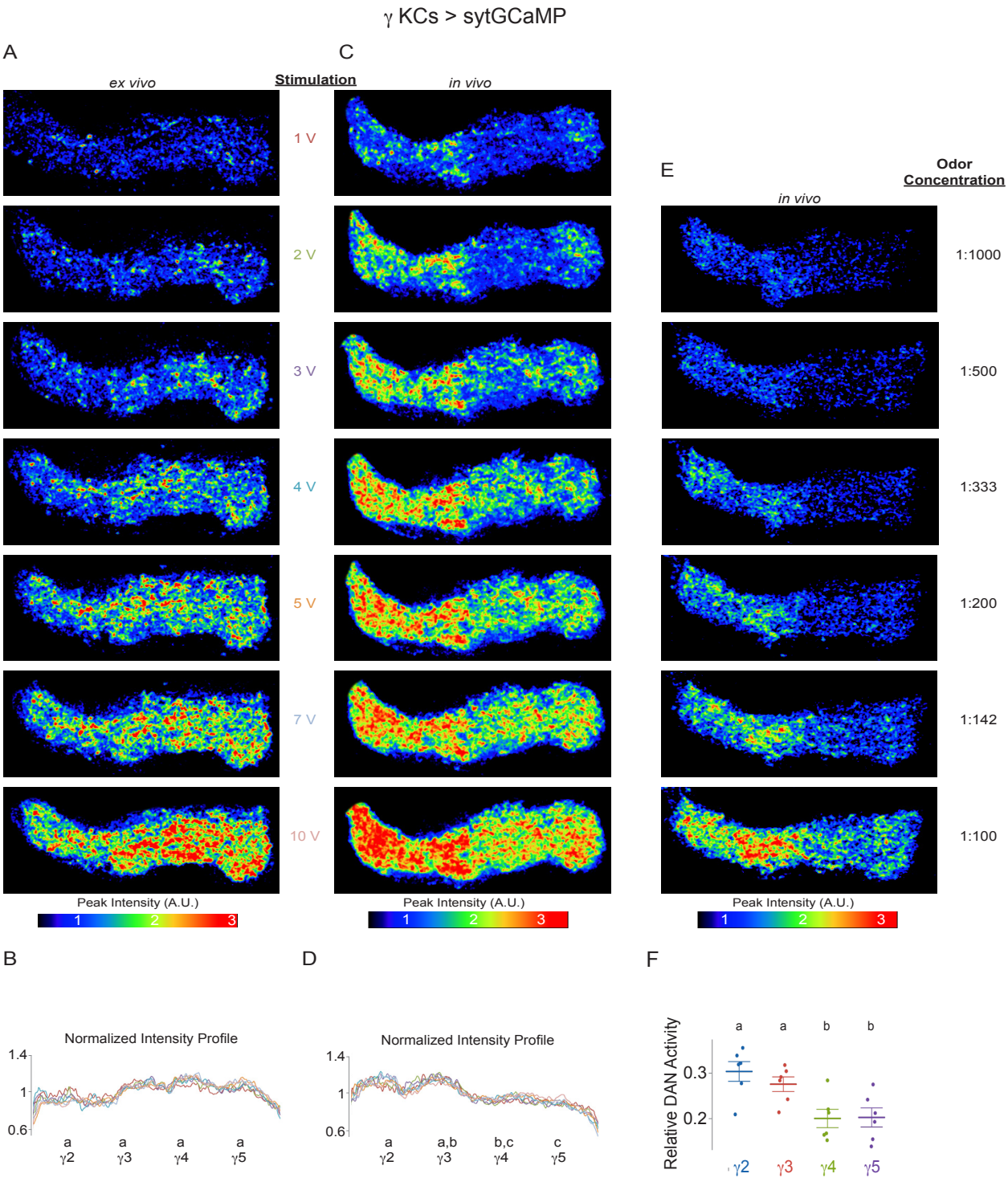
γ KCs > sytGCaMP
A
ex vivo
Stimulation
C
in vivo
E
Odor Concentration
in vivo
1 V
2 V
3 V
4 V
5 V
7 V
10 V
1:1000
1:500
1:333
1:200
1:142
1:100
Peak Intensity (A.U.)
1
2
3
B
Normalized Intensity Profile
1.4
1
0.6
a γ2
a γ3
a γ4
a γ5
D
Normalized Intensity Profile
a γ2
a,b γ3
b,c γ4
c γ5
F
Relative DAN Activity
0.3
0.2
a
a
b
b
γ2
γ3
γ4
γ5

by a mechanism that is active in a living fly but not in an explant. We therefore wondered whether there was any corresponding asymmetry with the movement-associated patterns of DAN activity described above. Analyzing the DAN activity levels across all recordings in each γ lobe compartment revealed that there was significantly more activity in the γ2-γ3 compartments compared with the γ4-γ5 compartments (Figure 4.6F). This correlation between higher spontaneous DAN activity and heightened KC presynaptic Ca^{2+} suggests the possibility that active modulation by the DANs that tile the γ lobe may regulate synaptic signaling within each compartment.

Dopaminergic Neurons Dynamically Modulate Kenyon Cell Synapses

We next asked whether acute alterations to the state or circumstance of an animal are sufficient to modify the pattern of presynaptic Ca^{2+} along KCs. Given that sucrose ingestion elicits the reciprocal pattern of DAN activity (high γ4/γ5 and low γ2/γ3, Figure 3.3B) as that associated with flailing behavior (Figure 3.3D-E), we reasoned that this appetitive reward might alter the distribution of presynaptic Ca^{2+} across lobe compartments. While it has been suggested that neuropeptide-mediated hunger signals suppress the synaptic output of specific DANs[302], overnight fasting of flies did not change the profile of presynaptic Ca^{2+} along γ KCs (Figure 4.5B). However, following sucrose ingestion, the odor-evoked syt-GCaMP signal in the γ4 and γ5 compartments relatively increased, while the response in the γ2 compartment relatively

decreased (Figure 4.7A). Sucrose ingestion therefore differentially modulates the olfactory responses of KC synapses across the γ lobe compartments, paralleling the bidirectional pattern of DAN activity evoked by this appetitive reward.

To confirm that the sugar-induced modification of KC synaptic responses is mediated by DANs, and not through other signaling downstream of sugar ingestion, we used the R58E02 promoter to drive expression of the P2X2 channel in a subset of DANs, including those innervating the γ4 and γ5 compartments excited by sugar-feeding. Stimulation of R58E02+ DANs shifted the profile of subsequent odor-evoked Ca^{2+} along γ KC axons, relatively increasing the signal in the distal lobe compartments while decreasing it in the proximal compartments, closely resembling the changes induced by sucrose ingestion (Figure 4.7B). ATP application in control animals, lacking P2X2 expression, had no effect on the distribution of presynaptic Ca^{2+} (Figure 4.7C) confirming the specificity of this manipulation. Thus, both exogenous and physiological activation of DAN reinforcement pathways can modulate the state of KC synapses with precise spatial localization. In both cases, transient DAN activation resulted in changes in odor-evoked presynaptic Ca^{2+} that persisted for the duration of an experiment (up to ~1 hour, Figure 4.7D). Intense salient experiences, like tethering or sugar ingestion, therefore appear sufficient to modulate the state of KC synapses with enduring consequences for how subsequent olfactory signals are processed.

Figure 4.7, Dopaminergic Neurons Shape the Distribution of Presynaptic Ca^{2+} Along KC Axons. A, Representative odor-evoked KC syt-GCaMP response before and after sucrose ingestion (bottom left). Normalized intensity profiles pre- and post-sugar ingestion and the change due to sugar feeding (post-pre) for the representative images are shown (top right). Average change in normalized intensity profile induced by sugar ingestion (bottom right, n = 11 flies). **B,** Schematic of γ lobe P2X2 expression under the 58E02 promoter (top left) and representative odor-evoked responses in γ KCs expressing syt-GCaMP, pre- and post-activation of 58E02+ DANs with ATP (bottom left). Normalized intensity profiles and change due to DAN activation for the representative images (top right). Average change in normalized intensity profile induced by DAN activation (bottom right, n = 10 flies). **C,** As in **B**, but in control flies lacking P2X2 expression (n = 6 flies). **D,** Representative time course for experiment shown in **B** shows that transient DAN-activation using P2X2 (indicated by dashed line) induces a persistent shift in the pattern of odor-evoked presynaptic Ca^{2+} along KC axons. The ratio of the peak odor-evoked syt-GCaMP signal for KC axon segments in the γ4 and γ2 compartments is plotted over the course of an experiment. All KC heatmaps in this figure represent peak fluorescence to odor stimulation. Error bars in all panels are SEM. Significant differences in relative compartment intensity compared to wild-type are indicated as follows: *$p < 0.05$, **$p < 0.005$, and ***$p < 0.0005$.

Figure 4.7

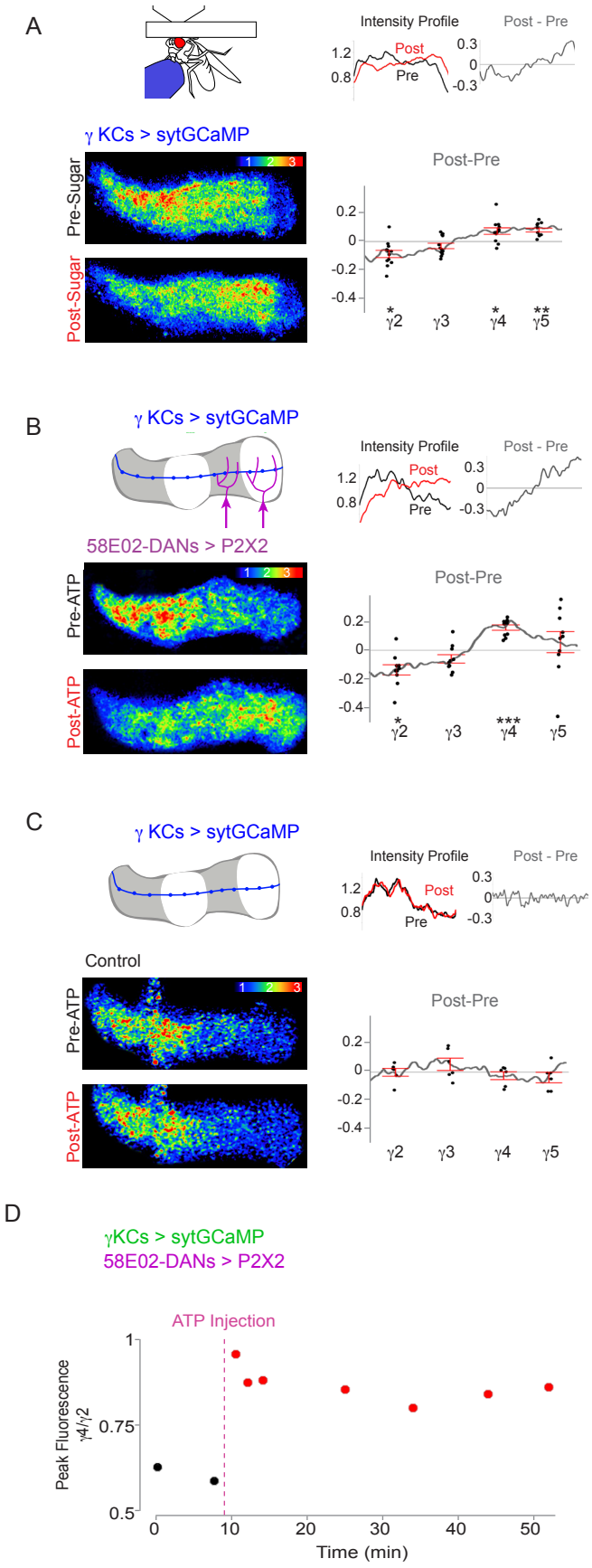
A
Intensity Profile
Post - Pre
Post
Pre
γ KCs > sytGCaMP
Pre-Sugar
Post-Sugar
Post-Pre
γ2
γ3
γ4
γ5
B
γ KCs > sytGCaMP
58E02-DANs > P2X2
Pre-ATP
Post-ATP
C
γ KCs > sytGCaMP
Control
D
γKCs > sytGCaMP
58E02-DANs > P2X2
ATP Injection
Peak Fluorescence γ4/γ2
Time (min)

Dopaminergic Signaling Modulates Synaptic Responses Along KC Axons

As DANs can co-release additional neurotransmitters along with dopamine[303–305], we sought to verify that dopaminergic signaling directly contributes to the compartmentalized synaptic modulation we observe. At least two of the four *Drosophila* dopamine receptors, DopR1 and DopR2, are highly expressed within the lobes and are known to be essential for the formation and maintenance of learned olfactory associations[206,222,306]. However, how deficits in dopamine reception alter odor processing in the mushroom body has never been functionally investigated. We therefore examined olfactory responses in mutants for these receptors and observed that the profile of odor-evoked syt-GCaMP fluorescence along γ KCs is strikingly inverted in DopR2 mutants (Figure 4.8A). Selective knock down of DopR2 in γ KCs using RNAi significantly altered the pattern of odor-evoked synaptic Ca^{2+} along their axons (Figure 4.8B-C), confirming that dopamine signaling acts presynaptically in KCs to shape odor processing along the lobe.

DopR1 mutants exhibited a subtler phenotype, displaying a somewhat more uniform distribution of Ca^{2+} across compartments relative to wild-type controls (Figure 4.8D). Subsequent investigations in the lab have revealed that the DopR1 mutant, originally thought to be a null-mutation[307], used for these experiments is actually a hypomorph. Therefore, we cannot rule out the possibility that a null mutant would lead to

Figure 4.8, Dopaminergic Signaling Pathways Modulate Presynaptic Ca^{2+} in KCs. A, Representative odor-evoked response of γ KCs expressing syt-GCaMP in *DopR2* mutant and wild-type flies (top). Fluorescence in other lobes is masked for clarity. Average normalized odor-evoked profile across the γ lobe and compartmental averages (bottom) in flies mutant for *DopR2* (red, n = 8) and wildtype (black, n = 8) are shown. **B,** As in **A,** but comparing γ KC-specific knock- down of *DopR2* using RNAi (red, n = 14) to wildtype flies (black, n = 5). **C,** Whole brain mRNA transcript levels quantified by RT-PCR for the indicated dopamine receptors in animals expressing DopR2-RNAi pan-neuronally using the synaptobrevin promoter (left) relative to transcript levels in Gal4 driver only control (right). **D,** Representative odor-evoked syt-GCaMP fluorescence in WT and *DopR1* mutant flies (top). Intensity profiles (bottom) for WT (black, n = 8 mushroom bodies) and *DopR1* (red, n = 7 mushroom bodies) flies show that *DopR1* profiles are somewhat more uniform, with a slight but significant difference in Ca^{2+} distribution apparent in γ5. **E,** As in **D,** but for DopR1, DopR2 double mutant, n = 8 mushroom bodies. **F,** As in **D** but for the dopamine reuptake transporter (DAT) mutant, n = 5. All KC heatmaps in this figure represent peak fluorescence to odor stimulation. Error bars in all panels are SEM. Significant differences in relative compartment intensity compared to wild-type are indicated as follows: $*p < 0.05$, $**p < 0.005$, and $***p < 0.0005$.

Figure 4.8

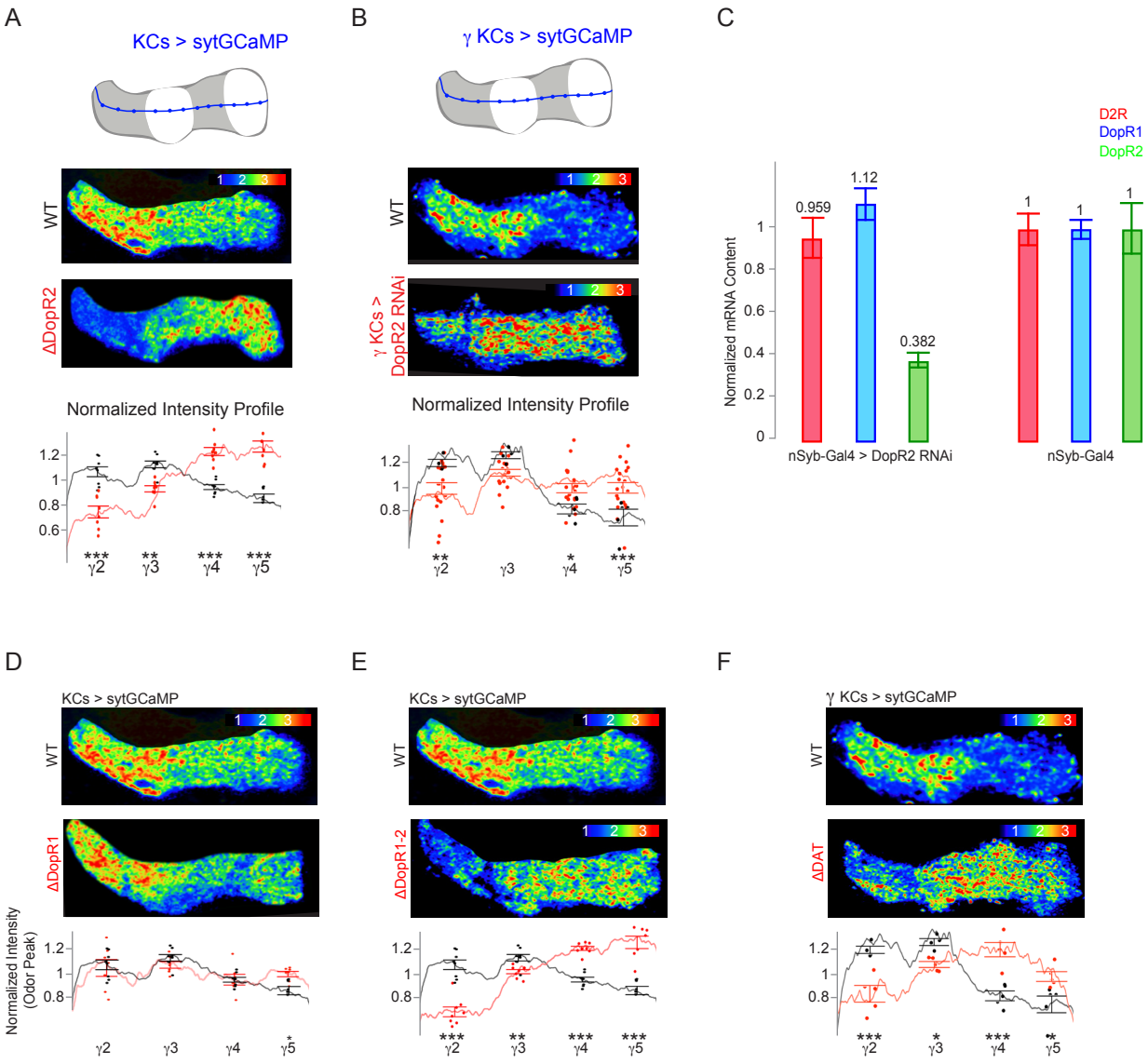
A
KCs > sytGCaMP
WT
ΔDopR2
Normalized Intensity Profile
B
γ KCs > sytGCaMP
WT
γ KCs > DopR2 RNAi
Normalized Intensity Profile
C
D2R
DopR1
DopR2
Normalized mRNA Content
0.959
1.12
0.382
1
1
1
nSyb-Gal4 > DopR2 RNAi
nSyb-Gal4
D
KCs > sytGCaMP
WT
ΔDopR1
Normalized Intensity (Odor Peak)
E
KCs > sytGCaMP
WT
ΔDopR1-2
F
γ KCs > sytGCaMP
WT
ΔDAT

a more significant phenotype. Interestingly, the distribution of synaptic Ca^{2+} in DopR1/DopR2 double mutants was still asymmetric (Figure 4.8E), suggesting the possibility that additional dopamine receptors or other neuromodulatory or peptidergic pathways that innervate the mushroom body[114,115,308] may contribute to the patterning of presynaptic Ca^{2+} in KCs. We also examined synaptic responses in mutants for the dopamine reuptake transporter (DAT) which mediates the clearance of dopamine from the synaptic cleft[309–311] and impairs dopamine signaling independent of any specific receptor. We found the profile of odor-evoked presynaptic Ca^{2+} in DAT mutants was significantly altered, resembling the phenotype of the DopR1/DopR2 mutant (Figure 4.8F). These manipulations of dopamine detection and handling confirm that dopaminergic signaling contributes to the precise spatial topography of presynaptic Ca^{2+} along KC axons, providing a functional link between molecular and neural mechanisms.

The capacity of the DAN network to differentially modify the synapses along a KC axon greatly expands the computational power of each KC. While many modulatory mechanisms work at the level of cell-wide properties, the fact that dopamine independently adjusts each KC synapse suggests that it is the synapse, rather than the neuron as a whole that should be considered the computational unit of the MB. This focus on synaptic properties mirrors many approaches in neural network modeling, in which learning signals are used to modify synaptic weights rather than cell-wide properties of individual units[312]. While the pattern of synaptic connectivity is certainly an important aspect of circuit function, it has become clear that modifications to synaptic

properties are just as important. Because each DAN subset targets a discrete compartment, which is co-innervated by a unique and genetically identifiable set of output neuron dendrites, we were able to ask how modulation by subsets of DANs changes KC-MBON signaling in the targeted compartment. This investigation forms the basis of the next chapter.

Chapter 5

Dopaminergic Modulation of Kenyon Cell-MBON Neurotransmission

Our experiments indicate that dopaminergic modulation can acutely modify presynaptic Ca^{2+} in discrete subcellular domains along individual KC axons. If this presynaptic modulation results in altered neurotransmission to the MBONs, our data would suggest that the state of the DAN network can dynamically regulate how olfactory information is conveyed to the different output pathways of the mushroom body. Individual MBONs can drive different types of behavior such as approach or avoidance, and it has been suggested that tuning the strength of KC-MBON synapses could shift the balance of activity in the MBON population in order to bias the fly's behavior[117,118,212,216]. However, it has not yet been directly shown that dopaminergic signaling modifies these synaptic connections. We therefore asked whether the presynaptic KC modulation described above might be translated into differential signaling from a KC to each of its postsynaptic MBONs.

MBON Odor Responses Mirror Compartmentalized Kenyon Cell Ca^{2+}

Heterogeneous neurotransmission from the synapses along a single axon has been described in the cortex and hippocampus as a possible substrate for independent plasticity between a neuron and its many postsynaptic targets[297,298,313]. However, rarely has it been possible to trace the propagation of neural signals from nearby synapses on the same axons to distinct postsynaptic neurons. We took advantage of the compartmentalized architecture of the MB to examine whether localized synaptic modulation along the same KC axons results in differential functional responses across the MBONs that tile the lobe. We expressed soluble GCaMP6s in pairs of γ MBONs (γ2/γ4 or γ3/γ5, Figures 2.3C, 5.1A), and simultaneously measured dendritic Ca^{2+} responses to the same odor stimuli in their segregated projections. Within the same fly, a given odor presentation consistently evoked more robust responses in the γ2 and γ3 MBONs in comparison to γ4 and γ5 MBONs (Figure 5.1B), paralleling the differences in presynaptic Ca^{2+} exhibited by KC axons in response to odor (Figure 4.3C). In contrast, direct stimulation of KCs in a brain explant elicited essentially equivalent responses across MBONs (Figure 5.1C), again mirroring what we observed in KC Ca^{2+} in the explant (Figure 4.3D). Thus, in the absence of *in vivo* modulation, KCs have the inherent capacity to transmit equivalent signals to the different output pathways of the lobe. These results suggest the possibility that the olfactory responses of MBONs innervating each compartment may be differentially tuned by the activity of their cognate DANs.

Figure 5.1, MBON Odor Responses Mirror Compartmentalized Kenyon Cell Ca^{2+}. **A,** Schematic shows pairs of MBONs expressing soluble GCaMP6s used for functional imaging in **B** and **C**. **B and C,** Representative heatmaps of evoked fluorescence (top left in each panel, ΔF/F0), time courses (bottom left), and scatterplots (right) of responses to odor stimuli (blue line) in pairs of MBONs *in vivo* (**B**, n = 8 for γ2 versus γ4, n = 11 for γ3 versus γ5) and evoked by calycal stimulation in a brain explant (**C**, n = 8 for each pair). Values marked with different lowercase letters represent significant differences ($p < 0.05$ by t test with correction for multiple comparisons).

Figure 5.1

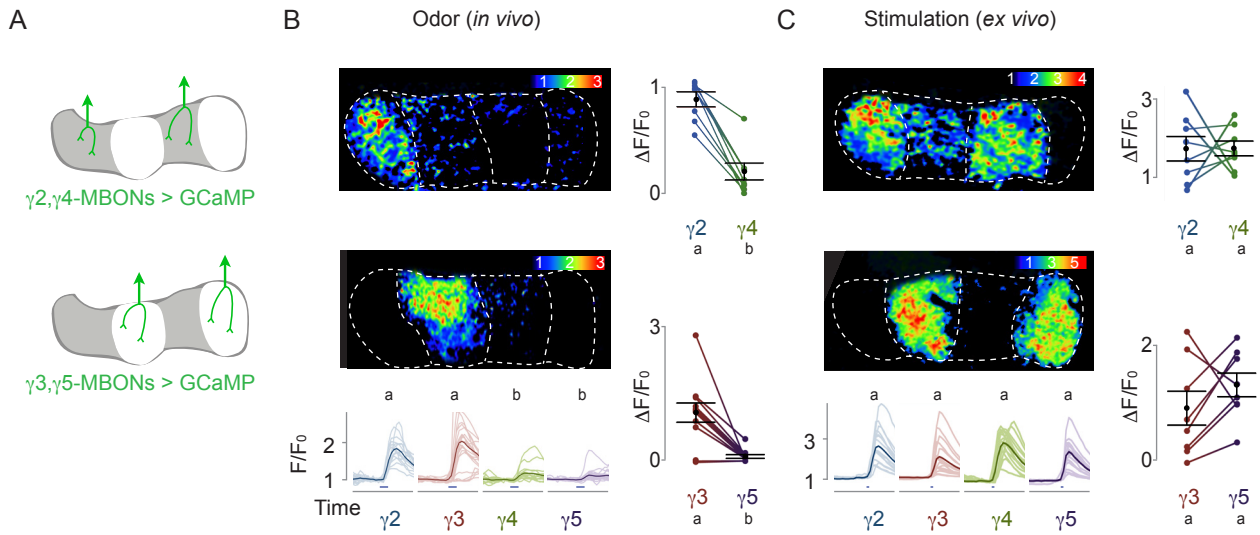
A
γ2,γ4-MBONs > GCaMP
γ3,γ5-MBONs > GCaMP
B
Odor (in vivo)
C
Stimulation (ex vivo)
ΔF/F0
F/F0
Time
a
a
b
b
γ2
γ3
γ4
γ5

Dopamine Potentiates KC-MBON Synapses

The correlation between the pattern of presynaptic Ca^{2+} in the KCs and the response magnitudes of the MBONs in each compartment suggest that the same DAN activity that was sufficient to modulate KC Ca^{2+} distribution might also alter the strength of KC-MBON synaptic transmission. We therefore used whole-cell electrophysiology recordings to examine whether DAN activity modulates KC-MBON neurotransmission at the resolution of individual synaptic events. We performed voltage-clamp recordings of the γ4 MBON, as it innervates the compartment in which we observed the most robust dopamine-dependent modulation of KC presynaptic Ca^{2+} (Figure 4.7B). Recordings were carried out in a brain explant, where reduced basal activity allows for the measurement of well-isolated synaptic currents and provides precise control over the neuromodulatory state of synapses. We stimulated KC dendrites in the calyx to evoke excitatory postsynaptic currents (EPSCs) in the γ4 MBON and observed that the strength of these synaptic inputs drastically increased following acute activation of the R58E02+ DANs expressing the P2X2 channel (Figure 5.2A). The amplitude of spontaneous synaptic events was also potentiated whether DANs were activated by stimulation of P2X2 or a red-shifted channelrhodopsin variant (Figure 5.2B). The average latency of EPSCs after KC stimulation was 3.8±0.1 ms, consistent with monosynaptic transmission[154,314], thereby identifying the KC-MBON synapses as the site of dopaminergic modulation. Focal application of the inhibitory neurotransmitter GABA onto KC dendrites in the calyx resulted in the loss of synaptic events, further

Figure 5.2, Dopamine Potentiates KC-MBON Synaptic Transmission. A, Schematic of experimental setup. Synaptic currents were measured in the γ4 MBON (green) by voltage-clamp recordings in response to direct KC stimulation by acetylcholine iontophoresis in the calyx (Stim). P2X2-expressing R58E02+ DANs (magenta) were activated by local ATP injection (left). Representative γ4 MBON recordings (center) show overlay of ten KC stimulations pre- (grayscale) and post- (redscale) activation of R58E02+ DANs by ATP injection. Note the potentiation evident in both spontaneous and evoked EPSCs. Vertical line denotes 2-ms KC stimulation. Amplitude of evoked currents in the γ4 MBON pre- and post-ATP injection (right, average of ten stimulations each in n = 5 recordings). **B,** Mean γ4 MBON spontaneous EPSC profiles (left) and histogram of EPSC amplitudes (right) with (red) and without (black) ReaChR expressed in R58E02+ DANs (n = 5 flies ReaChR, n = 6 flies control, $p < 0.0005$). **C,** GABA injection into the KC dendrites in the MB calyx suppresses spontaneous EPSCs measured in the γ4 MBON. **D,** Representative KC spike trains evoked by 2 pA current steps in KC current clamp recordings before and after activation of R58E02+ DANs through P2X2 (left). Mean (+/- SEM) number of spikes evoked by current injection in KC current clamp recordings show no apparent change in KC properties following DAN activation (right, n = 6 flies, $p > 0.6$).

Figure 5.2

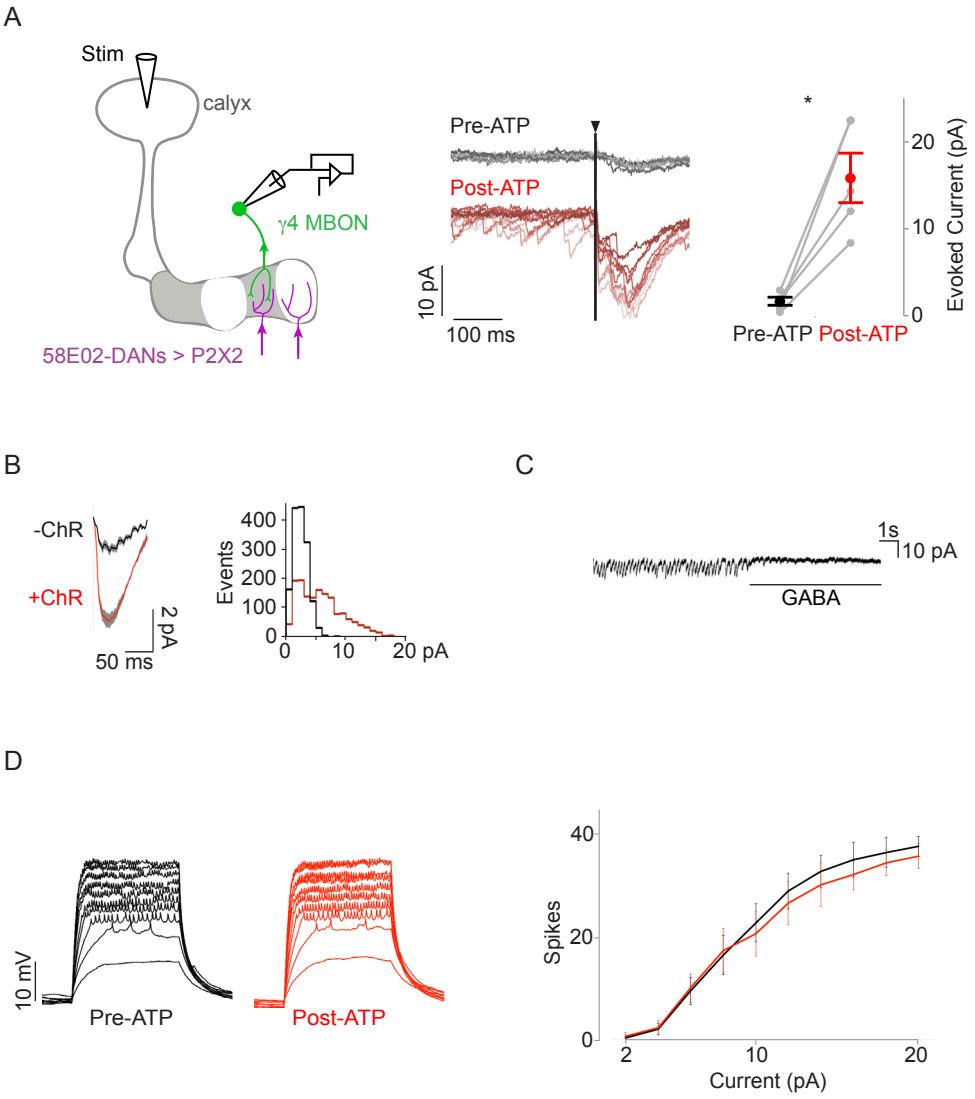
A
Stim
calyx
γ4 MBON
58E02-DANs > P2X2
Pre-ATP
Post-ATP
10 pA
100 ms
*
20
10
0
Evoked Current (pA)
Pre-ATP Post-ATP
B
-ChR
+ChR
2 pA
50 ms
400
300
200
100
0
Events
0
10
20 pA
C
1s
10 pA
GABA
D
10 mV
Pre-ATP
Post-ATP
40
20
0
Spikes
2
10
20
Current (pA)

substantiating KCs as the source of this potentiated synaptic input (Figure 5.2C). In contrast to the prominent modulation of synaptic currents, activation of R58E02+ DANs had no apparent effect on the baseline membrane voltage or evoked spiking of γ KCs, as measured through whole-cell recordings (Figure 5.2D). Dopaminergic modulation therefore locally potentiates neurotransmission at KC-MBON synapses without appearing to change the overall excitability of KCs, providing a mechanism to alter the propagation of olfactory signals to each MBON without modifying the underlying KC odor representation.

Compartmental Specificity of Dopaminergic Modulation

While the anatomic compartmentalization of DAN innervation points to localized modulation, dopamine has been shown to adjust circuit properties at a distance from its site of release[311]. To probe the spatial specificity of KC-MBON synaptic modulation, we asked whether the dopaminergic modulation of KC-MBON synapses is spatially restricted to the compartments innervated by activated DANs. Functional imaging revealed that the dendritic Ca^{2+} response of the γ4 MBON to direct KC stimulation was enhanced after activation of R58E02+ DANs (Figure 5.3A-B), consistent with the potentiation we measured by electrophysiology. Likewise, activation of the γ2 DAN strengthened the γ2 MBON response to KC stimulation (Figure 5.3C-D), verifying that dopaminergic potentiation of KC-MBON synaptic signaling is a common modulatory

Figure 5.3, DAN Potentiation of KC-MBON Signaling is Compartment-Specific. Schematic (top), time courses (bottom left), and quantification of responses to KC stimulation (bottom right) before and after ATP injection were recorded in **A,** the γ4 MBON with activation of the γ4-γ5 (R58E02+) DANs (n = 6), **B,** the γ4 MBON with no P2X2 expression (control), **C,** the γ2 MBON with activation of the γ2 DAN (n = 6), **D,** the γ2 MBON with no P2X2 expression (control), **E,** the γ2 MBON with activation of the γ4-γ5 DANs (n = 6), and **F,** the γ4 MBON with activation of the γ2 DAN (n = 6). All pairwise comparisons plot mean ± SEM. Significance of change after activation is indicated as follows: *$p < 0.05$ and **$p < 0.005$.

Figure 5.3

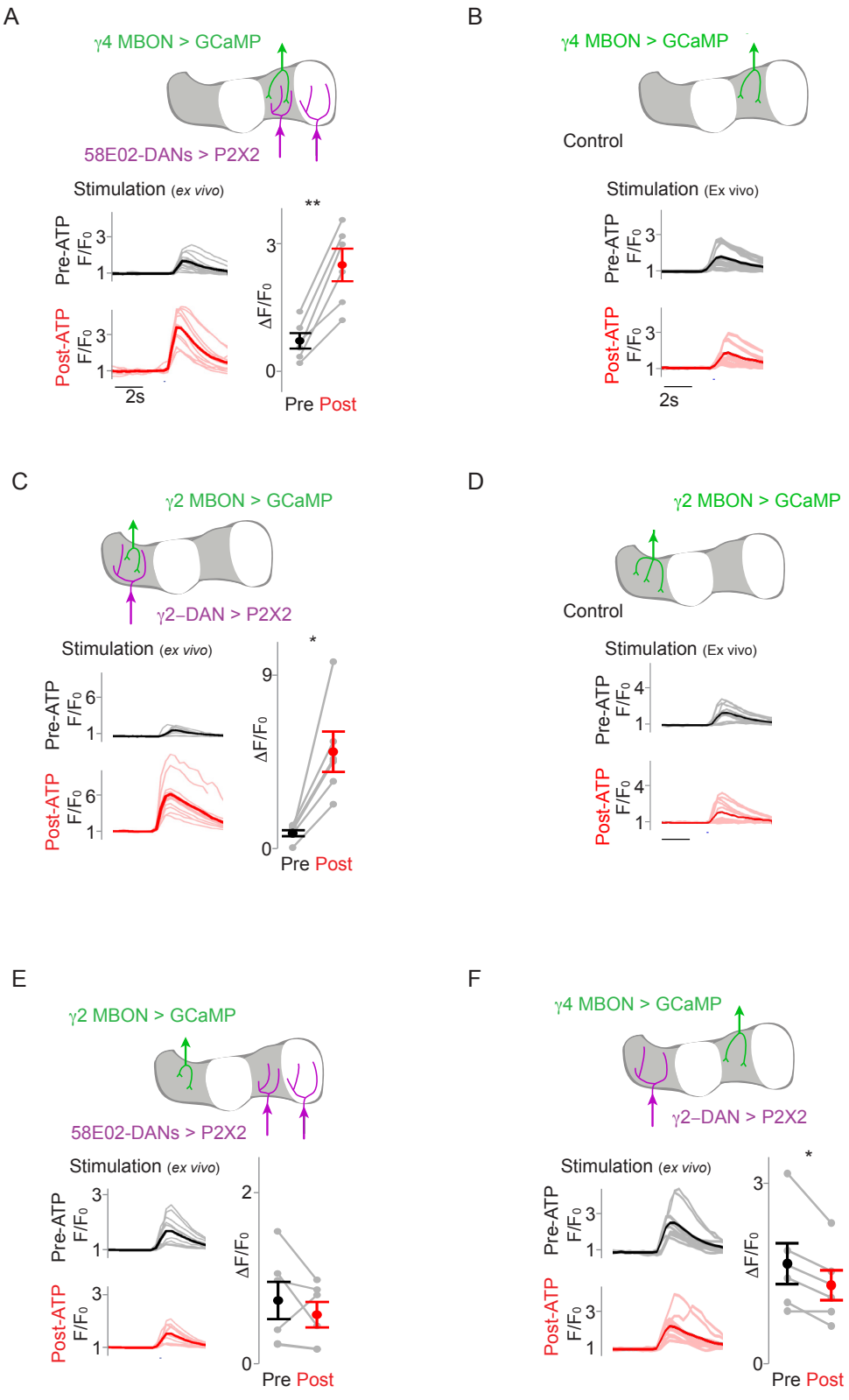
A
γ4 MBON > GCaMP
58E02-DANs > P2X2
Stimulation (ex vivo)
Pre-ATP F/F0
Post-ATP F/F0
2s
**
ΔF/F0
Pre Post
B
γ4 MBON > GCaMP
Control
Stimulation (Ex vivo)
Pre-ATP F/F0
Post-ATP F/F0
2s
C
γ2 MBON > GCaMP
γ2–DAN > P2X2
Stimulation (ex vivo)
Pre-ATP F/F0
Post-ATP F/F0
*
ΔF/F0
Pre Post
D
γ2 MBON > GCaMP
Control
Stimulation (Ex vivo)
Pre-ATP F/F0
Post-ATP F/F0
E
γ2 MBON > GCaMP
58E02-DANs > P2X2
Stimulation (ex vivo)
Pre-ATP F/F0
Post-ATP F/F0
ΔF/F0
Pre Post
F
γ4 MBON > GCaMP
γ2–DAN > P2X2
Stimulation (ex vivo)
Pre-ATP F/F0
Post-ATP F/F0
*
ΔF/F0
Pre Post

mechanism across different γ lobe compartments. In contrast, activation of the R58E02+ DANs, had no effect on the γ2 MBON response to KC stimulation (Figure 5.3E), while activation of the γ2 DAN actually resulted in a small, but significant, depression of activity in the γ4 MBON (Figure 5.3F). These experiments indicate that the segregated innervation of DAN axons in the lobe permits spatially restricted potentiation of KC-MBON neurotransmission, localized to the synapses within a compartment.

State-Dependent Changes to the Pattern of MBON Activity

Having demonstrated that DAN activity can potentiate KC-MBON signaling in a brain explant, we asked whether activation of DANs, either by exogenous activation or through reward signaling, was sufficient to change MBON odor responses *in vivo*. We therefore compared odor-evoked activity of the γ4 MBON, prior to and after stimulation of the γ4 DANs expressing P2X2 under the R58E02 promoter. After DAN stimulation the responses of the γ4 MBON to all odors tested were significantly potentiated (Figure 5.4A) while γ2 MBON responses remained unaffected (Figure 5.4B). Together, these observations indicate that localized dopaminergic modulation can independently regulate neurotransmission between the same KC ensemble and each of its MBON partners, permitting an odor stimulus to drive distinct patterns of output activity in different contexts. We next compared the odor-evoked responses of the γ4 and γ2

Figure 5.4, State-Dependent Modulation of MBON Odor Responses. A, Schematic (left) and quantification of γ4 MBON odor responses before and after stimulation of the γ4-γ5 (R58E02+) DANs (n = 6, right). **B,** As in **A**, but γ2 MBON response with activation of the γ4-γ5 DANs was quantified (n = 6). **C,** Ratio between odor-evoked responses in the γ4 MBON and γ2 MBON before and after sugar feeding (n = 10). All pairwise comparisons in this figure represent the mean (±SEM) with significant changes indicated as follows: *$p < 0.05$, **$p < 0.005$, and ***$p < 0.0005$.

Figure 5.4

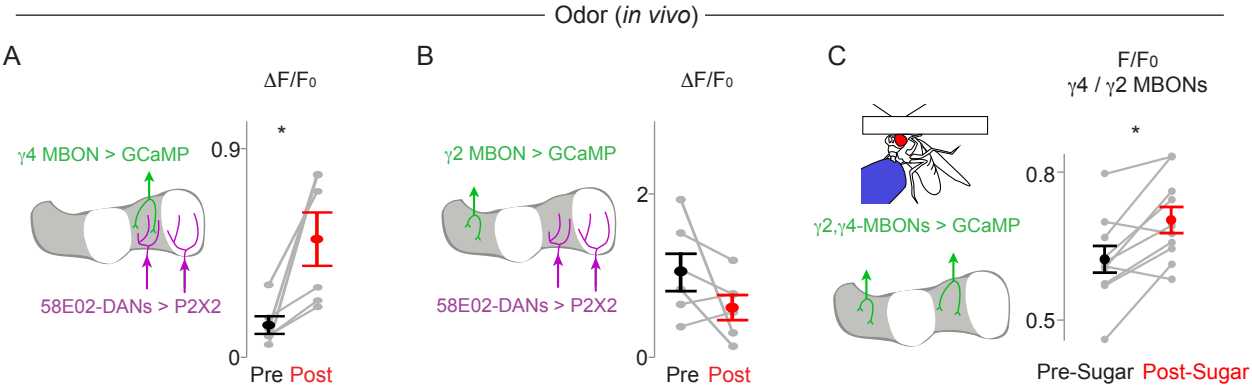
Odor (in vivo)
A
ΔF/F0
γ4 MBON > GCaMP
58E02-DANs > P2X2
0.9
0
*
Pre Post
B
ΔF/F0
γ2 MBON > GCaMP
58E02-DANs > P2X2
2
0
Pre Post
C
F/F0
γ4 / γ2 MBONs
γ2,γ4-MBONs > GCaMP
0.8
0.5
*
Pre-Sugar Post-Sugar

MBONs prior to and after sugar feeding, an appetitive stimulus that activates the γ4/γ5 DANs and inhibits the γ2/γ3 DANs (Figure 3.3B). Sucrose ingestion resulted in an enhancement of the γ4 MBON odor response relative to the γ2 MBON response (Figure 5.4C), mirroring the spatially precise alteration of presynaptic Ca^{2+} along KC axons following a sugar reward (Figure 4.7A). Acute changes to the state of an animal can thus rapidly gate the transmission of olfactory signals through the MBONs of a lobe, producing a different pattern of output activity to the same odor stimulus.

DAN Activity Bidirectionally Modulates KC-MBON Signaling

Dopamine can modulate synaptic communication in diverse ways—including potentiation or depression of neurotransmission and modifications to both short- and long-term plasticity[20,41]. Our data indicate that activation of DANs through salient experiences or exogenous stimulation is sufficient to modify the basal state of the KC synapses within a compartment, with enduring consequences for how all subsequent olfactory signals are processed. This finding can potentially explain why salient experiences that do not involve associative training can still lead to changes in subsequent animal behavior[315–317]. In contrast, during associative learning the contingent pairing of olfactory and reinforcement pathways is thought to selectively alter neurotransmission from odor-selective KC ensembles to allow formation of specific olfactory memories[133]. We therefore asked whether coincident activation of KCs and

DANs might elicit a distinct form of synaptic modulation in comparison to the potentiation we observe when DANs are activated independently of KC stimulation due to the changing context of an animal. We found that temporally pairing R58E02+ DAN activation with KC stimulation significantly depressed KC-evoked responses in the γ4 MBON, in contrast to the robust potentiation induced by activation of DANs without simultaneous KC activity (Figure 5.5A-D). Alternating temporally paired and unpaired stimulation protocols resulted in depression and potentiation within the same preparation, indicating that KC-MBON synapses are capable of rapid bidirectional plasticity (5.5B-C). Conversely, repetition of the paired protocol generally resulted in further depression or no additional change, while repetition of unpaired DAN activation maintained or increased responses (Figure 5.5E-G). Furthermore, the potentiated state induced by unpaired DAN activation was maintained through several rounds of KC stimulation (Figure 5.5H). Thus, the rapid depression and potentiation induced by alternating protocols (Figure 5.5B-C) is not simply the effect of rebounding from an extreme state. Depression of KC-MBON signaling was restricted to the compartment innervated by the activated DANs, suggesting similar spatial specificity for these opposing forms of modulation (Figure 5.5I).

If plasticity of KC-MBON signaling were limited to the KCs that were concurrently activated during an olfactory experience, our observations would provide a mechanistic basis for the odor-specific modulation thought to underlie learned olfactory associations within the mushroom body. We therefore monitored responses of the γ4 MBON to two

Figure 5.5, DAN Activity Bidirectionally Modulates KC-MBON Signaling. A, Schematic (left) and experimental design (right) for **B-I**. The γ4 MBON responses to direct KC stimulation were recorded before and after R58E02+ DAN activation that was either temporally paired or unpaired with KC stimulation. Dashed lines here and below represent >45s delays. **B,** Representative time course of γ4 MBON GCaMP fluorescence in response to direct KC stimulation in which R58E02+ DANs expressing P2X2 were alternately activated in the absence of KC stimulation (unpaired), or synchronously with KC stimulation (paired). Paired KC-DAN activation resulted in depression of MBON responses that had been previously potentiated (gray lines in **D** and **G**). Time courses (top) and heatmaps (bottom) of the γ4 MBON response with stimulation protocol indicated between recordings. Blue lines indicate KC stimulation. **C,** Same as in **B**, but demonstrating unpaired protocol after paired protocol. **D,** Changes in γ4 MBON responses to KC stimulation following activation of 58E02+ DANs that was either paired (left, n = 6, starting from a potentiated state) or unpaired (right, n = 12, starting from a depressed state) with KC stimulation (as in **B-C**). **E-G**, As in **B-D** but for a protocol in which the same protocol (either paired or unpaired) was repeated twice rather than alternating between protocols. Magenta lines in **G** are for repeated protocols (as in **E-F**, gray lines are same data from **D**, showing alternating protocols. **H,** As in **B-G**, but for a series of KC stimulations in which there was only a single, unpaired activation of R58E02+ DANs, showing that γ4 MBON responses are stable over successive recordings after potentiation by dopamine. **I,** Stimulation of R58E02+ DANs had no effect on γ2 MBON responses to KC stimulation whether KC-DAN activation was synchronous (paired) or DANs were activated independently of KC stimulation (unpaired). All pairwise comparisons in this figure represent the mean (±SEM) with significant changes indicated as follows: *$p < 0.05$, **$p < 0.005$, and ***$p < 0.0005$.

Figure 5.5

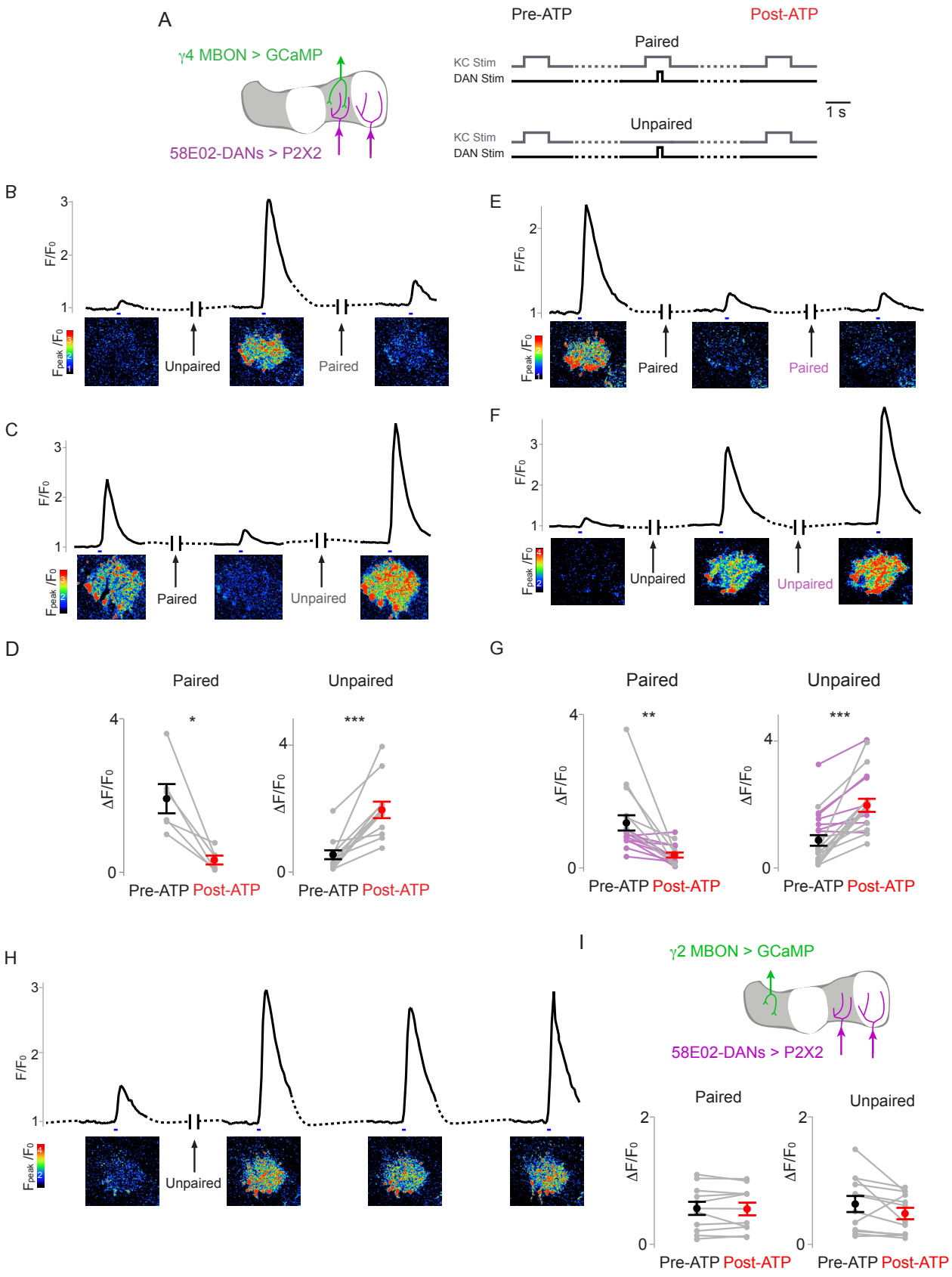
A
γ4 MBON > GCaMP
58E02-DANs > P2X2
Pre-ATP
Post-ATP
Paired
KC Stim
DAN Stim
1 s
Unpaired
KC Stim
DAN Stim
B
F/F0
Fpeak /F0
Unpaired
Paired
E
F/F0
Fpeak /F0
Paired
Paired
C
F/F0
Fpeak /F0
Paired
Unpaired
F
F/F0
Fpeak /F0
Unpaired
Unpaired
D
Paired
Unpaired
ΔF/F0
*
***
Pre-ATP Post-ATP
Pre-ATP Post-ATP
G
Paired
Unpaired
ΔF/F0
**
***
Pre-ATP Post-ATP
Pre-ATP Post-ATP
H
F/F0
Fpeak /F0
Unpaired
I
γ2 MBON > GCaMP
58E02-DANs > P2X2
Paired
Unpaired
ΔF/F0
Pre-ATP Post-ATP
Pre-ATP Post-ATP

alternately presented odors and then paired one odor with stimulation of R58E02+ DANs expressing P2X2. Following DAN activation, the response of the paired odor relative to the unpaired odor was significantly reduced (Figure 5.6A-B). Similar odor-specific depression of KC-MBON synapses was also observed in other studies[119,226], confirming this result. Thus DAN activity can bidirectionally modulate KC-MBON signaling, allowing for both odor-independent synaptic potentiation, as well as odor-specific depression.

The role of the MBONs in regulating various aspects of fly behavior have been examined in several other labs[100,117,119,216,226]. These behavioral studies allow us to consider our findings concerning plasticity of the KC-MBON synapses in light of their findings, which suggest that a fly's decision to approach or avoid an odor is a function of the net activity in the population of MBONs. Some MBONs bias the fly to approach an olfactory stimulus while others lead to avoidance[118]. As a consequence of learning, the balance of activity among the MBON population in response to a given odor is shifted, leading to a change in subsequent odor responses[216]. Integrating our findings with this body of literature reveals a plausible model for the circuit mechanism for dopaminergic signaling in the formation of olfactory associations. For example, activation of the γ4 MBON has been shown to drive avoidance behavior, while the γ4 DAN is activated by appetitive stimuli, such as sucrose ingestion (Figure 3.3B). Thus, when exposure to a specific odor is paired with a reward, the paired activation of odor-specific KCs and the sugar-responsive γ4 DAN leads to depression of the synapses between those KCs and

Figure 5.6, Mechanisms of DAN Modulation for Associative Learning. A, Change in γ4 MBON response to an odor that was paired with R58E02+ DAN activation using P2X2, relative to a second odor that was unpaired (n = 10). **B,** Representative example showing depressed response in the γ4 MBON to an odor that was paired with R58E02+ DAN activation using P2X2, while the unpaired odor response is unchanged. **C**, The potentiation of MBON olfactory responses by unpaired DAN activation is independent of odor identity. The responses of the γ4 MBON to hexanol and isobutyl acetate were equivalently enhanced after activation of R58E02+ DANs, such that the ratio of the responses remained unchanged (n = 6 flies, $p > 0.6$). This is in contrast to the odor-specific depression evident using these same odors, after pairing one odor with DAN stimulation as shown in **A**. **D,** Representative trace showing changes in γ4 MBON responses to KC stimulation in a brain explant following forward paired KC-DAN stimulation, unpaired DAN stimulation, and reverse paired KC-DAN stimulation (courtesy of Annie Handler). **E,** Model for how dopamine-mediated synaptic depression underlies associative learning in the MB. In the naïve fly (left), the KC response to an innately neutral odor leads to activation of both attraction-inducing and avoidance-inducing MBONs. The balance of activity in the MBONs leads to a net neutral response. During appetitive learning (center) the pairing of odor sensation and activity in the reward-responsive DANs (such as the γ4 DANs) leads to long-term depression of the synapses between the odor-responsive KCs and MBONs (such as the γ4 MBONs) that promote avoidance behavior. When the fly is subsequently exposed to the trained odor (right) the weakened response in the avoidance-promoting MBONs shifts the balance of activity in the MBON population, leading to net attraction. All pairwise comparisons in this figure represent the mean (±SEM) with significant changes indicated as follows: *$p < 0.05$, **$p < 0.005$, and ***$p < 0.0005$.

Figure 5.6

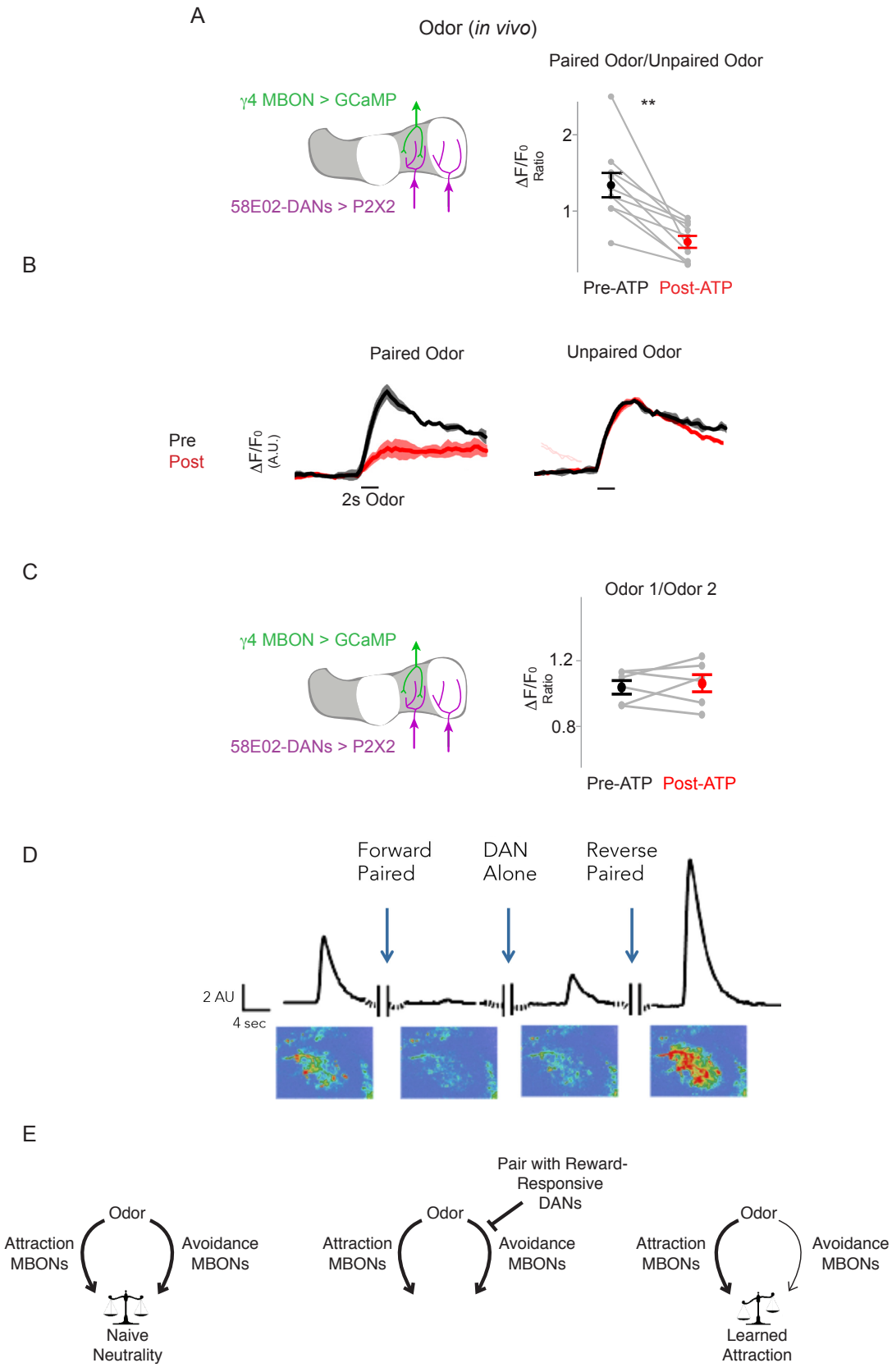
A
Odor (in vivo)
Paired Odor/Unpaired Odor
γ4 MBON > GCaMP
58E02-DANs > P2X2
**
ΔF/F0 Ratio
2
1
Pre-ATP
Post-ATP
B
Paired Odor
Unpaired Odor
Pre
Post
ΔF/F0 (A.U.)
2s Odor
C
Odor 1/Odor 2
γ4 MBON > GCaMP
58E02-DANs > P2X2
ΔF/F0 Ratio
1.2
0.8
Pre-ATP
Post-ATP
D
Forward Paired
DAN Alone
Reverse Paired
2 AU
4 sec
E
Odor
Attraction MBONs
Avoidance MBONs
Naive Neutrality
Pair with Reward-Responsive DANs
Odor
Attraction MBONs
Avoidance MBONs
Odor
Attraction MBONs
Avoidance MBONs
Learned Attraction

the γ4 MBON (Figure 5.6A-B). When the fly is then re-exposed to that odor, the γ4 MBON response has been weakened, thus reducing its avoidance-inducing effect, and shifting the fly's behavior towards approach of the now-appetitive odor (Figure 5.6E).

Temporal Control of DAN-induced Synaptic Plasticity

While the extensive MB literature provides a satisfying framework for understanding dopaminergic modulation in the context of associative conditioning, the role of the odor-independent potentiation that we observe from unpaired DAN activation is less clear. One line of research has suggested that locomotor-induced DAN activity in the absence of odor presentation is responsible for the active erasure of memories, a process that is abrogated by the lack of such activity when the fly is quiescent, such as during sleep, when the MB circuit is effectively consolidating memories[223,274,306]. These findings suggest the possibility that in addition to forming memories, the DANs are responsible for erasing associations that are no longer predictive or relevant[211,274].

Regardless of the specific behavioral role, our findings confirm that dopamine can induce different, sometimes opposing, forms of plasticity in a neural circuit[41,318–321] and that the mode of modulation is dependent upon the timing of the DAN signal relative to KC activity[322]. Therefore, together with Annie Handler, another student in the lab, we

asked whether varying the pairing protocol might also affect the form or strength of plasticity observed. Indeed, we found that reversing the order of KC-DAN pairing, where R58E02+ activation preceded KC stimulation, resulted in even stronger potentiation when compared with unpaired DAN activation of equivalent strength (Figure 5.6D). Such reversal of the pairing order between the conditioned (CS) and unconditioned stimulus (US) has also been shown to induce opposing effects on the valence of the learned behavioral response to the CS[322,323]. Thus, our results suggest that dopaminergic signaling in the MB can implement different types of plasticity in the KC-MBON synapses with exquisite temporal and spatial precision.

The diversity of plasticity mechanisms under control of DAN signaling in the MB raises a number of interesting questions about the mechanisms underlying such plasticity. cAMP signaling pathways have been shown to be an important component of learning in the MB as well as many other circuits that implement learning[227–229,324–326]. It has been proposed that the primary cellular means for detecting coincident CS and US activity in the KCs is through the Ca^{2+} sensitive adenylyl cyclase, *rutabaga*[327,328]. However, our finding that the direction of plasticity induced is extremely sensitive to the relative timing of these two signals suggests that the order of signals, and not simply their coincidence, is detected at the molecular level. A recent demonstration that the rules of plasticity differ across the compartments of the MB[211] indicates that further investigations will be needed to reveal how distinct modulatory mechanisms are mediated throughout the MB.

Together with behavioral and functional studies from several other labs[118,119,211,212,226], we believe that our findings regarding dopaminergic modulation of KC-MBON synapses contribute to a plausible model for the role of the MB in associative learning. These results, however, have also revealed additional complexity within the MB circuitry, suggesting that the DANs represent the fly's locomotor state in addition to reinforcement signals, and that dopamine can induce different types of plasticity depending on the timing and position of its release. While our findings indicate that the extreme behavioral states present in a tethered fly are sufficient to induce DAN-mediated modulation of MB signaling (Figures 4.3C, 5.1), it will be interesting to determine whether, and how, patterns of DAN activity during more naturalistic behaviors might modify the flow of sensory information through the MB. Furthermore, while the studies mentioned above have demonstrated the general effects of exogenous MBON activation and suggested how learning might adjust these responses to change the fly's behavior, we have a very limited understanding of the neural pathways downstream of the MBONs and the specific mechanisms by which they control the fly's actions. Our preliminary attempts to address these questions are described in the next chapter.

Chapter 6

Linking the MB to the Execution of Flexible Behaviors

The results described here, combined with decades of behavioral genetic and functional investigations of the MB, provide a starting circuit model for how a single sensory input can lead to different patterns of output circuit activity depending on the present context or past experiences of an individual animal. Olfactory sensory stimuli are represented by the activation of a sparse subset of KCs such that each odor has a unique representation at this input layer to the MB. When an odor is paired with a salient contextual cue, such as sugar or an electric shock, strong dopaminergic signals that follow the odor will lead to weakening of the synapses between the KCs activated by that odor and the MBONs in the same compartments as the activated DANs. In this way, the MB acts like a switchboard, where the routing of the same odor-specific KC input to different MBONs is controlled by the network of DANs. By changing the balance of activity in the different MBONs, the net output of this circuit can shift the fly's behavioral response towards approach or avoidance depending on which DANs were co-activated when the animal encountered the odor. Importantly, we find depression of KC-MBON synapses only occurs when the odor precedes the DAN activity and predicts

the reinforcement signal. Reversing the temporal order of DAN and KC activation indicates that the odor is not predictive of the US, and instead of depressing these synapses, will actually potentiate them, consistent with behavioral studies showing that conditioned odor preferences similarly depend on timing[322,323,329]. Finally, ongoing fluctuations in the DANs that represent the behavioral state of the fly might serve as a modulatory signal to affect immediate behavior, or to prime the circuit for learning–a question we will return to below. However, it remains unclear how the output pathways from the MB are actually linked to different motor programs or action sequences necessary for moving towards or away from an odor source. In the preliminary results described in this chapter, we describe a novel closed-loop olfactory system that is compatible with functional imaging of the MB circuitry, facilitating our ongoing investigations of the downstream targets of the MB.

Studying Olfactory Navigation in Individual Flies

Flies and other animals display a range of behavioral strategies for tracking towards appetitive odors[330,331]. One well-described chemotactic strategy, which is prevalent across many species, is anemotaxis, in which an animal will turn upwind upon encountering an appetitive olfactory cue[332–338]. Anemotactic strategies provide an appealing target of analysis for understanding the execution of olfactory-guided behaviors in the fly. For one, the decision to turn upwind could reflect a discrete binary

choice, potentially mediated by relatively simple circuit mechanisms, amenable to functional studies. Furthermore, we hypothesized that allowing flies to use mechanosensation of wind-direction as an additional source of information, as might happen in a natural setting, could help generate more robust chemotaxis assays. Many behavioral assays, such as the T-maze traditionally used in the *Drosophila* field to examine odor preferences[66], have relied on end-point measurement of the movement of a large population of tens of flies towards or away from an odor source. However, there are distinct advantages to using single animal tracking as a readout of odor preferences[220,336,339] if individual behavior is sufficiently robust. Incorporating wind-direction cues that allow for naturalistic anemotactic behaviors is therefore a promising approach for the design of single-animal assays of olfactory navigation.

In order to investigate how MB output circuitry impinges on pathways underlying olfactory navigation we sought to devise a behavioral setup that is compatible with 2-photon imaging, in which a tethered fly can perform odor-tracking behaviors. It has been increasingly appreciated that the interplay of motor execution and sensory feedback plays an integral role in the neural circuits responsible for sensorimotor processing[340,341]. Our goal was therefore to mimic the relevant wind-direction cues and sensory feedback that a fly would encounter while freely walking in an odor plume. We designed an apparatus in which a head-fixed fly can walk comfortably on a spherical treadmill. As the fly walks, the rotation of the ball is tracked in real-time and used to

adjust the angle of an air- and odor-delivery tube directed at the fly in closed loop with the fly's turns.

The first iteration of this closed loop system was a relatively simple design in which the air-delivery tube was attached to an arm that was driven around the fly by a servo motor (Figure 6.1A). The fly was either glued to a pin at the thorax for purely behavioral experiments or mounted in a custom imaging chamber based on Green et al.[342] for functional experiments, and placed on an air-supported foam ball[343]. We tracked the rotation of the ball using FicTrac software[344] and used the calculated heading changes of the fly to direct the motor, adjusting the angle of the air tube in real time. While this system has the benefit of simplicity of design, its main drawback is that the range of tube-motion is limited to approximately 180 degrees due to obstruction of complete revolution by necessary structural components (Figure 6.1A). While this limitation did not preclude the use of this system to investigate odor-tracking behavior (see below), it does present certain problems. In particular, rotations beyond the available angles necessitate rapid swinging of the arm from side to side and disruption of continuous airflow – leading to sensory stimuli that we found to be extremely salient to the fly as evidenced by the prominent responses elicited in relevant neural circuits. Such artifacts necessitated discarding significant portions of certain datasets. Furthermore, as our goal was to simulate a realistic virtual environment for the fly, the presence of these discontinuities might contribute to a loss of the closed loop illusion. We therefore designed a second iteration of our closed loop olfactory system in which

Figure 6.1, A Closed Loop System for Virtual Olfactory Navigation. A, 3D rendering of the first iteration of the closed loop olfactory environment. A head-fixed fly is positioned comfortably on an air-supported foam ball. A small tube carrying an air stream is positioned near the fly. The angle of the wind/odor stream is controlled by a servo motor whose activity is yoked to the real-time calculation of changes in the fly's heading on a virtual 2D plane. Movement of the tube angle is limited to approximately 180 degrees. **B,** 3D rendering of the second iteration of the closed loop system in which the air stream can fully rotate around the fly. Cutaway view shows inner mechanism by which a fixed air inlet is coupled to a rotating output stream. Central blue part remains fixed while outer gray piece is rotated by the gear belt. Air enters through the air inlet and is routed to an air channel at the interface between the two parts. Air-tightness is ensured by O-rings above and below the channel.

Figure 6.1

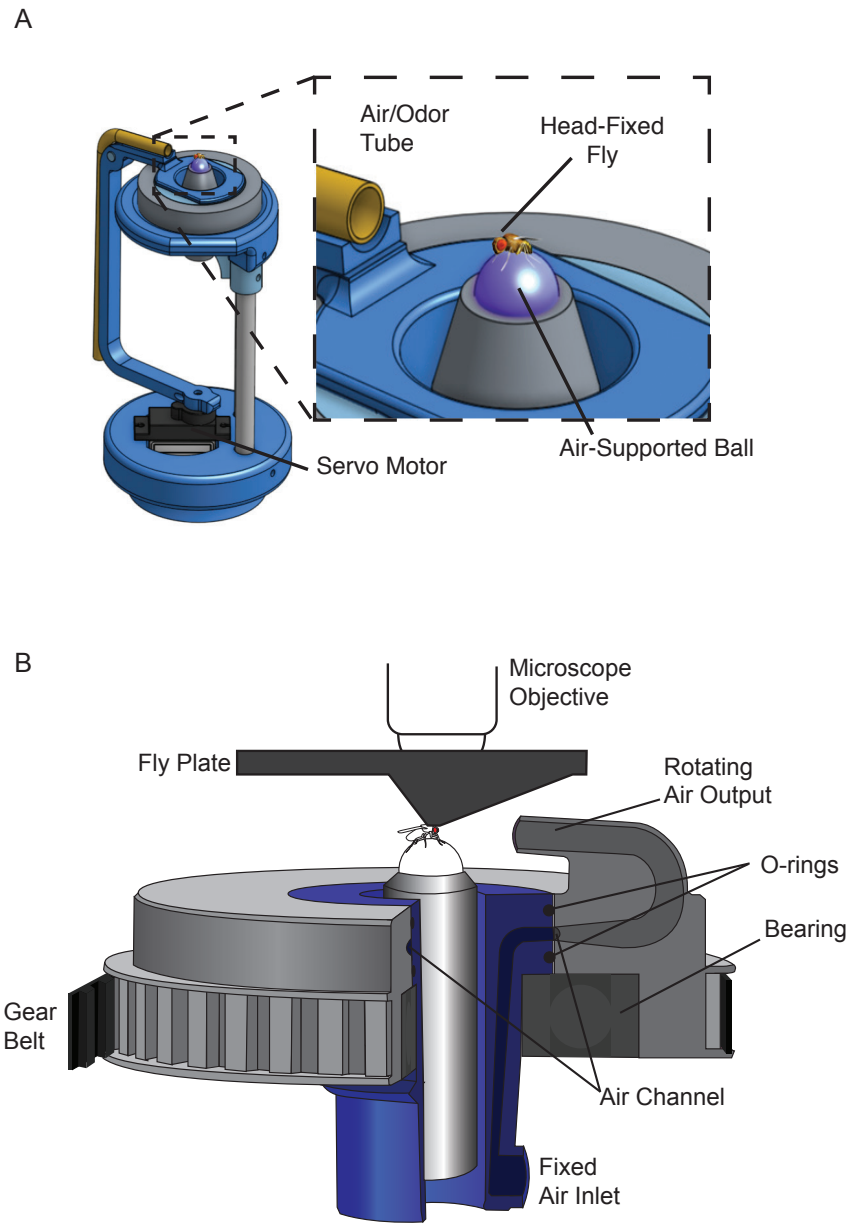
A
Air/Odor
Tube
Head-Fixed
Fly
Servo Motor
Air-Supported Ball
B
Microscope
Objective
Fly Plate
Rotating
Air Output
O-rings
Bearing
Gear
Belt
Air Channel
Fixed
Air Inlet

the air-delivery tube was able to move continuously through the entire 360 degrees around the fly (Figure 6.1B). This system uses a stepper motor coupled to a custom rotary union via a gear belt. The rotary union unit receives the air stream via a fixed input connection, while the output tube facing the fly can rotate continuously without limit. Both systems proved to be capable of inducing and recording robust upwind odor tracking behavior (see below) and we therefore pool data from both systems or indicate which system was used where relevant.

Closed Loop System Verification

While flies have sensory bristles distributed over their entire bodies, the aristae, feather-like sensory bristles extending from the third antennal segment, are the primary sense organs associated with detection of wind direction[345]. We therefore measured the position of the aristae of a mounted fly and found that changing the airflow direction of our closed loop system led to appropriate deflections of the aristae (Figure 6.2A). Together with the odor-tracking results described below, this suggests that our air-delivery apparatus can faithfully simulate the change in sensory input associated with a change in relative wind direction. How the sensation of wind direction in the aristae is encoded and relayed to the relevant navigational circuitry in the fly brain remains an interesting question for future study.

Figure 6.2, Naturalistic Anemotaxis in a Virtual Olfactory Environment. A, Verification that changes in wind direction in closed loop systems appropriately deflect the aristae. A fly was placed in the closed loop system and the position of the aristae (Ar), featherlike sensory hairs that extend from the antennae (An), were imaged using the brightfield microscope. Dashed box shows position of imaging field of view (left). Angles of aristae were manually traced when the airflow was turned off (center, blue) and with the airflow on (right) and the airtube positioned directly in front of the fly (yellow), to the fly's right (green) or left (red). Manual tracing of the aristae angles in all cases matched expected deflections. (Fly drawing modified from www.flinnsci.com). **B,** Representative 2D trajectories of the same fly walking for 5 minutes on the spherical treadmill in the dark with the airflow turned off (left, 'asensory') and with airflow turned on and closed loop system engaged (right). In 'asensory' condition, the fly is unable to maintain a stable heading without sensory feedback and generally walks in circles within a small area. In closed loop the fly can maintain a relatively straight heading over extended periods of time (Courtesy of Ari Zolin). **C,** Representative example of heading relative to wind direction (top) and **D,** 2D trajectory of a fly exposed to multiple presentations of apple cider vinegar odor while walking in the closed loop system. Each time the odor is presented (red), the fly robustly walks upwind, evident above by maintenance of a heading near 0, and below by the upwind trajectory. Odor offset often leads to increased turning that resembles local search behavior. **E,** Heading traces as in **C,** aligned to time of odor onset shows robust upwind turning in response to 49 odor presentations in n=7 flies.

Figure 6.2

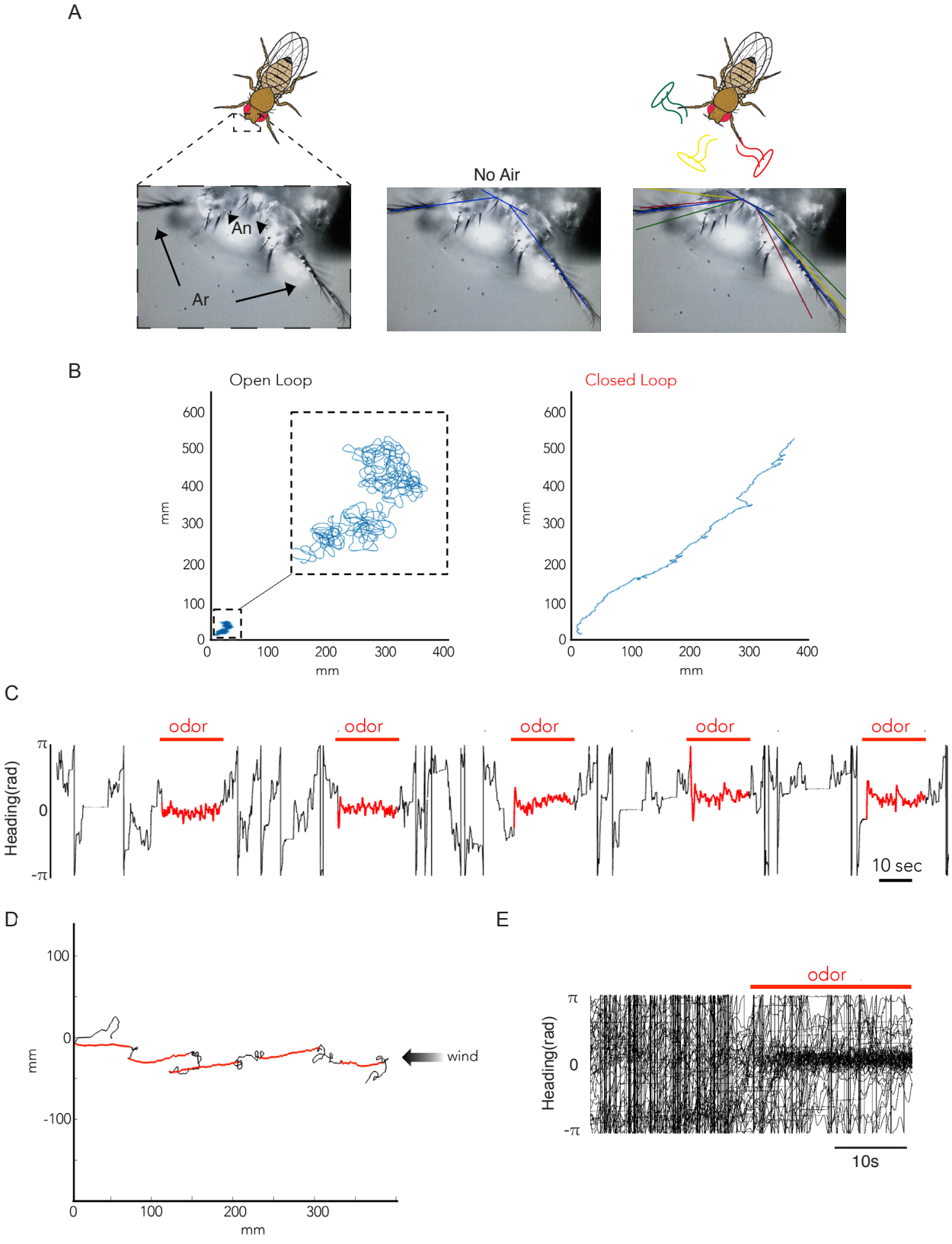
A
No Air
An
Ar
B
Open Loop
Closed Loop
mm
C
odor
Heading(rad)
10 sec
D
wind
E
10s

Flies walking in virtual visual environments have been shown to maintain a relatively fixed heading over long periods of time[342,346]. However, when the visual feedback is removed, the heading direction of these flies will drift over time since they no longer have the sensory feedback needed to remain on course[346]. If we compare the fictive 2D trajectory of the same fly walking on a ball in the absence of sensory feedback or in our closed loop virtual reality system, we find that the fly can maintain a relatively straight, long path when in closed-loop, but walks in circles when deprived of this sensory feedback (Figure 6.2B). This is consistent with the idea that the fly is indeed using the wind direction as a salient directional cue in order to maintain a constant heading direction. We next asked whether flies in closed loop would engage in anemotactic behavior in response to the presentation of appetitive odor. Indeed, we find that flies track relatively straight upwind when presented with the appetitive odor of apple cider vinegar, and often perform what appears to be local search behavior at odor offset[347] (Figure 6.2C-E). Thus, we have developed what we believe to be the first head-fixed preparation in which a fly can engage in naturalistic odor tracking behavior while walking.

Linking MBONs to Olfactory Navigation Behavior

Our preliminary results are in line with what has previously been observed in flies and other insects[333,337,338], suggesting that when flies detect an appetitive odor, they

can rely on directional signals conveyed by the wind to track towards the odor source. Therefore, the neural circuits that assess olfactory cues must ultimately converge with pathways that relay wind direction information, such that odor valence gates wind-tracking behavior. However, in our odor-tracking experiments, the olfactory stimulus is inherently linked to the wind, as in the context of natural odor plumes, since it is delivered by integration into the carrier air-stream in the same tube. We therefore optogentically activated the majority of OSNs to evoke a fictive olfactory response independent of wind. This type of stimulation has been previously shown to effectively drive upwind tracking in freely walking flies[336] and allows us to fully decouple 'odor' sensation from wind presentation. We expressed csChrimson in the majority of OSNs using the ORCO-Gal4 promoter and found that optogentic activation of this peripheral sensory population indeed evoked robust anemotaxis behavior, which was apparent from their maintenance of an upwind heading to a clean air stream in the closed loop paradigm (Figure 6.3A, D). We observed no obvious change in heading direction or walking velocity of flies in which OSNs were activated in the absence of airflow (Figure 6.3B) or when flies lacking csChrimson expression were stimulated with light (Figure 6.3C). Thus, the activation of olfactory sensory circuits increases the behavioral relevance of wind direction and causes the fly to turn upwind and attend to this directional cue.

We next asked whether the MB output pathways, which have been shown to represent learned and context-dependent odor valence, might directly influence upwind

Figure 6.3, Activation of Olfactory Sensory Neurons and MBONS Gates Upwind Odor Tracking. A, Representative trace of heading of a fly expressing csChrimson under control of ORCO-Gal4. Fly is in closed loop system with a constant, clean, airstream. Green lights indicate exposure to a 630nm LED, showing that optogenetic activation of OSNs leads to upwind tracking behavior in the absence of odor. **B,** When the wind flow is turned off, LED exposure has no apparent effect on the behavior of the same fly. **C,** LED exposure also has no apparent effect on control flies without csChrimson expression. **D,** Heading traces from 30 LED exposures in 6 flies aligned to the time of LED onset in ORCO>Chrimson flies shows that ORCO activity elicits robust upwind tracking behavior, apparent as maintenance of a heading near 0 (upwind). **E,** As in **D**, but for flies expressing csChrimson in the γ2 MBON, showing that this MBON elicits upwind tracking behavior (72 trials in n=8 flies). **F,** As in **D-E**, but for flies expressing csChrimson in the γ4 MBON, demonstrating a lack of upwind tracking, and instead, an increase in sharp turning when the LED is turned on (45 trials in n=5 flies).

Figure 6.3

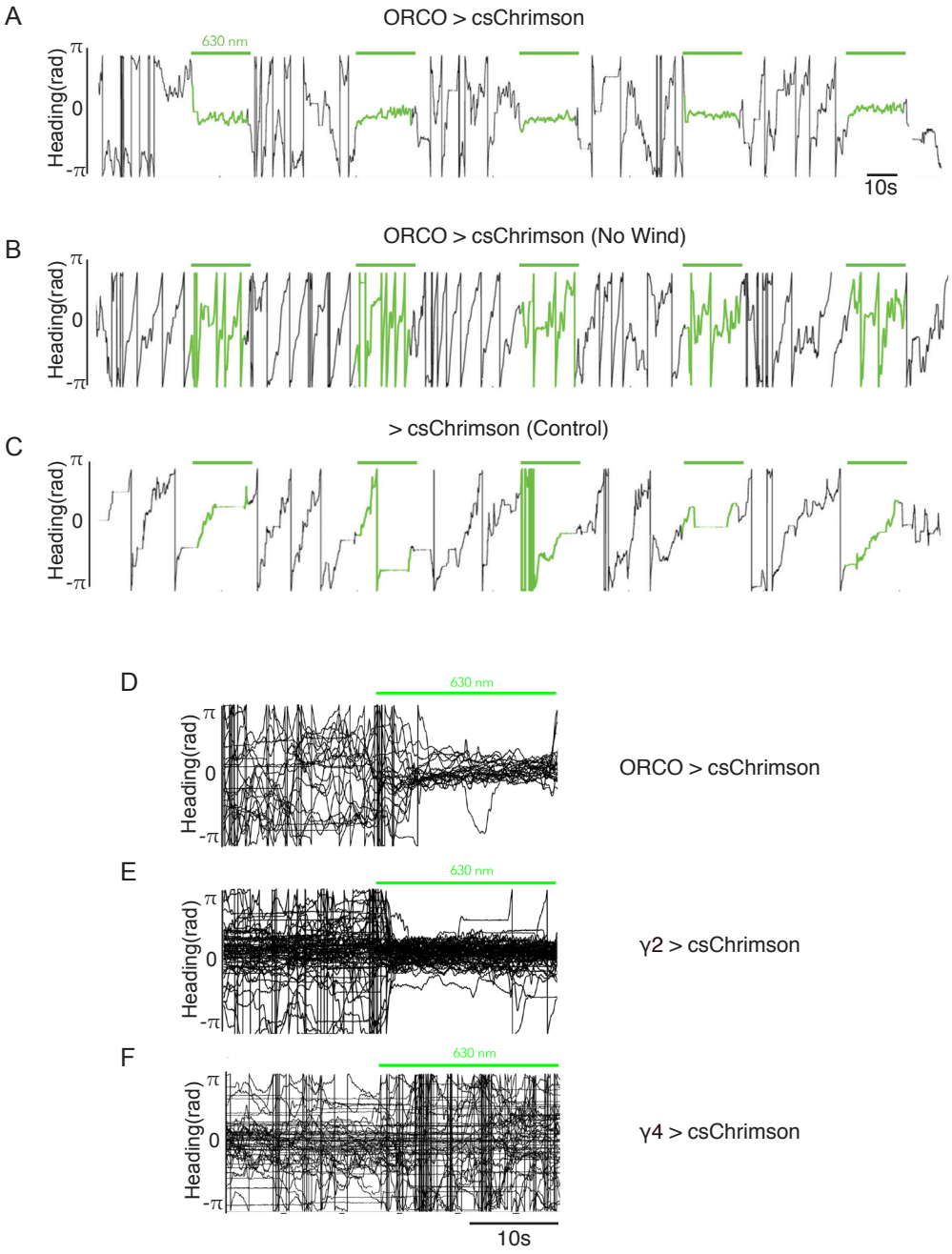
A
ORCO > csChrimson
630 nm
Heading(rad)
π
0
-π
10s
B
ORCO > csChrimson (No Wind)
C
> csChrimson (Control)
D
ORCO > csChrimson
E
γ2 > csChrimson
F
γ4 > csChrimson

turning. We expressed csChrimson under the control of split Gal4 lines, each of which selectively drives expression in a single or small subset of MBONs[114]. We then optogenetically activated each MBON class while the fly was walking in a clean air-stream in closed loop. Activation of either the γ2 or γ3 MBONs elicited robust upwind tracking (Figure 6.3E), in agreement with previous results showing that activation of these mushroom body output pathways replicates odor attraction in a population assay[118]. Thus, the olfactory-attraction mediated by MBONs may be, in part, implemented through a downstream circuit that relies on wind direction to guide anemotaxis in response to appetitive odors. Conversely, activation of the γ4 MBON, which has been shown to lead to avoidance[118], did not evoke upwind turning, and instead elicited increased turning rates in the closed loop system (Figure 6.3F). Taken together, these preliminary results suggest that circuits downstream of the MBONs mediate the convergence of odor valence representations with information about wind direction in order to guide anemotactic behavior.

We therefore used a newly developed trans-synaptic tracing mechanism, known as *trans*-TANGO[348], to identify neural loci that are both downstream of the MB and encode directional cues. In *trans*-TANGO, a modified glucagon receptor is expressed pan-neuronally, together with downstream machinery that initiates expression of a reporter gene, such as tdTomato, when the receptor is activated. A Gal4 driver line is used to drive expression of a glucagon construct that is tethered to the extracellular surface of presynaptic terminals. This system thus allows for anterograde labeling of

any neurons that are postsynaptic to those labeled by a Gal4 line of interest (Figure 6.4A). We crossed the *trans*-TANGO flies with selective split-Gal4 lines targeting individual MBON classes to visualize putative downstream neurons. From this labeling, it appears that MBONs synapse onto diverse neurons with projections in many different parts of the protocerebrum. However, an intriguing shared target of many MBON postsynaptic partners are the dorsal and medial layers of the fan shaped body (FSB) (Figure 6.4C), a part of the central complex (CX) which has been previously suggested to be downstream of MBONs based on anatomical proximity of neuronal processes[114].

The CX comprises a set of discrete neuropils in the central brain and is known to play roles in encoding spatial cues and controlling directional motion[349–353]. Work in recent years highlighted a set of neurons, known as EPGs, that innervate a donut-shaped structure called the ellipsoid body (EB) along with the linearly-arranged glomeruli of the protocerebral bridge (PB)[342,346,354] (Figure 6.4B). These neurons have been shown to function as a ring attractor, in which a single peak of activity travels around the span of the ellipsoid body and maintains a faithful record of the heading direction of the fly relative to a visual landmark[354]. We asked whether these same neurons might represent the fly's heading relative to the wind direction in the absence of visual feedback. In preliminary experiments, we expressed GCaMP in the EPG neurons and recorded their activity while the fly navigated within the closed loop paradigm. We found that the EPG activity peak was indeed well-correlated with the heading of the fly, with an arbitrary offset, replicating findings from visual virtual navigation (Figure 6.4D).

Figure 6.4, Convergence of Odor Valence and Wind Direction in the FSB. A, Schematic demonstrating the use of the *trans*-TANGO system in order to label neurons that are postsynaptic to the γ2 MBON. A Gal4 line is used to express one part of the *trans*-TANGO system, a synaptically localized, membrane-tethered glucagon, along with a visualizable reporter (γ2 MBON, red). A pan-neuronally expressed modified glucagon receptor is activated only in neurons that are postsynaptic to the targeted γ2 MBON. Receptor activation leads to expression of another reporter (green). Many MBONs appear to synapse onto neurons that project to the FSB. **B,** Schematic of the protocerebral bridge (PB), fan-shaped body (FSB) and ellipsoid body (EB), three components of the central complex (CX). The PB is made up of 18 glomeruli that are roughly linearly aligned along the posterior edge of the brain. The patterns of innervation by different neurons in the FSB define discrete rows and columns. Many neurons innervating the EB tile the circumference of the structure into discrete wedges. Color-coding indicates wedges and glomeruli that are connected by a subset of CX neurons. Adapted from Turner-Evans and Jayaraman[355]. **C,** *trans*-TANGO labeling of neurons downstream of several MBONs highlights their common projections to the dorsal and medial layers of the FSB. **D,** Representative recording of peak of GCaMP fluorescence of EPG neurons in the wedges of the EB (grayscale) aligned with the fly's heading direction (red) while the fly navigates in the closed loop system. Adding in the odor of apple cider vinegar leads the fly to track in a relatively upwind direction. **E,** As in **D**, but imaging the PFN neurons along the span of the FSB. When the wind is temporarily turned off, the heading no longer aligns with the peak of activity in the FSB, but snaps back into place when the wind returns. (Note that in **D** and **E**, the wedge phase has been shifted by an arbitrary offset in order to maximize alignment with heading over the course of the recording, as described in Seelig et al.[346])

Figure 6.4

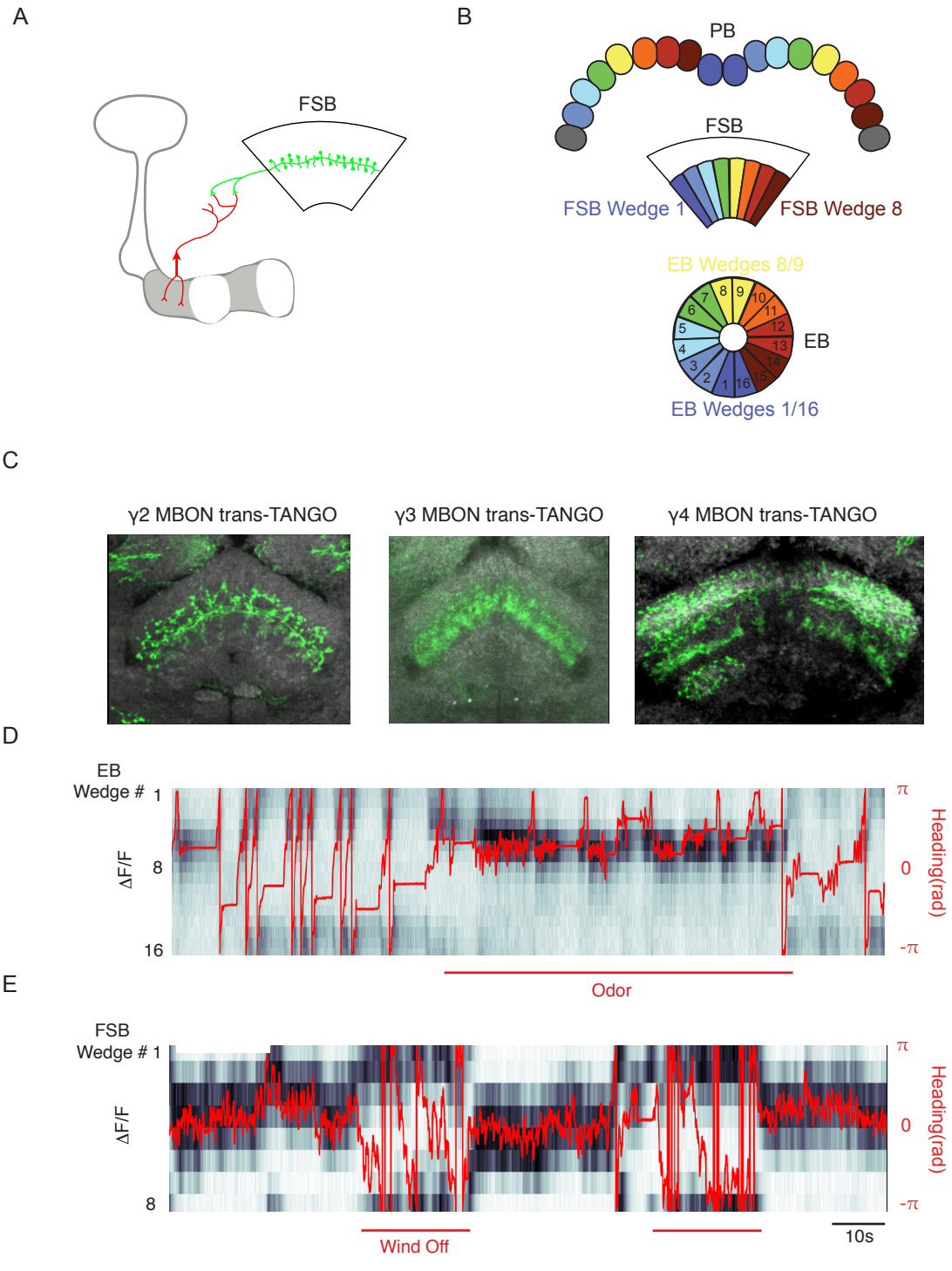
A
FSB
B
PB
FSB
FSB Wedge 1
FSB Wedge 8
EB Wedges 8/9
EB
EB Wedges 1/16
C
γ2 MBON trans-TANGO
γ3 MBON trans-TANGO
γ4 MBON trans-TANGO
D
EB
Wedge #
1
8
16
ΔF/F
π
0
-π
Heading(rad)
Odor
E
FSB
Wedge # 1
8
ΔF/F
π
0
-π
Heading(rad)
Wind Off
10s

This correspondence was lost when the wind source was turned off but the air tube was still yoked to the fly's position. This preliminary result suggests that wind direction can, indeed, be used to update and maintain this heading representation. It is, perhaps, unsurprising that multimodal sensory inputs are integrated into a unified heading signal in the EPGs, as it has been previously shown that olfactory inputs can modulate visual processing in flight[9]. In future experiments it will be interesting to extend on these observations and to determine whether this wind-direction information is relayed to the CX through the same types of neurons that convey visual directional cues[350].

The highly recurrent circuit organization of the CX[356] suggests that there are multiple copies of EPG-like heading signals carried by different neural populations in this neuropil[342,346,357] (Figure 6.4B). We therefore asked whether neurons innervating the fan shaped body, and therefore poised to interact with the putative MBON targets identified by *trans*-TANGO, also represent the fly's heading direction relative to the wind. We expressed GCaMP in a set of neurons, known as PFN neurons, which extend projections into the same layers of the FSB that were identified as targets of MBONs in our *trans*-TANGO labeling. The PFNs also innervate the noduli and the PB, a shared target of EPGs, suggesting they may carry a heading representation (private communication from Cheng Lyu). We observed a single peak of activity along the span of the FSB columns that provided a faithful representation of the fly's heading relative to the wind direction (Figure 6.4E). As observed when imaging the EPG heading signal, temporarily removing the wind flow resulted in uncoupling of the PFN activity peak from

the fly's heading direction, while restoring the wind induced the PFN peak to 'snap back' into alignment with the heading. Interestingly, these preliminary recordings in both the PFNs and EPGs showed no obvious change in signal intensity upon odor presentation. This implies that the encoding of spatial orientation in these neurons is distinct from the representation of a goal (an attractive odor source) that might lead to the maintenance of an upwind heading.

These results suggest that the FSB is likely to be one point of convergence between odor-valence decisions carried by the MBONs and wind-direction information contained in the activity of the PFNs. While it remains to be seen whether and how this convergence might impact the fly's behavior in response to an odor, we believe that the FSB provides a promising target for future investigation of how olfactory-based decisions are translated into action. Another region of interest highlighted by *trans*-TANGO as a target of several MBONs is the lateral accessory lobe (LAL), a brain region that also contains the dendrites of many descending neurons[358,359], suggesting these neurons might directly influence motor control. There are likely to be multiple points of convergence of odor information and spatial orientation representations within the fly brain. For instance, airflow is also represented in the MB itself[360]. Nonetheless, our closed loop paradigm will serve as a powerful tool in future studies exploring the circuits that link MB output to the execution of anemotaxis behavior.

Dopaminergic Neurons Represent Details of Sensorimotor Context

Investigations into the neural circuits responsible for controlling action selection and modifying motor control based on experience have revealed that internal representations of behavior tend to appear in conjunction with the learning signals that motivate future choices. For instance, it appears that the presence of locomotor signals in the dopaminergic circuitry of the basal ganglia may be important for invigorating movement[33,276,361,362]. Our discovery of locomotor-related signals in the reinforcement-signaling DANs of the MB (Figure 3.3D-E) suggests that this connection between reward representation and motor state is conserved across distantly related species, pointing to an intrinsic connection between the roles of these seemingly distinct neural codes. However, this initial observation was made in a dangling fly – a seemingly extreme behavioral state with unknown ethological significance. Initial recordings of DAN activity while the fly walked on a spherical treadmill revealed that the correlations apparent in a dangling fly were not maintained during more naturalistic walking (Figure 3.4B). Therefore, in collaboration with Ari Zolin, another student in the lab, we decided to investigate the role of the γ lobe DANs in representing the fly's actions in a more relevant behavioral context: tracking towards an appetitive odor stimulus in our closed loop olfactory paradigm.

In trying to understand the relevance and purpose of the locomotor signals in learning centers, we again simultaneously recorded the activity of several genetically distinct subpopulations of DANs and used the compartmental organization of the MB lobes to unambiguously identify each subset (Figure 3.2). Making use of a closed loop paradigm allowed us to record detailed sensory and behavioral parameters while placing the fly in a context in which it could perform meaningful, sensory-guided behaviors. We began by recording from the γ lobe DANs in flies walking comfortably on the ball, but without providing a wind source or any other overt external sensory cues. In this 'asensory' setup, DAN activity was frequently coordinated (Figure 6.5A), but the correlations between DANs of different compartments and between DANs and the fly's behavior were significantly more complex than the simple binary states apparent in the flailing animal. While, on average, the activity in all compartments correlated with the initiation of walking bouts, the γ3 DANs were nearly perfectly correlated with this locomotor state, while the other DANs exhibited more variability (Figure 6.5B-C). Interestingly, there appeared to be a reciprocal opponency between the γ2 and γ4 DANs (Figure 6.5B-C), resembling the population-wide opponency apparent in the 'flail' and 'still' states (Figure 3.3D-E). Additional analysis revealed that during movement bouts, the activity of the γ4 DANs is correlated with the fly's forward velocity (Figure 6.5D,F). Thus the DAN population represents multiple aspects of the fly's locomotor state, in addition to internal DAN network dynamics.

Figure 6.5, DANs Represent Details of Sensorimotor Context. A, Overlay of net velocity of the fly walking on a spherical treadmill and neuronal activity in four of the dopaminergic neuron subpopulations innervating the γ lobe of the mushroom body in three representative animals expressing syt-GCaMP in all dopaminergic neurons and dsRed in KCs. **B-C**, Pearson correlation coefficient (r) of net motion and γ2 (top row, blue), γ3 (second row, red), γ4 (third row, green), or γ5 (bottom row, magenta) DAN activity as animals initiate (**B**) or terminate (**C**) locomotion. Columns correspond to all instances of locomotion initiation (**B**) or cessation (**C**) performed by an individual animal. Animals are ordered from lowest to highest average pearson correlation coefficient between net motion and γ2 DAN activity within each condition. n=36 animals initiating locomotion 1038 times (**B**). n=38 animals terminating locomotion 676 times (**C**). **D,** Representative trace showing that the activity in the γ4 DANs (green, average of left and right MBs) is roughly correlated with the forward velocity (black) of the fly during a walking bout. **G,** Representative trace showing that the difference between the syt-GCaMP fluorescence in the left and right γ4 DANs roughly correlates with the changes in heading of the fly walking in closed loop (black). **H,** Linear filters describing the relationships between behavioral parameters and γ4 DAN activity. Black traces represent average filters across n=10 flies, with filters fit from individual flies shown in gray. Filters suggest that forward velocity is positively correlated with average γ4 DAN activity (top), odor sensation leads to increases in γ4 DAN activity (middle) and air tube angle is correlated with the difference between the γ4 DAN activity on the left and right sides of the brain (bottom). These filters look similar across closed loop (left) and white noise (right) conditions, indicating that they are not significantly effected by the state-change associated with closed loop behavior, and that the Left-Right difference represents sensation of wind direction and not turning behavior. Courtesy of Ari Zolin (**A-G**) and Rich Pang (**H**).

Figure 6.5

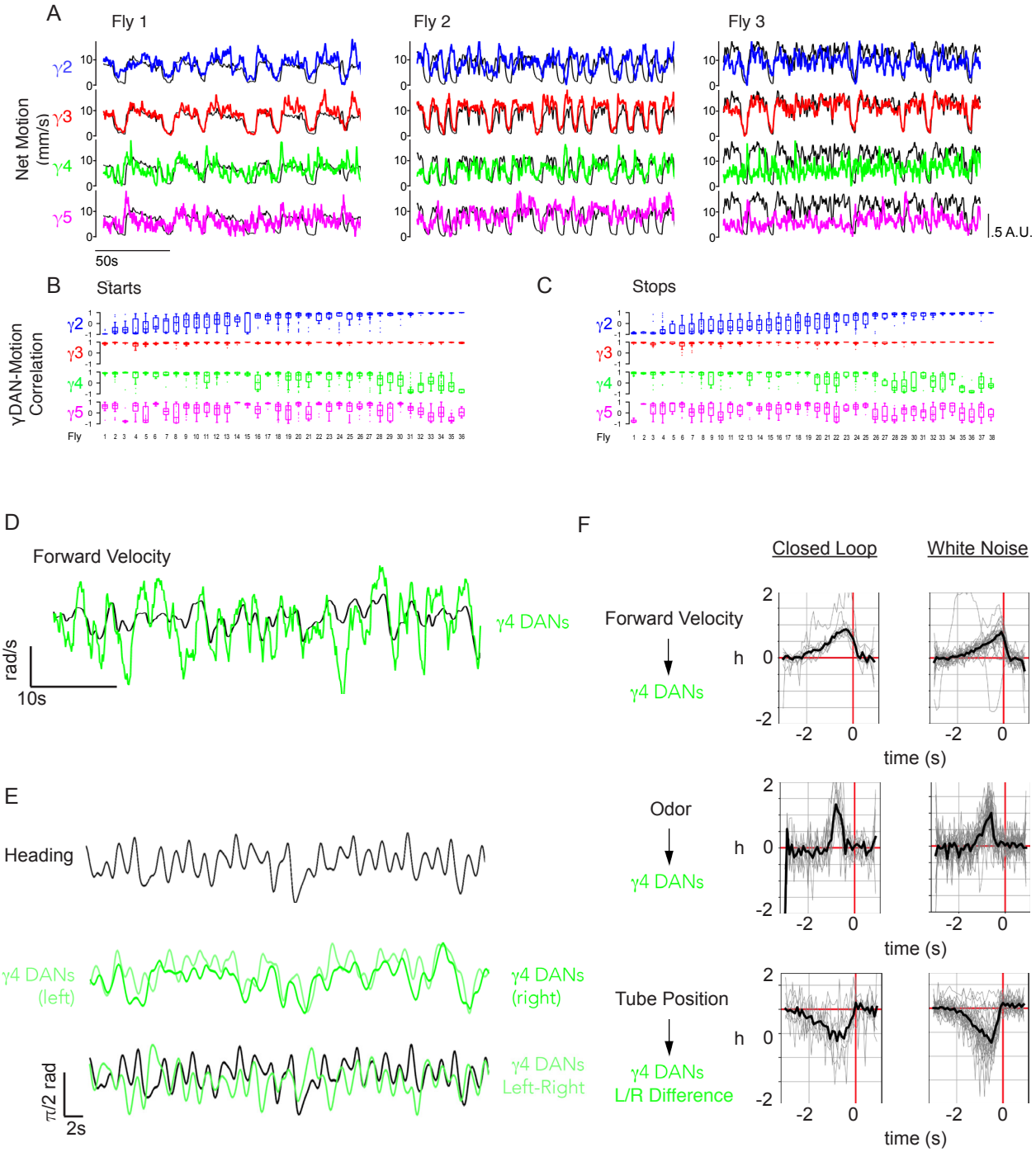
A
Fly 1
Fly 2
Fly 3
γ2
γ3
γ4
γ5
Net Motion (mm/s)
50s
.5 A.U.
B
Starts
γDAN-Motion Correlation
Fly
C
Stops
D
Forward Velocity
γ4 DANs
rad/s
10s
E
Heading
γ4 DANs (left)
γ4 DANs (right)
γ4 DANs Left-Right
π/2 rad
2s
F
Closed Loop
White Noise
Forward Velocity
γ4 DANs
Odor
γ4 DANs
Tube Position
γ4 DANs L/R Difference
h
time (s)

We next asked whether allowing the fly to navigate relative to the wind direction in our closed loop system would reveal additional aspects of behavior that might be encoded by the DAN population. During upwind tracking, we noticed that while the activity of most γ lobe DANs was bilaterally equivalent, the activity of the γ4 DANs was significantly different between the right and left MBs. The deviation between the two sides correlated well with the left and right turns made by the fly, indicating that the γ4 DANs represent an additional aspect of the fly's behavior: the small turns within the air stream required to maintain an upwind direction (Figure 6.5E-F). Because the movement of the air tube and changes in the fly's heading are linked in the closed loop condition, it is impossible to determine whether this γ4 DAN difference represents the act of turning or the sensation of changing wind direction. We began a collaboration with Rich Pang, a student from Adrienne Fairhall's Lab at the University of Washington, to quantitatively describe the different states within the DAN network and how they depend on behavior and sensory inputs. We exposed the fly to a white noise stimulus of air tube motion that replicated the statistical properties of tube movement observed in closed loop, but was uncorrelated with the fly's behavioral output. These experiments revealed that the difference between right and left γ4 DAN activity is actually a representation of the changes in wind direction induced by turning, and not the act of turning itself (Figure 6.5F). Thus in the closed loop paradigm, the γ4 DAN activity reflects both sensory feedback resulting from changes in wind direction as well as the fly's forward velocity.

Finally, we asked whether the DANs might represent additional sensory- or motor-related signals in the context of olfactory navigation. We presented flies in the closed loop paradigm with pulses of apple cider vinegar odor while recording from the γ lobe DANs. We found that the γ4 DANs gave the most robust responses to the presentation of this appetitive odor, with other compartments only weakly responding or being inhibited, though the odor responses were somewhat variable. In order to determine the contributions of odor-related signals and velocity representations, respectively, to γ4 DAN activity, we again turned to a white noise stimulus paradigm. Using the same white noise air tube motions describe above, we added in a series of randomized odor pulses. Rich Pang fit linear filters to the behavioral and functional imaging data and found that both odor presentation and forward velocity contribute to the γ4 DAN activity, and confirmed that the left-right difference between γ4 DANs correlates with air tube motion (Figure 6.5F). The γ4 DAN activity therefore contains complex, multiplexed information encompassing aspects of behavioral state as well as multimodal sensory inputs that include reward signals, wind direction, and odor responses.

Investigations into the functional properties of the MB circuitry have revealed how the specialized circuit architecture that first drew the interest of neurobiologists over 150 years ago is ideally suited to dynamically assign meaning to sensory inputs based on experience. Our own work has helped to describe the specific mechanisms by which dopaminergic modulation within the compartments of the MB lobe contribute to this

flexibility. However, very little is known about how the odor valence, shaped by the population of DANs and carried in the joint activity of the MBONs, is translated into appropriate, odor-guided behavior. Using a closed loop, virtual wind environment in which flies can perform realistic olfactory navigation, we have begun to observe and perturb the activity of neurons within and downstream of the MB. We believe this tool will be instrumental for future experiments that explore how MBON activity is translated into action.

Our findings thus far demonstrate that in addition to reinforcement signals, the MB DANs encode specific parameters of the fly's locomotor state. This detailed behavioral representation again draws an interesting parallel to the dopaminergic circuits of the mammalian striatum. Striatal DANs have been shown to represent and contribute to specific aspects of animal activity, including movement initiation, vigor, action sequences and action selection[32,33,276,293,361,363,364]. Interestingly, just as we see differences in the types of behavioral and sensory signals that are represented in the distinct MB compartments, regional specializations and differences between subcompartments of the striatum have also been described[32,365,366]. As in studies of these mammalian systems, our ability to parse the correlations between DAN activity and behavioral parameters was aided by advances in techniques that allowed us to simultaneously record from identifiable subpopulation of DANs, as well as the development of novel behavioral paradigms that are compatible with functional imaging and the execution of meaningful actions.

The parallels between the MB and the basal ganglia raise several interesting questions for future investigation. The dopaminergic locomotor signals in the striatum have been suggested to be specifically linked to the initiation of motivated actions, perhaps with the expectation of reward[33,34,240,269,291]. This leads us to ask whether the MB DANs might similarly show distinct representations of goal-oriented movements. Preliminary investigations using our closed loop system suggest that γ4 DAN activity is specifically enhanced when the fly is motivated to track upwind towards an appetitive odor. Additionally, ongoing experiments, and recent reports[367], indicate that perturbing MB DAN activity can lead to increases or decreases in motivated locomotion, paralleling the effects that changes in dopaminergic activity have on mammalian behavior, whether due to experimental manipulations or disease[33,225,361,365,368]. It thus appears that the control of motivated behaviors and reinforcement learning in highly divergent species rely on shared dopaminergic circuits whose coordinated activity acts to modulate the flow of sensory information and impart meaning to sensorimotor experience.

Chapter 7

Discussion

In the work described here, we took advantage of the orderly architecture of the *Drosophila* MB to gain insight into how neuromodulatory mechanisms mediate flexible circuit processing. Recent data[118,119,125] and our own experiments (Figure 6.3E-F) suggest that the ensemble of MBONs act in concert to bias an animal's behavioral response to an odor, such that altering the balance of their activity can modify the olfactory preferences of both naïve and trained animals. We showed that compartmentalized dopaminergic signaling permits independent tuning of synaptic neurotransmission between an individual KC and its repertoire of postsynaptic MBON targets. As a consequence, a single odor representation can evoke different patterns of output activity depending on the state of the animal and the dopaminergic network. Thus, we reveal how a distributed neuromodulatory network is poised to direct plasticity across all the compartments of the MB and selectively route olfactory signals through different MBONs, allowing for adaptive behavioral responses based on the acute needs or past experience of the animal.

Neuromodulation: A Challenge and a Guide

The awesome complexity of the nervous system presents a daunting and exciting challenge for neuroscientists studying animals from worms to humans. The intricate wiring in our brains and bodies must somehow give rise to our ability to sense, reason and imagine. The task of understanding neural circuit function would be challenging enough if the hundreds of trilliions of synaptic connetions in our brains were fixed. The fact that these connections are constantly being modified, and that this modulation is inherent to our ability to generate flexible behaviors suggests an insurmountable roadblock. However, while the dynamic nature of circuit function certainly presents some difficulties, exploring the modulation of neural circuits can also provide insights that help explain the relationships between the structural organization of specific brain regions and their functions.

One of the most ubiquitous sources of behavioral modulation across all animals is satiety state, and investigations of the relevant modulatory pathways have improved our understanding of the neural circuits controlling food-related actions. Animals must adjust their behaviors depending upon their level of hunger in order to ensure the availability of nutrients necessary for survival. Internal sensation of nutrient availability is therefore a potent modulator of neural circuits that control behaviors related to the acquisition of food. In mammals, the identification of hunger-activated AgRP neurons

has greatly accelerated our understanding of the circuits that are modulated by hunger in order to lead to increased food-seeking and intake[369,370]. Interestingly, activity in these hunger-activated neurons can serve as a negative-valenced reinforcement signal[371], while satiety state also affects food-reward related signals in brain regions involved in learning[372], including DANs in the striatum[373]. In the *Drosophila* MB, satiety state has also been shown to influence the formation of long term memory[374,375] and to control the excitability of specific DANs, thereby gating the expression of appetitive memories[302], thus demonstrating an additional role of the DANs in mediating the effect of internal state on MB circuitry. In collaboration with Leslie Vosshall's lab, we explored the effect of satiety state on the sugar-ingestion responses of a set of gustatory interneurons in the *Drosophila* subesophageal zone. We found that the activity of these neurons in response to sugar ingestion is significantly modulated by both the quality of the food source as well as the satiety state of the fly (Figure 7.1). When the fly is sated, these neurons respond transiently to sugar intake, while in hungry flies, they exhibit a sustained sugar response (Figure 7.1E-G). These findings helped to explain how these neurons might function to control the fly's feeding behavior under different conditions, and opened up new avenues of exploration of a pharyngeal gustatory pathway[376]. In all of these instances, investigations into the modulation of specific circuits by hunger-mediated modulatory pathways led to the elucidation of neural mechanisms for animals to adjust their feeding-related behaviors. Thus, neuromodulatory mechanisms can serve as a handle into the dissection of complex neural circuits and the behaviors they control.

Figure 7.1, Satiety State Modulates Activity in a Gustatory Pathway. A, Representative IN1>GCaMP6s responses recorded in the same 24-hr-fasted female before, during, and after 1 M sucrose ingestion. Still images captured by the video camera (a–d; see **B** for corresponding raw traces), with the eye pseudocolored in red and 1 M sucrose drop in blue (top). Heatmap of IN1 neuron activity in response to indicated stimuli (bottom). **B,** Trace of IN1 fluorescence in a.u., with letters a–d indicating the corresponding still image and activity heatmaps in **B**. **C,** Fluorescence traces are normalized using F_0. The gray lines show data from individual flies; bold green and blue lines show average traces for the indicated stimuli. **D,** Peak of stimulus-evoked IN1 neuron activity ($p < 0.05$, one-way ANOVA with pairwise post hoc Bonferroni test; error bars indicate mean ± SEM; n = 4–6). **E,** Normalized IN1 neuron activity in fed or 24-hr-fasted flies to 1 M or 100 mM sucrose. Mean traces for indicated stimuli and conditions (colored lines) ± SEM (gray). Summed histogram of ingestion duration (bottom). **F,** Peak of stimulus-evoked IN1 neuron responses to indicated stimuli and conditions ($p < 0.05$, unpaired Student's t test with Bonferroni correction; error bars indicate mean ± SEM; n = 5–6). **G,** Area under the curve (A.U.C.) measurement of the GCaMP6s signal showing the persistent activity of IN1 neurons to indicated stimuli and conditions ($p < 0.05$, Student's t test with Bonferroni correction; error bars indicate mean ± SEM, n = 5–6). Adapted from Yapici et al.[376]

Figure 7.1

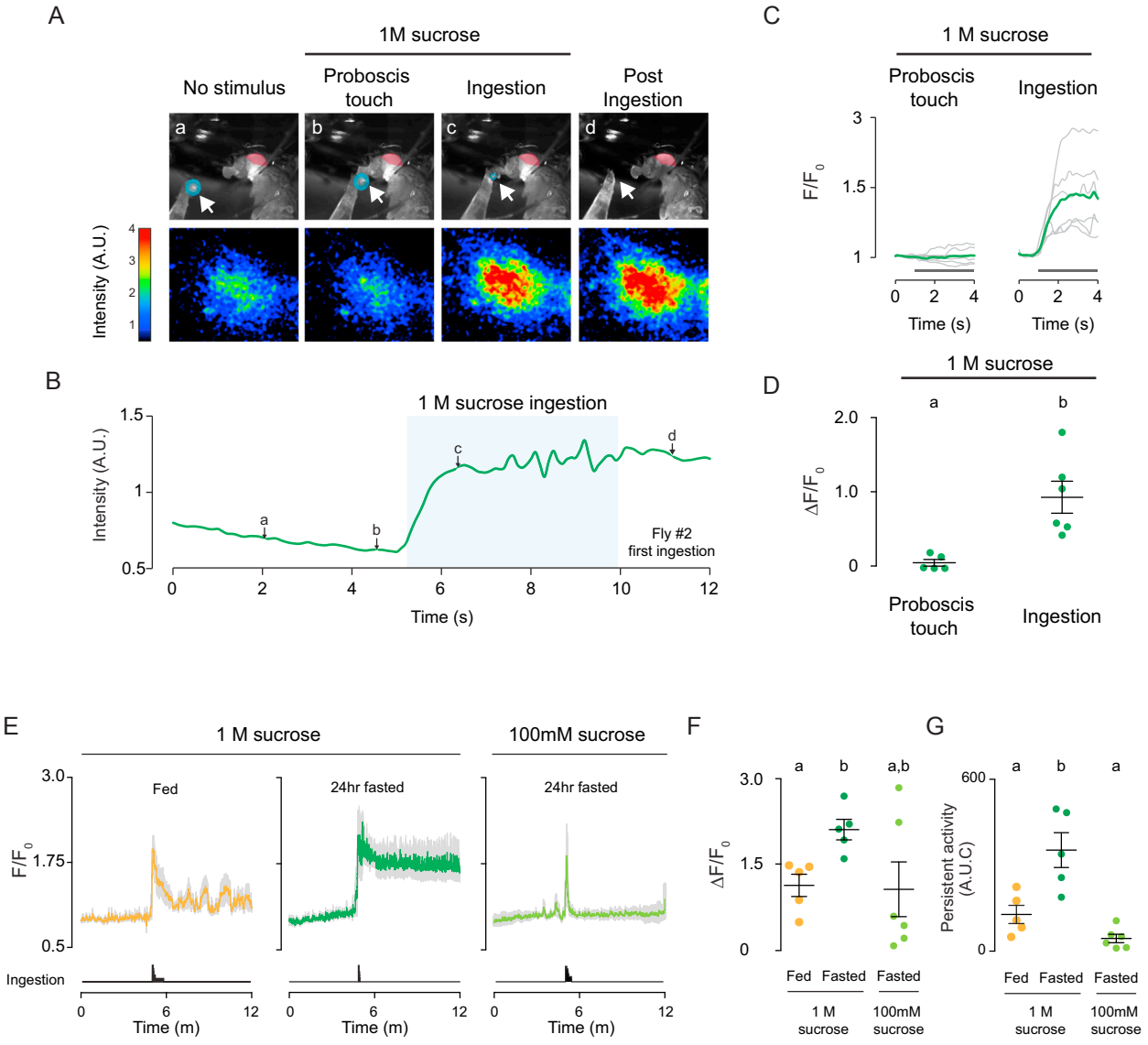
A
1M sucrose
No stimulus
Proboscis touch
Ingestion
Post Ingestion
a
b
c
d
Intensity (A.U.)
B
1 M sucrose ingestion
Intensity (A.U.)
Fly #2 first ingestion
Time (s)
C
1 M sucrose
Proboscis touch
Ingestion
F/F0
Time (s)
D
1 M sucrose
ΔF/F0
Proboscis touch
Ingestion
E
1 M sucrose
100mM sucrose
Fed
24hr fasted
24hr fasted
F/F0
Ingestion
Time (m)
F
ΔF/F0
Fed
Fasted
Fasted
1 M sucrose
100mM sucrose
G
Persistent activity (A.U.C)
Fed
Fasted
Fasted
1 M sucrose
100mM sucrose

Our investigations into dopaminergic modulation of the MB[377], together with many other studies of the MB's role in learning and context-dependent behavior, have likewise shed light on some of the organizational principles within the MB circuitry. Our demonstration that individual KC synapses can be independently modulated by dopaminergic inputs underscores the significance of the compartmentalized organization of the MB lobes. This circuit architecture allows for the flow of sensory information to be independently modulated within each compartment, resulting in precise control of each set of MBONs and their collective downstream influence on behavior. Descriptions of the plasticity rules at KC-MBON synapses and at parallel fiber output synapses in other cerebellum-like structures have informed computational analyses suggesting that optimal encoding for associative learning may dictate the choice of specific connectivity parameters at the input layers of these structures[112]. Finally, our demonstration of coordinated DAN network activity representing many parameters of the sensorimotor state of the fly helps to explain the potential role of the recurrent circuitry in the MB and related structures. Thus, our studies of dopaminergic modulation in the MB help elucidate the elegant relationship between structure and function in this neural circuit.

Nonetheless, it is important to recognize the limitations of our findings. In particular, while we investigated the immediate effects of dopamine-induced plasticity within particular γ lobe compartments, it is known that the MB is responsible for many different forms of memory, some of which are thought to result from interactions

between multiple compartments. Recent studies have begun to explore these differences, suggesting that the learning rules may differ between compartments based on the form of memory they encode[133,211]. Thus, additional investigations into the diverse capabilities of this brain structure are likely to further expand our understanding of the many different ways that dopamine and other neuromodulators affect circuit function.

Mechanisms for Spatiotemporal Precision of DAN Modulation

The interplay between structural and functional studies in the MB help to explain the mechanisms by which DANs control the flow of sensorimotor information with striking spatiotemporal precision. We demonstrated that dopaminergic modulation of both KC presynaptic Ca^{2+} and KC-MBON synapses appears to be restricted to the precise compartmental boundaries (Figures 4.3A-B, 5.3)[226]. This spatial precision is remarkable in that the boundaries between compartments span only a few microns and dopamine has been shown to be capable of acting over considerable distances via diffusion[311]. Our functional findings, however, are nicely supported by recent EM studies that examined the distribution of DAN synapses within a MB lobe[305]. These studies revealed that while dopaminergic synapses are not always co-localized with KC-MBON synapses, they invariable appear within approximately 2 microns of each synapse in a compartment. This short distance should allow for dopamine released by DANs to reach

all synapses within a compartment through local diffusion, while significantly greater distances would have to be traversed to affect synapses in neighboring compartments. Thus, detailed anatomic studies provide a plausible physical mechanism to explain the spatial precision of neuromodulation we demonstrate, while our functional observations of this precise targeting enlighten us as to the utility of this structural organization.

In addition to the selective targeting of specific KC synapses, we also found that MB DANs can induce opposing forms of synaptic plasticity depending upon the precise temporal ordering of activation of KCs and DANs (Figures 5.3-5.6). While it has long been held that *rutabaga*, a Ca^{2+} dependent adenylyl cyclase, mediates detection of coincident odor stimulation of the KCs with DAN activity[75,228], our findings necessitate a more nuanced understanding. Rather than a single mechanism for coincidence detection, the bidirectional modulation of KC-MBON signaling we observe suggests the presence of molecular mechanisms for the detection of three distinct temporal patterns of dopamine release: forward paired, backward paired and unpaired.

Ongoing studies in our own lab and others have suggested that these distinct forms of plasticity may be mediated by at least two different dopamine receptors, DopR1 and DopR2[223,306], through distinct downstream signaling cascades. One model suggested that the choice of engaging one pathway versus the other might be a function of differences in dopamine affinity between the two receptors[306], thereby distinguishing

between low and high levels of dopamine release. This proposed mechanism parallels the notion that dopamine-affinity differences between the D1 and D2 dopamine receptors are responsible for the selective engagement of the direct and indirect striatal pathways by phasic and tonic DAN activity in the striatum, respectively[378]. However, an increasing accumulation of evidence suggests that this hypothesis is unlikely to fully explain the modes of plasticity observed in the MB. For one, the dichotomy suggested in the mammalian circuitry has recently come into doubt, as increasingly detailed analyses have revealed commingling of receptors between the two pathways[378]. Furthermore, while the classical viewpoint held that the direct pathway was responsible for driving locomotion and the indirect pathway was involved in opposing movement, more recent studies have suggested that both pathways contribute to different aspects of action sequences[361,362], further muddying the previously proposed distinctions. Meanwhile, within the MB circuitry, significant questions remain about how these distinct forms of plasticity are implemented. In the experiments described here, we found that identical levels of DAN stimulation were able to alternately recruit opposing types of plasticity, based solely on the relative timing of their activation (Figure 5.6D). A difference in receptor affinity would therefore be unable to explain this distinction. Additionally, both dopamine receptors have been shown to induce the production of cAMP[223], raising questions as to how downstream pathways can distinguish between their activation. Thus, how these different patterns of dopamine release recruit distinct, opposing modes of plasticity at KC-MBON synapses remains an interesting open question.

Ongoing studies in our lab have begun to trace the distinct molecular underpinnings of the bidirectional modulation induced by forward and backward KC-DAN pairing in the MB. Future experiments will continue to explore the mechanisms by which these opposing pathways are engaged in the fly depending upon the precise temporal relationship of convergent inputs. We hope that by interrogating how these complementary forms of plasticity work to guide behavior in the fly, we will also help to resolve the ongoing uncertainties about specific mechanisms of dopaminergic modulation in other model organisms.

Modern Tools for Linking Animal Behavior with Neural Circuits

The digital revolution has unleashed a steady stream of tools that have dramatically changed most scientific fields. The wide availability of electronics, such as digital recording devices and affordable data processing and storage options, allows for the study of animal behavior with a resolution that was previously unattainable. Olfactory preference and learning assays in *Drosophila* have traditionally used population assays, such as the T-maze designed for the original learning demonstrations in the Benzer lab[66]. While such assays established the foundations of the entire field of learning and memory in *Drosophila*, there is much to be gained from the analysis of individual, rather than population activity. For one, it has been shown that interactions between flies can effect their collective behavior[379], potentially confounding

the interpretation of any given behavioral phenotype. Furthermore, tracking the behavior of individual animals over time allows for higher resolution analysis of their behaviors, providing insight into the specific actions that lead to the endpoint measurements often recorded in population assays[380]. This type of high resolution behavioral tracking has led to insights into the structure of animal behavior in many different model organisms[211,220,363,381–383]. In mice, for instance, novel methods of recording and analysis coupled with neural recordings are beginning to delineate the contributions of the direct and indirect striatal pathways to behavior, as described above[382]. The application of modern methods in machine learning have increasingly improved the resolution and accuracy of the automated classification of behaviors, giving insight into the structure of behavioral transitions and the neural mechanisms underlying them[384–386]. Recent studies of behavior in the nematode, *C. elegans*, have utilized automated behavioral tracking of worms to link various neuromodulatory systems with the expression of individuality in behavioral patterns[387], while others have attempted to decipher the circuit basis for integration of sensory information in order to execute an appropriate response[388]. These studies, among many others, indicate how the increased capacity for monitoring individual animals has contributed to our understanding of the link between neural circuitry and the execution of specific behaviors.

In *Drosophila,* single animal tracking assays have also proven to be extremely useful. Tracking the trajectories of individual flies in an odor choice task has identified

neural circuits that appear to accumulate sensory evidence and use that information to make behavioral decisions[220,389]. Other studies have used high resolution behavioral data to begin to dissect the strategies used by flies to navigate towards or away from various stimuli[118,211]. Such analyses have revealed that flies can use distinct tracking strategies to approach different appetitive odors[390], and suggested that flies might perform path integration in order to return to the site where they received an appetitive stimulus[347]. Thus, the development of tools for monitoring the behaviors and olfactory preferences of individual flies in our own lab and others[220,336,339] has begun to provide new insight into the behavioral strategies and neural circuits used.

With the development and refinement of assays to measure individual animal behavior comes the possibility of measuring neural activity in the context of specific behaviors of interest. In certain vertebrate systems, continuing improvements in electronics miniaturization allows for the possibility of mounting recording devices on a freely behaving animal[381,391,392]. In many cases, however, and certainly in flies, the best tools available for high resolution neural recordings require placing the animal in a head-fixed apparatus (although see Grover et al.[393] for an intriguing exception). This necessity for head-fixed recordings while trying to monitor naturalistic, individual animal behaviors provides a formidable challenge. In freely behaving animals, the actions taken, almost invariably, will cause some change in the animal's environment, which is then sensed by the animal. Such feedback may be inconsequential in peripheral sensory circuits with relatively invariant responses to specific stimuli. As we move into higher brain circuits,

however, where patterns of activity rely upon multimodal integration and state-dependent modulation, the lack of this closed loop interaction between animal behavior and sensory input becomes highly problematic. For this reason, there has been an increasing push for placing head-fixed animals in realistic virtual environments, meant to mimic the experience of unrestrained behavior[341,394–396]. In flies, the development of virtual environments containing visual landmarks has contributed greatly to our understanding of navigational decisions made in flight[397] and the spatial representations of environments maintained in the central complex, described above[342,343,346].

Here too, improvements in the available technology have contributed greatly to our ability to create virtual environments that elicit naturalistic behaviors. In the case of the closed loop olfactory system describe here, the use of high resolution 3D printing technology, fast image analysis software for the tracking of spherical treadmill rotation[344] and affordable microprocessor-based electronics platforms, such as Arduino, facilitated the design, prototyping and execution of multiple iterations of this system. The finished product allows us to monitor and manipulate the activity of neural circuits in the fly brain while the animal executes realistic olfactory anemotaxis behavior (Figures 6.2-6.5). This system is now being used in the lab to directly explore how the dopamine-induced plasticity we observed in the MBONs correlates with the individual behavioral responses to odors. Recording from the population of DANs during navigation in this apparatus has also given us insight into the role of this modulatory network in the execution of goal-

directed behaviors. As is often the case, however, as the resolution and sensitivy of our tools improves, they continue to reveal additional questions for future study.

The Dopaminergic Network and the Encoding of Behavioral State

Our ongoing examination of the DAN network in the context of olfactory navigation (Figure 6.5) highlights what can be learned from new tools, but also raises additional questions. By recording from the DAN population while animals navigate in a virtual olfactory environment, we have identified a detailed representation of the sensorimotor state of a fly in the DAN network activity. These investigations paint a picture of the MB DAN system that increasingly resembles what is known about dopaminergic circuits of the basal ganglia. As in mammalian DANs, we observe motion related signals in parallel with reward representations. These patterns of activity correlate with multiple behavioral parameters, such as locomotor state and velocity, as well as sensory inputs, such as odor stimuli and wind direction. Because these DANs are genetically identifiable across animals, we are able to precisely quantify these relationships and determine that the same individual dopaminergic neurons that respond to reinforcement stimuli also represent these aspects of locomotion. Finally, by recording the activity in this modulatory network across different internal states and sensory environments, we are beginning to identify changes in network parameters that suggest a role in encoding motivational state–a hypothesis which we are primed to

investigate through perturbations of particular circuit elements. In addition to helping us to understand the role of the DAN network in the MB circuitry, it is our hope that insights gained in this relatively simple nervous system might help to clarify the complexity and controversies regarding the role of DANs in the basal ganglia.

Nonetheless, these investigations have also raised many questions as to the function of these dopaminergic signals in the MB. One possibility is that these ongoing patterns of motor-related dopaminergic activity might actively modulate MB activity, thereby contributing to the ongoing behavior of the fly. This possibility has gained support from studies suggesting that the MB, and the DAN network, does, indeed, play a significant role in controlling fly behaviors such as food-seeking[136], sleep[118,124] and context-dependent odor responses[127,307]. This idea is also consistent with our demonstration of robust odor-independent potentiation of KC-MBON synapses by the ongoing DAN activity in a tethered animal (Figure 5.4). We found, for instance, that in our *in vivo* preparations, the odor responses of the γ2 and γ3 MBON are much greater than those in the γ4 and γ5 MBONs (Figure 5.1), likely due to the ongoing aversive signal in the γ2-γ3 DANs during flailing (Figures 3.3D-E, 4.6F). Since the γ2-γ3 MBONs have been shown to drive approach behavior[118] (Figure 6.3E), these results lead us to speculate that when the fly is in a particularly dire situation, any incoming odor stimulus is considered more attractive than it otherwise would be. This makes intuitive sense and is in line with behavioral experiments which have demonstrated that flies show reduced odor aversion (or, in other words, increased odor attraction) following exposure to an

electric shock[315]. Conversely, when the fly is in a particularly rewarding situation (leading to higher activity in the γ4-γ5 DANs and increased odor responses in the avoidance-inducing γ4-γ5 MBONs), incoming odors should be interpreted as being less attractive, leading the animal to remain in its current, rewarding, situation. Thus, the ongoing activity of the distributed DAN network, encoding information about an animal's current environmental context and behavioral state, is poised to continuously reconfigure the activity patterns of the MBON population to allow for adaptive odor responses based on the acute needs of the animal.

However, there are several other possible roles for the ongoing DAN activity that may occur instead of, or in parallel with, direct modulation of fly behavior[275]. For instance, given the prominent role of the DANs in associative learning, it is possible that the behavioral modulation of DAN activity may serve to gate the capacity for learning. The idea that learning rules can be altered has been explored in the locust MB, where octopaminergic modulation has been shown to control the timing windows for STDP[129]. It has also been suggested that one role of the dopaminergic circuitry of the basal ganglia is to gate the updating of goals or context in the prefrontal cortex[291]. Interestingly, it was recently demonstrated that the locomotor state of mice has a robust effect on their ability to learn in an eyeblink conditioning task[398]. If learning is similarly contingent upon behavioral state in the fly, reafferent motor signals in the DANs might serve as the mediators of this gating mechanism. In parallel with the development of the closed loop apparatus described here, Thomas Graham, a postdoc in the lab, has

developed a high-throughput assay for measuring anemotaxis behavior in freely behaving flies. Analysis of learning effectiveness in individual, freely behaving flies might allow us to begin to investigate the possibility that learning is contingent upon the locomotor state of the fly at the time of training. This system can also be used to explore the possibility that motor-related DAN activity might be relevant in operant learning, where rather than learning an association between two stimuli controlled by the experimenter, the fly must execute a particular behavior in order to lead to a rewarding stimulus [399].

Finally, there is experimental and computational support for the idea that the ongoing activity of the DANs might direct the formation, consolidation and erasure of memory traces in the MB. In an intriguing demonstration of the capacity of the MB as a general-purpose learning machine, Ardin et al. showed that a MB-like circuit could be used to record visual snapshots along the foraging route of an ant, in a way that could then be used to chart a course back to the home nest[195]. This model utilized a periodic plasticity-inducing signal to record each snapshot, but this role would likely be played by the DANs in an actual MB. Thus, it is easy to imagine that the motor signals represented in the DANs might serve as salience detectors, indicating the significance of the current context, and forming a plasticity window in the MB synapses. Indeed, the idea that the MB plays a role in the detection of salient or novel sensory cues has also recently found experimental support[123]. Other experimental results have suggested that the ongoing DAN activity might be important for the consolidation of memories for longer term

storage[272] and that movement-related DAN signals are particularly important for the active forgetting of previously learned associations[274,306]. Thus, the complex encoding of movement in the DAN network raises many intriguing questions and possibilities for the roles of these neuromodulatory signals.

A Recurrent Neuromodulatory Network

Understanding the potential significance of the DAN network in the various behavioral roles described above will require investigation into the functional effects of dopaminergic release on downstream effectors. Our investigations of dopamine-mediated plasticity at KC-MBON synapses aids in our understanding of the role of DANs in the formation of associative memories, while hinting at additional forms of plasticity that might underlie other functions of this circuit. The tools and protocols we used here are likely to be similarly effective in further exploring the other, non-associative effects of DAN activity in the MB. However, the interconnectedness of the MB circuitry and the complexity of the interactions between the different neuronal classes will also necessitate the development of new tools and technologies. For instance, recent EM studies of the MB have demonstrated the presence of a number of unexpected synaptic relationships in the MB lobes, including direct synaptic connections between DANs and MBONs and axo-axonic connections between KCs[305]. A more complete understanding of the effects of dopaminergic modulation on the MB will

therefore rely upon our ability to isolate different pairs of synaptically connected populations for independent manipulation.

Furthermore, our DAN population imaging demonstrated that the dopaminergic inputs to each compartment represent both appetitive and aversive stimuli through bidirectional changes in their activity, and that DANs and MBONs of different compartments are functionally linked through complex multisynaptic interactions. Thus DANs may not act independently but, as a consequence of their rich interconnectivity, provide a coordinated representation of reinforcement experiences to orchestrate plasticity at KC-MBON synapses throughout the mushroom body. One implication of the functional interdependence of DANs is that positive or negative reinforcement may be conveyed to an odor by either the activation or suppression of specific DANs in different compartments. Indeed, behavioral studies suggest a requirement for DANs activated by aversive stimuli in appetitive learning[219] and a role for sugar-responsive DANs in relative aversive learning[400]. Intriguingly, midbrain DANs responsive to punishment and reward also project to distinct targets in the mammalian brain and display a similar functional opponency as a consequence of reciprocal network interactions[29,36,239,401]. Thus the concerted and partially antagonistic action of neuromodulatory pathways responsive to stimuli of opposing valence may represent a general and conserved circuit principle for generating adaptive behavioral responses.

While DAN network activity regulates the transmission of olfactory information to MBONs, the extensive feedback we observe between MBONs and DANs suggests that the net output of the mushroom body can dynamically shape the activity of the dopaminergic network. Such recurrent connectivity is a fundamental feature of circuits that use information from one moment to shape neural function at later time-points[402,403]. Thus the patterning of MBON activity by an animal's state or experience has the potential to both bias its immediate olfactory behavior as well as influence future responses through positive or negative feedback onto different DANs. An interesting consequence of this arrangement is that the plasticity induced on MBON odor responses by a previously learned association will influence the dopaminergic activity elicited by that odor. A recent study investigated a particular MBON-DAN feedback circuit and found that this recurrence allows the fly to re-evaluate an odor that was previously associated with an appetitive sugar reward[285]. When the fly is re-exposed to an appetitively trained odor, but denied the expected reward, the modulated pattern of activity in the DANs leads to the formation of a parallel, aversive 'disappointment' memory[285]. Interestingly, the withholding of a reward in this paradigm leads to a change in DAN activity that is reminiscent of the RPE that emerges in mammalian DANs when an expected reward is denied.

The complexity of activity patterns in the DAN network and the feedback connections between MBONs and DANs emphasizes the need to identify the sources of synaptic input onto the DANs. Recent studies have begun to trace specific sensory

pathways that feed into the DANs, including gustatory projection neurons[404] and afferents from the LH branch of the olfactory pathway[405]. However, these circuits likely represent only a small fraction of the inputs onto the DANs, and unfortunately, at present there are no effective means for retrograde tracing of neural circuits in the fly. In place of genetic tracing mechanisms, EM reconstructions of progressively larger portions of the fly brain, in larvae and adults, have begun to provide some insight into the circuitry upstream of the DANs[165,305,406]. The picture emerging from this connectomic data is that the DANs are likely to receive synaptic input from hundreds or thousands of different sources. Understanding how the complex activity patterns in the DAN network emerge will therefore require identification of which input synapses are particularly significant in controlling DAN activity in different behavioral or sensory contexts.

Towards an Understanding of a Complete Flexible Sensorimotor Circuit

The ultimate role of the nervous system is to use the totality of sensory information available to select the set of actions that will give an animal the greatest chance of surviving in its environment. Thus, tracing the route of neural circuits that link sensory input to behavioral output, and understanding how sensory signals are processed and transformed along the way is a fundamental goal of neuroscience. In the simplest cases, studies of monosynaptic reflex arcs, in which a specific stimulus elicits an acute, innate response, have elucidated basic properties of input-output coupling in

neural circuits[407]. In organisms with relatively simple nervous systems, sensorimotor circuits spanning a small number of synaptic connections have been used to investigate various forms of non-associative learning and context-dependent modulation of behavior[17,77,408]. Meanwhile, studies of neural circuits underlying innate behaviors in *Drosophila* have provided valuable insight into the computational principles that lead from sensation to appropriate behavioral responses. For instance, the delineation of the olfactory and gustatory processing pathways underlying male *Drosophila* courtship behaviors identified circuit motifs, such as balanced coupling of feedforward excitation and inhibition, that might serve to gate entry into particular behavioral states[164,409]. Recent investigations in the *Drosophila* visual system identified a set of optic lobe neurons that detect approaching dangers and directly connect to a neuron that induces rapid escape behavior[410,411]. These studies revealed an elegant neurophysiological circuit for the selective activation of these neurons by looming stimuli as well as a neural circuit mechanism for selecting the type of escape behavior to execute. These findings, among many others, exemplify the types of insights that have been gained by leveraging the tools of modern neuroscience to the tracing and interrogation of sensorimotor pathways.

The MB sits at the nexus between the mostly feed-forward sensory processing steps of the olfactory sensory circuitry and the output circuits that control the execution of the entire behavioral repertoire of the fly. Thus, understanding how the dopaminergic network shapes the flow of sensory information through the MB helps to fill in an

essential link that brings us closer to the complete tracing of a sensorimotor circuit connecting complex, arbitrary sensory stimuli with flexible behavioral output. Our investigations are built on the solid foundation of knowledge about the early stages of sensory processing, from sensation at the periphery through the olfactory PNs that carry odor signals to the KC dendrites in the MB calyx. The sensory signals passing through these early layers are filtered and transmitted into the expanded coding space available in the large population of KCs as a sparse encoding of odor identity. The coordinated activity of the DAN network, representing both salient external stimuli and the internally generated behavioral state of the fly, precisely modifies synaptic connectivity in the MB lobes. In doing so, they condense the sparse KC odor code into a lower dimensional representation of odor valence in the MBON population that encapsulates the learned experience and current circumstances of the individual. Our development of a closed loop olfactory navigation system has allowed us to further investigate the MB circuitry in the context of a fly engaged in realistic odor tracking behavior. Going forward, this system will provide the opportunity to explore how the patterns of modulated activity in the MBON population lead to the execution of specific odor-related behaviors. In doing so, we will come closer to the goal of tracing the flow of flexible sensorimotor processing from sensory input to behavioral output.

Conclusion

Together with decades of research on this fascinating structure, the work we present here suggests that the MB embodies many of the properties that we associate with neural circuits responsible for higher cognitive functions. It serves as a convergence point for multimodal signals representing a range of sensory stimuli as well as internal and behavioral state information. This convergence allows for sensory processing to be modulated in complex ways, such that the behavioral response of the fly takes into account a whole range of relevant contextual information. Furthermore, through the use of neuromodulatory mechanisms with long-lasting effects on the MB circuitry, the fly's decisions rely not only on current circumstances but are informed by its previous experiences. These properties of the MB, combined with the striking functional and anatomical resemblance between the MB and circuits in the vertebrate brain, indicate that the insights we describe here might shed light on the neural mechanisms underlying our ability to learn about and adjust to the world around us. These findings and parallels suggest that the ability to generate flexible behavioral responses based on experience, whether past or present, may rely on common integrative brain structures in which neuromodulatory networks act with exquisite spatial and temporal precision to shape sensory processing.

Materials and Methods

Generation of syt-GCaMP Transgenic Flies

The coding sequence for GCaMP6s[246,412] (Addgene Plasmid #40753) was appended to the *Drosophila* synaptotagmin 1 coding sequence (DGRC Stock #4839) with an intervening 3xGS linker by PCR and Gibson Assembly[279]. The resulting product (syt-GCaMP) was ligated into pJFRC- 10xUAS (Addgene Plasmid #36432) and pJFRC-LexAOP (Addgene Plasmid #26224) and used to generate transgenic flies by PhiC31-based integration into attp40, attp5 and VK00005 by Bestgene Inc. Additional transgenics were generated in which GCaMP6s was tethered to synaptogyrin (DGRC Stock #17821) but preliminary expression studies in Kenyon cells revealed inferior presynaptic localization with fluorescence along the shaft of axons lacking presynaptic sites (data not shown).

Fly Strains

Flies were maintained on conventional cornmeal-agar-molasses medium at 23-25°C and 60-70% relative humidity, under a 12 hr light: 12 hr dark cycle.

Strains and sources

VT026001-Gal4, VT043657-Gal4, VT203149-Gal4 (Vienna *Drosophila* Resource Center (VDRC); https://braingazer.org/brainbaseweb); R25D01-Gal4, R93B07-Gal4, R66C08-Gal4, R16A06-Gal4, R35B12- Gal4, R53C03-LexA, R25D01-LexA, R14C08-LexA, R58E02-Gal4, R58E02-LexA, R60A06-Gal4, R37G12[413], 83F01-Gal4[376],

MB298B, MB77B, MB83C[118] (http://flweb.janelia.org/cgi-bin/flew.cgi), *trans*-TANGO[348] (gift from Mustafa Talay and Gilad Barnea), UAS-GCaMP6s, UAS-tdTomato, LexAOP-tdTomato, LexAOP- ReaChR[259], MZ19-Gal4[414], ORCO-Gal4, nSYB-Gal4, VGlut-Gal4, UAS-DopR2-RNAi (TRiP.HMC02893, generated by the TRiP at Harvard Medical School (NIH/NIGMS R01-GM084947)) (Bloomington *Drosophila* Stock Center); MB247-DsRed[99] (gift from Andre Fiala, University of Göttingen); MB247-LexA[280] (gift from Scott Waddell, University of Oxford); LexAOP-P2X2[258] (gift from Orie T. Shafer, University of Michigan); OK107-Gal4[264]; TH-Gal4[415]; DDC-Gal4[416]; Tub>Gal80>[310] (gift from Kristin Scott, University of California, Berkeley); fmn dDAT mutant[307]; DopR1attP, DopR2attP[164], DopR1attP-DopR2attP Double Mutant (Gift from Daisuke Hattori); UAS-C3PA-GFP, LexAOP-SPAGFP-T2A-SPAGFP[300]; UAS-FLP, brp>STOP>GFP[164,417] (gift from Larry Zipursky, University of California, Los Angeles).

Detailed fly genotypes used by figure (with neuronal expression description):

Figures 2.2B,2.3B,4.4A:
LexAOP-SPA-T2A-SPA;MB247(KCs)-LexA, LexAOP-SPAGFP

Figures 2.3C, 5.1, 5.4C,:
UAS-GCaMP6s;VT026001(γ4-MBON)-Gal4,UAS-GCaMP6s/R25D01(γ2-MBON)-Gal4
UAS-GCaMP6s/UAS-GCaMP6s;R93B07(γ3-MBON)-Gal4/R66C08(γ5-MBON)-Gal4

Figure 2.3D:
UAS-C3PA-GFP/UAS-C3PA-GFP;TH(DAN subset)-Gal4, DDC(DAN subset)-Gal4/UAS-C3PA-GFP

Figure 3.1C:
MZ19(PN subset)-Gal4/UAS-tdTomato;UAS-FLP,brp>STOP>GFP

Figure 3.1D-E:
MZ19(PN subset)-Gal4/UAS-sytGCaMP;UAS-tdTomato

Figure 3.1F:
VGlut(motorneurons)-Gal4;UAS-sytGCaMP

Figures 3.2B,D, 3.3, 3.4, 6.5:
UAS-sytGCaMP, MB247(KCs)-DsRed;TH(DAN subset)-Gal4, DDC(DAN subset)-Gal4

Figure 3.2C:
UAS-GCaMP6s; TH(DAN subset)-Gal4, DDC(DAN subset)-Gal4

Figure 3.5A:
UAS-sytGCaMP, MB247(KCs)-DsRed/R58E02(γ4-5 DANs)-LexA;TH(DAN subset)-Gal4, DDC(DAN subset)-Gal4/LexAOP-P2X2

Figure 3.5B:
UAS-sytGCaMP, MB247(KCs)-DsRed/R25D01(γ2 MBON)-LexA;TH(DAN subset)-Gal4, DDC(DAN subset)-Gal4/LexAOP-P2X2

Figure 3.5C:
UAS-sytGCaMP, MB247(KCs)-DsRed/R93B07(γ3 MBON)-LexA;TH(DAN subset)-Gal4, DDC(DAN subset)-Gal4/LexAOP-P2X2

Figure 3.5D:
UAS-sytGCaMP, MB247(KCs)-DsRed/R53C03(γ4 MBON)-LexA;TH(DAN subset)-Gal4, DDC(DAN subset)-Gal4/LexAOP-P2X2

Figure 3.5E:
UAS-sytGCaMP, MB247(KCs)-DsRed/R14C08-LexA(γ5 MBON);TH(DAN subset)-Gal4, DDC(DAN subset)-Gal4/LexAOP-P2X2

Figures 4.1B,D, 4.2A-D, 4.3A,C,D, 4.5A-B, 4.6, 4.7A, 4.8:
UAS-sytGCaMP;R16A06(γ KCs)-Gal4

Figure 4.1C:
UAS-tdTomato, UAS-sytGFP;VT043657-Gal4

Figure 4.2E:
R16A06(γ KCs)-Gal4

Figure 4.3A:
R58E02(γ4-5 DANs),LexA,LexAOp-tdTomato;VT026001(γ4-MBON)-Gal4, UAS-GCaMP6s/25D01(γ2-MBON)-Gal4

Figure 4.3B:
UAS-sytGCaMP/R58E02(γ4-5 DANs)-LexA;R16A06(γ KCs)-Gal4/LexAOP-tdTomato

Figures 4.3E, 4.4B:
hsFLP;UAS-sytGCaMP/UAS-tdTomato;R16A06(γ KCs)-Gal4/Tub>Gal80>

Figure 4.5C:
UAS-sytGCaMP;R35B12(α'β' KCs)-Gal4

Figure 4.7B,D:
UAS-sytGCaMP/R58E02(γ4-5 DANs)-LexA;R16A06(γ KCs)-Gal4/LexAOP-P2X2

Figure 4.7C:
UAS-sytGCaMP;R16A06(γ KCs)-Gal4/(LexAOP-P2X2)

Figure 4.8A-E:
UAS-sytGCaMP;;OK107(KCs)-Gal4

Figure 4.8A:
UAS-sytGCaMP;DopR2attP/DopR2attP;OK107(KCs)-Gal4

Figure 4.8B:
UAS-sytGCaMP/UAS-DopR2-RNAi;16A06(γ KCs)-Gal4

Figure 4.8C:
nSyb(neuronal)-Gal4nSyb(neuronal)-Gal4/UAS-DopR2-RNAi

Figure 4.8D:
DopR1attP/DopR1attP;OK107(KCs)-Gal4

Figure 4.8E:
DopR1attP, DopR2attP/ DopR1attP,DopR2attP;OK107(KCs)-Gal4

Figure 4.8F
dDAT mutant/dDAT mutant;R16A06(γ KCs)-Gal4/UAS-sytGCaMP

Figures 5.2A, 5.3A, 5.4A, 5.5A-H, 5.6:
UAS-GCaMP6s/R58E02(γ4-5 DANs)-LexA;VT026001(γ4-MBON)-Gal4,
UASGCaMP6s/LexAOP-P2X2

Figure 5.2B-C:
UAS-GCaMP6s/R58E02(γ4-5 DANs)-LexA;VT026001(γ4-MBON)-Gal4/LexAOP-ReaChR

Figure 5.2D:
UAS-GFP/R58E02(γ4-5 DANs)-LexA;R16A06(γ KCs)-Gal4/LexAOP-P2X2

Figure 5.3B:
UAS-GCaMP6s;VT026001(γ4-MBON)-Gal4,UAS-GCaMP6s/(LexAOP-P2X2)

Figure 5.3C:
R25D01(γ2 MBON)-LexA/UAS-P2X2;VT203149(γ2 DAN)-Gal4/LexAOP-GCaMP6s

Figure 5.3D:
R25D01(γ2 MBON)-LexA/(UAS-P2X2);LexAOP-GCaMP6s

Figures 5.3E, 5.4B, 5.5I:
R58E02(γ4-5 DANs)-LexA/UAS-GCaMP6s;25D01(γ2 MBON)-Gal4/LexAOP-P2X2

Figure 5.3F:
R53C03(γ4 MBON)-LexA/UAS-P2X2;VT203149(γ2 DAN)-Gal4/LexAOP-GCaMP6s

Figure 6.3A, D:
UAS-csChrimson; ORCO(OR83b, OSNs)-Gal4;

Figure 6.3C:
UAS-csChrimson;;

Figure 6.3E:
UAS-csChrimson;MB77B(γ2 MBON)split-Gal4

Figure 6.3F:
UAS-csChrimson;MB298B(γ4 MBON)split-Gal4

Figure 6.4C:
trans-TANGO x MB298B(γ4 MBON)split-Gal4
trans-TANGO x MB77B(γ2 MBON)split-Gal4
trans-TANGO x MB83C(γ3 MBON)split-Gal4

Figure 6.4D:
UAS-GCaMP6m;R60A06(EPGs)-Gal4

Figure 6.4E:
UAS-GCaMP6m;R37G12(PFNs)-Gal4

Figure 7.1:
UAS-GCaMP6s;83F01(IN1)-Gal4

Sparse Labeling

Sparse labeling of γ KCs for functional imaging (Figures 4.1C, 4.3E, 4.4B) was achieved by stochastic excision of ubiquitous Gal80 repression through expression of FLP-recombinase under the heat-shock promoter as described[418]. Briefly, flies with the genotype: hsFLP;UAS-sytGCaMP/UAS- tdTomato;R16A06(γ KCs)-Gal4/Tub>Gal80>, were incubated at 21°C to reduce spontaneous FLP-recombinase activation and transferred into new vials every 1-2 days. During the late pupal stage the vials were heatshocked by immersion in a 37°C water bath for 10-30 minutes and then returned to incubation at 21°C until dissection.

Imaging

All functional imaging experiments were performed on an Ultima two-photon laser scanning microscope (Bruker Nanosystems) equipped with galvanometers driving a Chameleon Ultra II Ti:Sapphire laser. Emitted fluorescence was detected with either photomultiplier-tube or GaAsP photodiode (Hamamatsu) detectors. Images were acquired with an Olympus 60×, 0.9 numerical aperture objective at 512 pixels × 512 pixels resolution. For fast-scanning volumetric imaging in vivo, the laser was directed through an 8kHz resonant scanning galvonometer and the objective was controlled by a piezo-electric Z- focus. Z-planes were defined in order to encompass the entire volume of the γ lobe. 12-18 planes were recorded, spaced ~2 μm apart and the entire volume was imaged at a rate of ~1.5Hz.

Photolabeling of neurons

To photolabel DANs innervating specific γ lobe compartments (Figure 2.3D) we expressed C3PA-GFP in most DANS driven by the combination of TH-Gal4 and DDC-Gal4. To label individual γ KCs (Figures 2.1C, 2.2B, 2.3A-B, 4.4A) we expressed SPA-GFP in all KCs driven by MB247-LexA. We targeted specific γ lobe compartments (for DAN labeling) or individual KC soma (for single KC labeling) using 925 nm laser illumination, a wavelength that does not cause significant photoconversion. To photolabel neurons, we defined an ROI in PrairieView Software in a single Z-plane and exposed the target area to 710 nm light (~10-30 mW at the back aperture of the objective) 10-15 times. After diffusion of the photoconverted fluorophores throughout the targeted neurons for 10-30 minutes, we imaged at 925 nm using 1 µm steps.

Functional Imaging

For *ex vivo* experiments brains were dissected in external saline (108 mM NaCl, 5 mM KCl, 2 mM CaCl2, 8.2 mM MgCl2, 4 mM NaHCO3, 1 mM NaH2PO4, 5 mM trehalose, 10 mM sucrose, 5 mM HEPES pH7.5, osmolarity adjusted to 275 mOsm), briefly treated with collagenase in external saline (2 mg mL-1, 30 sec), washed, and then pinned with fine tungsten wires to a thin Sylgard sheet (World Precision Instruments) in a 35 mm petri dish (Falcon) filled with saline. For *in vivo* imaging, flies were prepared as previously described [419]. Briefly, 2-5 day old flies were temporarily anaesthetized using CO2 (for <30 s) and then tethered to a piece of tape covering a hole in the bottom of a modified 35 mm petri dish using a human hair placed across the

cervical connectives. A small hole was cut into the tape, precisely above the head, to allow the top of the head capsule to extend above the plane of the tape. A dot of UV-curable glue (Loctite) was applied to the eyes to restrict head movement. The dish was then filled with external saline and the head capsule was opened by carefully cutting and folding back the flap of cuticle covering the dorsal portion of the head. Muscle 16 and obstructing trachea were removed with sharpened forceps. In ATP and acetylcholine injection experiments, the open head capsule was briefly bathed in collagenase (2 mg mL-1, 30 sec) to weaken the perineural sheath. Care was taken to keep the antennae and antennal nerves intact. On rare occasions, flies showed no movement or odor responses and were discarded. For closed loop behavior experiments (Figure 6.1-6.5) flies were glued into custom imaging chambers as previously described[342]. Chambers were milled out of delrin on a Roland 540 MDX CNC with Tool Magazine and Rotary Axis attachments.

Volumetric imaging of single KC in a brain explant

To visualize Ca^{2+} influx throughout the axonal arbor of a single KC (Figures 4.1B) with high spatial resolution, the same voltage was used to repeatedly iontophoretically stimulate the calyx with acetylcholine as described below, allowing for equivalent activation of the neuron at each of 45 planes spaced ~1 µm apart. The representative image shown is the maximum Z-projection of the peak intensity response to stimulation for each imaging plane. In comparison to volumetric imaging by resonant scanning used *in vivo* (below), this strategy yielded better image quality due to greater temporal averaging at this slower scanning rate.

Odor stimulation

Odor stimulation was achieved by directing a continuous stream (400-500 mL/min) of clean air through a 2 mm diameter teflon tube directed at the fly's antenna (carrier stream). 5-10% of the total airstream was diverted through the headspace of a 10 mL glass vial containing paraffin oil (odor stream). At a trigger, a custom-built solenoid valve controller system redirected the odor stream from a blank vial to a vial containing various odorants diluted in paraffin oil (Sigma) to a final volume of 1 mL. Final odorant dilutions were between 1:20-1:200, depending on the identity of the odorant. In experiments where odor concentration was varied (Figures 4.5B and 4.6E), the fraction of odor stream directed to the fly was adjusted to give final concentrations between 1:100 and 1:1000. Odorants used were isobutyl acetate (CAS #110-19-0), trans-3-hexen-1-ol (CAS #928-97-2), benzaldehyde (CAS #100-52-7), 3-octanol (CAS #589- 98-0), methancyclohexanol (CAS #589-91-3) and Apple Cider Vinegar (Heinz). In a subset of experiments, a fraction of the olfactometer output air stream was redirected to a mini-PID (Aurora Scientific) in order to measure odorant waveforms and ensure the consistency of odor presentations across trials. Given that we observed no difference in the patterns of pre-synaptic Ca^{2+} along KC axons or MBON responses to different odorants, we averaged responses across odors to generate the normalized odor-evoked syt-GCaMP profile in Figures 4.3 and to generate MBON response profiles in Figure 5.1.

Activation of P2X2-expressing Neurons by ATP Injection

To activate DANs or MBONs expressing P2X2, a glass stimulating electrode, pulled to a resistance of 7-10 MΩ, was filled with 2 mM ATP in external saline. Stimulating electrodes were positioned dorsal to the mushroom body's medial lobes, in the superior medial protocerebrum, at the site of rich γ4 and γ5 DAN dendritic and MBON axonal innervation. In some experiments tdTomato was co-expressed in R58E02+ DANs to serve as an anatomic guide. The stimulating electrode was coated with BSA-conjugated Texas Red Dye (Life Technologies) in order to visualize electrode position[67,68]. In experiments examining *in vivo* modulation of KC presynaptic Ca^{2+}, ATP was injected in short bursts (~15 pulses) over the span of 2-3 minutes, with >1 minute between the pre-injection odor stimulus and the start of injection and >1 minute recovery period following injection before post-injection odor stimulus. For the pairing protocols in Figure 5.6D, ATP was iontophoresed for 600ms at 5V alone (unpaired), immediately following a 500ms stimulation of KCs (forward paired) or ending 500ms before start of KC stimulation (reverse paired). For all other experiments involving ATP injection a single brief pulse of positive pressure was applied manually or using a custom-built pressure injector. Protocol for ATP stimulation in other experiments described below.

Calycal and Glomerular Stimulation

Glass stimulating electrodes were pulled to a resistance of 7–10 MΩ and then filled with 10 mM acetylcholine (Sigma) in external saline. Stimulating electrodes were positioned into the mushroom body calyx or the center of the DA1 glomerulus (Figure

3.1D) viewed under IR-DIC optics. Square voltage pulses (500 ms long, 0.1-10V for all imaging experiments, 0.1-2ms long, 10-100V for electrophysiology in Figure 5.2A) generated by a stimulator (Grass Technologies) were used to excite Kenyon cell or antennal lobe projection neuron dendrites. To account for variation in electrode tip and positioning, the iontophoretic voltage was titrated to evoke robust but non-saturating responses in the neurons being recorded. For Figure 4.1, the iontophoretic voltage was titrated until 1-2 KCs were stimulated, as evident by a sole active process running through the pedunculus where KC axons are unbranched, fasciculated, and parallel. For Figures 4.6, stimulation was performed twice at each voltage indicated between 1-10V.

Paired and Unpaired Stimulation Protocols

For 'paired' stimulation of DANs and KCs, KC stimulation and DAN activation via ATP injection were temporally paired as illustrated in Figure 7G. In experiments where KCs were directly activated (Figures 7H-I and S7C-J) KC stimulation was performed as described above for a duration of 500 ms, immediately followed by a 200 ms ATP injection via pressure injector as described above. For odor stimulation in vivo (Figure 7J), two odors (isobutyl acetate and hexanol) were each presented as described above at least 2 times with >45 seconds between exposure to establish stable baseline responses. One of the odors was then paired with a 200 ms pressure pulse of ATP beginning 500 ms after the start of the odor pulse. Each odor was used as the 'paired' odor in alternate experiments in order to control for any odor-specific effects. All DAN activation experiments were 'unpaired' unless noted. In 'unpaired' experiments, KC

stimulation or odor presentation were performed >45 seconds before and after ATP injection in order to temporally separate DAN and KC activation.

Recording Fly Motor Activity

To simultaneously record the dangling fly's motor activity during imaging (Figures 2B, 2D-2E, and S2) a Point Grey Firefly Camera with Infinity Lens (94 mm focal length) was focused on the fly, which was illuminated by infrared LED lights. Video was captured at 30 frames per second. Fly motion traces were extracted using a custom Matlab script that measures average absolute difference in pixel intensities between each frame and the preceding frame. Manual inspection of this automated analysis confirmed that it accurately registers the difference between the two behavioral states (flailing and quiescence) we observed in the tethered fly. Laser-scanning onsets and offsets, visible in the video recordings due to laser illumination through the head-capsule were used to align videos with imaging data. In light of the demonstrated correlation between DAN activity state and fly locomotion, we note that all other imaging experiments were performed without regard for the fly's behavioral state, which was presumably a comparable alternating pattern of flailing and pausing.

Sugar feeding

1-3 day old flies were fasted for 20-26 hours by transferring to an empty vial containing only a damp Kim- wipe. Flies were tethered for imaging as described above and positioned on the microscope. After recording baseline neural responses, a small wick of Kim-wipe fibers soaked in 0.2-1 M sucrose solution was positioned near the fly's

proboscis using a motorized micromanipulator (Scientifica). The wick was touched to the proboscis to initiate feeding. Blue food coloring was added to the sucrose solution and fly abdomens were inspected after each experiment to confirm sucrose ingestion. Data for flies that had not consumed the sucrose solution were discarded. We observed no apparent difference in evoked changes in KC activity depending on sucrose concentration so data from different stimulations were pooled. For DAN and MBON imaging 0.2 M sucrose solution was uniformly used. Sugar feeding for imaging of Pharyngeal Interneurons is described in Yapici et al.[376]

Electric Shock

The *in vivo* dissection dish described above was modified so that two steel threaded studs (McMaster-Carr) could be precisely positioned to make contact with either side of the fly's abdomen during tethering. The ends of the steel electrode leads were connected to a stimulator (Grass Technologies), which was used to apply a 500 ms pulse of 60-150V, comparable to the electrical shock parameters used in classical olfactory conditioning paradigms[420]. Current flow through the circuit was monitored by an oscilloscope and the stimulating voltage was adjusted to maintain approximately equivalent current flow across trials to compensate for buildup of resistance following shocking.

Simple Simulated Walking (Figure 3.4B)

A small foam ball (~1 mm diameter, Matsubara Sangyo Co.)[421] was positioned within the fly's grasp to allow the fly to 'walk' on the ball during imaging. Placement was adjusted to ensure free range of motion over 360°.

Closed Loop System

Air-supported foam ball was modified based on Seelig et al.[346] and Green et al.[342]. The ball was recorded using the camera/light setup described above at 60 fps. Ball rotation was calculated in real time using FicTrac software[344] running on Ubuntu 12.04 on computers with processors with speeds of at least 3GHz. FicTrac-calculated heading was transmitted to an Arduino Mega via serial port. Custom Arduino code was used to translate heading into tube position controlled by motors described below. For white noise stimuli, tube movement was controlled independently of tracking data using random movements with parameters based on previously recorded closed loop data. White noise odor presentations consisted of a combination of a) presentation of odors at random intervals (10-15s) and of random duration (1-5s) and b) m-sequence presentation with minimal duration of 500ms.

Both iterations of the closed loop air-delivery system were custom designed using OnShape (www.onshape.com) and 3D printed using Visijet Crystal material at XHD resolution in a 3DSystems Projet 3510 HD Plus. O-ring OD and ID Gland surfaces were designed with excess material for printing, then manually modified on a lathe for improved RMS [surface] finishing. Tube rotation for the first iteration 180 degree system

was driven by a MG90S High Torque Metal Gear Micro Servo (Adafruit Product ID 1143). Tube rotation for the second iteration 360 degree system was driven by a bipolar stepper motor (Pololu item #1206) controlled through a A4988 Stepper Motor Driver Carriers (Pololu #2980) coupled by a Dust-Free Timing Belt XL Series, 1/4" Width, (McMaster-Carr, 1679K121, Trade No. 130xL025) to the rotating tube system which rotated mounted on a Ultra-Corrosion-Resistant Stainless Steel Ball Bearing (3/4" Shaft Diameter, 1-5/8" OD, Mcmaster-Carr 5908K19). Air channel was kept airtight using oil-resistant o-rings (1/16 Fractional Width, Dash Number 020, Mcmaster-Carr 2418T126). Motor rotation was measured by a rotary encoder (CUI Inc., AMT10 Series) that was used in order to correct for skipped steps.

Image processing and Data Analysis

All image processing was done using FIJI/ImageJ (NIH). Further analysis was performed using custom scripts in ImageJ, Microsoft Excel, Matlab and R. When necessary, to correct for motion during *in vivo* imaging, recordings were stabilized using the TurboReg ImageJ plugin. When neurons were co-labeled with tdTomato, the MultiStackReg ImageJ plugin was used to stabilize the red channel and the transformations generated were applied to the green functional imaging channel. Images were smoothed with a Gaussian filter (s of 1-2 pixels). Areas outside of the γ lobes were partially masked in representative images for clarity as indicated.

Intensity profile plots (Chapter 4)

The frame containing the peak fluorescence (see below) from an odor stimulus was manually rotated so that the longitudinal axis of the γ lobe lay along the x-axis, with the lateral-most edge at x=0. Regions outside of the γ lobe, easily distinguishable from the dense KC labeling within the lobe, were manually masked in each image. To generate the intensity profile across the lobe, we averaged the intensity of all pixels along the y-axis, for each point x along the horizontal axis of the lobe. To account for variations in imaging orientation, the resulting profiles were normalized to the same length (1000 'pixels') by linear interpolation. The average raw profile length was 315 pixels with a standard deviation of 19 pixels. The resulting 1000 'pixel' profile plots were smoothed by calculating a moving average of 30 'pixels' (3% of the total profile length). Each intensity profile was normalized to its mean intensity value in order to allow for comparison across animals and conditions. Similar results were obtained from normalizing to the maximum intensity value or median intensity value. For every data point, the plots of 2 odor-evoked profiles were averaged to correct for any motion artifacts. Because we observed no difference in the Ca^{2+} profiles evoked by different odorants, we averaged data across odor stimuli. Initial experiments were carried out using the maximum intensity projection from volumetric imaging experiments. However, as we observed little variation in the intensity profile across imaging planes, we combined data from experiments collected in traditional galvo scanning mode at single planes with maximum intensity Z-projections from resonant scanning volumetric data.

When single planes were imaged, we chose planes that revealed the largest longitudinal portion of the lobe and contained γ2-γ5 compartments.

Quantification of neural activity using functional Ca^{2+} imaging is typically performed by normalizing the change in intensity by the pre-stimulus intensity (ΔF/F0). This normalization helps control for variations in reporter expression and imaging parameters so that comparisons can be made between different neurons or different experiments. In quantifying the modulation of KC synapses, however, we found this measure to be inappropriate. The asymmetric distribution of Ca^{2+} along KC axons is often apparent in the basal state, prior to odor stimulation. Differences in synaptic Ca^{2+} along KCs are not present in the brain explant indicating that they reflect in vivo modulation rather than differences in syt-GCaMP expression. Therefore, normalizing odor-evoked responses by the basal fluorescence values would serve to mitigate the modulation we were seeking to quantify. Thus to quantify Ca^{2+} distribution along the γ lobe we used the peak intensity values.

To calculate the change in intensity profiles due to artificial or physiological DAN activation from sugar feeding, we subtracted the average normalized intensity profile measured prior to DAN activation from the average normalized intensity profile after activation in each fly. The resulting difference plot was averaged across flies.

Compartmental border determination (Chapter 4)

To generate an average intensity value for each compartment of the γ lobe we needed to accurately define compartmental borders. In order to define consistent

compartmental borders, we used the strategy outlined in Figure 4.3A. Specifically, flies with fluorescently labeled DANs and/or MBONs (n=10 including TH-Gal4, DDC-Gal4>UAS-GCaMP6s; 58E02-LexA>LexAOP-tdTomato; 25D01-Gal4, VT026001-Gal4>UAS-GCaMP6s) were aligned and profiled as described above to generate the intensity profile plots for KCs. Regions of extrinsic neuron innervation in each compartment were used to generate average border positions, that divided the 1000 'pixels' along the x-axis. We defined the average γ2-3 border at pixel x=297, γ3-4 border at pixel x=560 and γ4-5 border at pixel x=821. The border positions were relatively consistent across animals but showed minor variability due to inevitable individual anatomic variation and differences in imaging orientation (see SEM depicted in Figure 4.3A). Therefore, to account for any potential uncertainty in the border assignment, we calculated the intensity value for each compartment by averaging pixels within the area comprising only the middle 50% of each compartment within the calculated borders. These values were used to calculate significance of intercompartmental differences within individuals, changes within compartments due to DAN activity and differences between control profiles and dopamine signaling mutants or RNAi.

For imaging of DANs and MBONs, ROIs were manually drawn based on the clear anatomic segregation of their innervation patterns in different compartments. For KC time-series traces ROIs were defined by compartmental border determination as described above. For single synapse time-series traces, circular ROIs were manually drawn around individual synapses along the length of the lobe, identified by puncta

labeled with syt-GCaMP. In sparsely labeled KC axons co-expressing syt-GCaMP and tdTomato, the tdTomato signal was first used to generate a mask in order to eliminate background signal due to low basal fluorescence outside of the labeled axons. The syt-GCaMP odor responses were then divided by the tdTomato signal on a pixel-by-pixel basis. For ΔF/F0 calculations in DANs and MBONs the difference between the pre-stimulus value (average of 4-5 frames ending >1 frame before stimulus) and post-stimulus value (average of the 2-3 frames spanning the peak of the stimulus evoked response) was divided by the pre-stimulus value.

Note that in the case of DAN population imaging (Chapter 3), the DANs exhibit strong fluctuations in their basal activity, making it inaccurate to define a single absolute baseline F0. The F0 values used in the heatmap images are therefore simply the immediate pre-stimulus average, as described above, and should not be interpreted as a true minimum baseline. Indeed, because all DAN populations appeared to fluctuate between high and low activity states, the representative traces and stimulus-triggered averages for DAN population activity were all normalized between 0 and 1, where 0 represents the minimum fluorescence of the DAN compartment during a trace and 1 represents the maximum. Raw fluorescence traces of DAN activity depicting the relative levels of activation due to different stimuli are presented in Figure 3.4A. The normalized DAN activity data was used to measure the integrated basal activity in Figure 4.6F. As a consequence, we potentially underestimate the differences between basal signals in each DAN population, as the raw intensities in γ2- γ3 were generally higher than those in γ4- γ5 (data not shown).

Stimulus-Triggered Averages

The normalized time series of syt-GCaMP fluorescence in each compartment were aligned to the time point when the stimulus was applied for each replicate. In the case of flailing behavior, the 'stimulus' refers to the time point at which bouts of leg flailing started and stopped, as identified in the fly motion traces and confirmed by manual video analysis. Traces beginning 5 seconds before the stimulus and ending 5 seconds after the stimulus were averaged and displayed.

Cross-correlation Analysis:

Motion-tracking data was aligned to functional imaging data as described above. Pearson product-moment correlation coefficients between pairs of DANs and between individual DANs and motion were calculated for a 60-120 second recording in each animal. The resulting correlation coefficients were averaged and used to generate the cross-correlogram shown in the figures.

Central Complex Imaging

For EB imaging (Figure 6.4D), the entire EB was imaged using volumetric imaging with 20 z-planes. The resulting volumes were max-projected perpendicular to the imaging plane to allow visualization of the ring-shaped EB. The area of the EB was then split into 16 wedge ROIs of equal angular size for fluorescence measurements. Fluorescence within each wedge was internally normalized. FSB imaging (Figure 6.4E)

except that the volume was z-projected and the span of the FSB was then manually splite into 8 ROIs of equal width.

trans-TANGO

trans-TANGO flies were processed according to Talay et al.[348]. Briefly, male flies were raised for at least 3 weeks at 18C and then immunostained as described above.

Statistical Analysis

Statistical analysis was performed using custom scripts in Excel and R. The significance of all results was tested by ANOVA followed by 2-tailed T-tests with Holm-Bonferroni post-hoc correction for multiple comparisons. Paired T-tests were used for changes in DAN activity due to all stimuli, compartmental differences in KC Ca^{2+}, KC Ca^{2+} changes due to DAN activation or sugar feeding, MBON activity differences and changes, DAN basal activity differences, and comparison of KC spiking due to current injection. Unpaired T-tests were used for DopR/dDAT mutant/RNAi and comparisons of EPSC amplitudes due to optogenetic DAN activation. To measure the significance of changes in DAN activity within each compartment due to exogenous stimuli or changes in behavioral state, DAN activity values were calculated by averaging the fluorescence intensity for 5 frames prior to the stimulus and for the 5 frames spanning the peak of the stimulus evoked response. The same windows were used for all compartments and all individuals within each panel. Changes within each compartment were then measured by paired-T-test (Table 3.1). In some experiments (as indicated), each mushroom body of an animal was treated as an independent sample.

DAN Linear Filters (Figure 6.5H)

Each filter depicts the best-fit relationship between two signals, a predictor (forward velocity, odor, time derivative of air tube angle) and a target (γ4 DAN average activity or difference between left and right γ4 DAN activity). The filter h-values are the weights applied to the predictor signal at different time delays to best predict the target. The best-fit h-values were determined by minimizing the (squared) error between the weighted sum of the predictor values (I.e. the target estimate) using the h-values as the weights, and the true value of the target, averaged over all time points in the trial.

Optogenetic Activation of DANs (Figure 5.2B)

Flies expressing ReaChR, a red-shifted channelrhodopsin variant, in DANs using 58E02-LexA, LexAOP- ReaChr transgenes, were placed on food containing 400 μM all-trans retinal, a ReaChR cofactor, for 18-36 hours prior to dissection. Targeting of the γ4 MBON soma was carried out under fluorescence guidance, using the minimum possible intensity and duration of illumination by a 490 nm LED. Nevertheless, upon initiation of whole-cell recording, we observed that γ4 MBONs exhibited significantly larger excitatory postsynaptic potentials (EPSPs) and excitatory postsynaptic currents (EPSCs) when the 58E02-LexA, LexAOP-ReaChr transgenes were present in comparison to control animals lacking ReaChr expression. This observation suggests that ReaChr stimulation during dissection of the brain from its capsule under white light LED illumination and targeting of the γ4 MBON soma under fluorescence illumination is sufficient to activate DANs and alter properties of synaptic transmission.

Optogenetic Activation of OSNs and MBONs (Figure 6.3)

csChrimson expressing flies were place on the closed loop system as described above. A 630nm LED was positioned approximately 2 inches above the fly and powered by an LED driver or standalone power source.

Larval NMJ Immunostaining

Wandering third instar larvae were fileted in PBS. Dissected larvae were fixed for 2 min in Bouin's solution (Sigma) then rinsed with PBS 4 times and blocked in 5% Normal Goat Serum in PBS + 0.1% TritonX-100 for 2 hours at RT. Primary antibody 1:250 mouse anti-DCSP-2 (6D6) (Developmental Studies Hybridoma Bank), 1:50 mouse anti-Bruchpilot (NC82) (Developmental Studies Hybridoma Bank) and 1:10,000 rabbit anti-GFP (Life Technologies A-11122) was incubated overnight 4°C. Larvae were washed extensively in PBS + 0.1% TritonX-100 then incubated for 2 hours at RT with 1:400 goat anti-mouse Alexa Fluor 633 (Life Technologies A-21052), 1:400 goat anti-rabbit Alexa Fluor 488 (Life Technologies A- 11034) and 1:500 Rhodamine Red-X conjugated goat anti-Horseradish Peroxidase (Jackson ImmunoResearch Laboratories 123-295-021). Larvae were then washed extensively in PBS + 0.1% TritonX-100 and mounted in Vectashield (Vector Laboratories). Images were captured on a Zeiss LSM 880 using a Plan-Apochromat 40X (1.4 NA) Oil DIC objective.

Adult Brain Immunostaining

Day 1 adult brains were dissected in 1X PBS pH 7.4 then immediately transferred to cold 1% PFA (Electron Microscopy Sciences) and fixed overnight at 4oC. Following overnight incubation samples were washed in PAT3 Buffer (0.5% BSA/0.5% Triton/1X PBS pH 7.4) 3 times. Brains were blocked in 3% Normal Goat Serum for 90 minutes at RT. Primary antibody 1:1000 rabbit anti-GFP (Life Technologies A- 11122) was incubated 3 hours at RT then overnight at 4°C. Brains were washed extensively in PAT3 Buffer. Secondary antibody 1:400 goat anti-rabbit Alexa Fluor 488 (Life Technologies A-11034) was incubated 3 hours at RT then 5 days at 4°C. Brains were washed 3 times in PAT3 Buffer then once in 1X PBS. Samples were mounted in Vectashield (Vector Laboratories). Images were captured on a Zeiss LSM 880 using a Plan-Apochromat 20X DIC objective.

RNA Isolation and qRT-PCR

Total RNA was isolated from dissected brains of day 1 adult females. RNA was extracted using Qiazol reagent (QIAGEN) then column purified by RNeasy micro kit (QIAGEN). cDNA was generated using Quantitect Reverse Transcriptase kit (QIAGEN). Taqman real-time qPCR experiments were performed on a QuantStudio 12K Flex Real-Time PCR System (ThermoFisher Scientific) following the manufacturer's instructions. Data were analyzed using the comparative 2ΔΔCt method using alphaTub84B as an endogenous control. The average fold-change relative to the pan-neuronal nsyb-GAL4 driver line alone was calculated. The following Taqman assays from ThermoFisher

Scientific were used: alphaTub84B (Dm02361072_s1), DopR1 (Dm02134814_m1), DopR2 (Dm02151745_m1), and D2R (Dm01845575_m1).

Electrophysiology

γ4 MBON and KC soma were targeted for patch recording by fluorescence from expression of soluble GCaMP or CD8-GFP. Dissected brain explants were treated with 2 mg mL−1 collagenase (Sigma) in external saline for ~30 sec to soften the perineural sheath and pinned to a Sylgard sheet. The exposed neuropil was then continuously perfused (about 2–3 mL min−1) with perfusion saline (108 mM NaCl, 5 mM KCl, 2 mM CaCl2, 8.2 mM MgCl2, 26 mM NaHCO3, 1 mM NaH2PO4, 5 mM trehalose, 5 mM sucrose, 5 mM HEPES, osmolarity adjusted to 275 mOsm). The perfusion saline was continuously bubbled with 95% O2/5% CO2 and reached a final pH of 7.3. To gain access to the soma, the sheath was broken by positive pressure from ejection of saline through a large bore broken electrode.

Intracellular recordings were performed with fire-polished patch electrodes (10–15 MΩ for MBONs, 15-20 MΩ for KCs) filled with internal saline (130 mM potassium aspartate, 8 mM KCl, 0.2 mM MgCl2, 5 mM sucrose, 10 mM HEPES pH 7.3, 10 mM EGTA). Current traces were acquired in voltage-clamp mode (for MBONs and KCs) and current-clamp mode (for KCs) using a Multiclamp 700B amplifier, digitized at 10 kHz and filtered at 1 kHz. The membrane potential of voltage clamp recordings was nominally -70 mV, a voltage at which unclamped action potentials rarely break through and could be readily detected by their large amplitude. Evoked EPSCs were stimulated

by acetylcholine iontophoresis into the calyx as described above. For each experiment, the responses to a train of 10 identical stimulation voltages, spaced 3 s apart were recorded before and after DAN activation. The data plotted in Figure 5.2A are the peak amplitude from stimulus-triggered averages for each experiment before and after DAN activation. In rare cases where stimulation evoked MBON spikes despite the voltage clamp, those responses were excluded from the average. We note that EPSC durations are likely exaggerated by low-pass filtering due to the high access resistance (50-100 MΩ) common to whole-cell recordings from *Drosophila* neurons[336].

In Figure 5.2BA, spontaneous EPSCs from 30-60 s traces (1 per fly) were analyzed in Clampfit (Molecular Devices), using a template search algorithm, with the template defined by the prominent EPSCs in the modulated MBON prep. As EPSCs in the unmodulated state were sometimes too small for reliable detection, this template search algorithm likely results in an underestimate in the difference in EPSC amplitude due to DAN stimulation.

To confirm that the spontaneous ESPCs measured in the MBON originated from KC activity (Figure 5.2B), we filled a fine electrode with 0.2 M GABA in external saline. After recording baseline EPSCs, the GABA electrode was moved from a position within the perfused saline to within the center of the mushroom body calyx. No further positive pressure was required to eject GABA. GABA applied in this manner rapidly inhibited measured EPSCs and EPSPs but did not suppress occasional spontaneous spiking in the MBON in current clamp recordings (data not shown.)

References

1. Swanson, L. W., Newman, E. A., Araque, A., Dubinsky, J. M., King, L. S. & Himmel, E. *The beautiful brain: the drawings of Santiago Ramón y Cajal*. (2016).

2. Morgan, J. L. & Lichtman, J. W. Why not connectomics? *Nat. Methods* **10,** 494–500 (2013).

3. Bargmann, C. I. Beyond the connectome: How neuromodulators shape neural circuits. *BioEssays* **34,** 458–465 (2012).

4. Marder, E. Neuromodulation of Neuronal Circuits: Back to the Future. *Neuron* **76,** 1–11 (2012).

5. Albert, P. R. & Benkelfat, C. The neurobiology of depression--revisiting the serotonin hypothesis. II. Genetic, epigenetic and clinical studies. *Philos. Trans. R. Soc. Lond. B. Biol. Sci.* **368,** 20120535 (2013).

6. Cooper, S., Robison, A. J. & Mazei-Robison, M. S. Reward Circuitry in Addiction. *Neurotherapeutics* **14,** 687–697 (2017).

7. Pagano, G., Niccolini, F. & Politis, M. The serotonergic system in Parkinson's patients with dyskinesia: evidence from imaging studies. *J. Neural Transm.* (2017).

8. Riederer, P. & Wuketich, S. Time course of nigrostriatal degeneration in Parkinson's disease. *J. Neural Transm.* **38,** 277–301 (1976).

9. Wasserman, S. M., Aptekar, J. W., Lu, P., Nguyen, J., Wang, A. L., Keles, M. F., Grygoruk, A., Krantz, D. E., Larsen, C. & Frye, M. A. Olfactory neuromodulation of motion vision circuitry in Drosophila. *Curr. Biol.* **25,** 467–72 (2015).

10. Root, C. M., Ko, K. I., Jafari, A. & Wang, J. W. Presynaptic facilitation by neuropeptide signaling mediates odor-driven food search. *Cell* **145,** 133–144 (2011).

11. Maimon, G. Modulation of visual physiology by behavioral state in monkeys, mice, and flies. *Curr. Opin. Neurobiol.* **21,** 559–564 (2011).

12. Su, C. Y. & Wang, J. W. Modulation of neural circuits: How stimulus context shapes innate behavior in Drosophila. *Curr. Opin. Neurobiol.* **29,** 9–16 (2014).

13. Palmer, C. R., Kristan, W. B. & Jr. Contextual modulation of behavioral choice. *Curr. Opin. Neurobiol.* **21,** 520–6 (2011).

14. Rogers, R. D. The roles of dopamine and serotonin in decision making: evidence from pharmacological experiments in humans. *Neuropsychopharmacology* **36,** 114–32 (2011).

15. Huertas, M. A., Schwettmann, S. E. & Shouval, H. Z. The Role of Multiple Neuromodulators in Reinforcement Learning That Is Based on Competition between Eligibility Traces. *Front. Synaptic Neurosci.* **8,** 37 (2016).

16. Aggarwal, M., Hyland, B. I. & Wickens, J. R. Neural control of dopamine neurotransmission: Implications for reinforcement learning. *Eur. J. Neurosci.* **35,** 1115–1123 (2012).

17. Mackey, S. L., Kandel, E. R. & Hawkins, R. D. Identified serotonergic neurons LCB1 and RCB1 in the cerebral ganglia of Aplysia produce presynaptic facilitation of siphon sensory neurons. *J. Neurosci.* **9,** 4227–35 (1989).

18. Chao, M. Y., Komatsu, H., Fukuto, H. S., Dionne, H. M. & Hart, A. C. Feeding status and serotonin rapidly and reversibly modulate a Caenorhabditis elegans chemosensory circuit. *Proc. Natl. Acad. Sci.* **101,** 15512–15517 (2004).

19. Seamans, J. K. & Yang, C. R. The principal features and mechanisms of dopamine modulation in the prefrontal cortex. *Prog. Neurobiol.* **74,** 1–57 (2004).

20. Tritsch, N. X. & Sabatini, B. L. Dopaminergic Modulation of Synaptic Transmission in Cortex and Striatum. *Neuron* **76,** 33–50 (2012).

21. Kreitzer, A. C. & Malenka, R. C. Striatal Plasticity and Basal Ganglia Circuit Function. *Neuron* **60,** 543–554 (2008).

22. Roseberry, T. K., Lee, A. M., Lalive, A. L., Wilbrecht, L., Bonci, A. & Kreitzer, A. C. Cell-Type-Specific Control of Brainstem Locomotor Circuits by Basal Ganglia. *Cell* **164,** 526–37 (2016).

23. Schultz, W., Dayan, P. & Montague, P. R. A neural substrate of prediction and reward. *Science (80-.).* **275,** 1593–1599 (1997).

24. Watabe-Uchida, M., Eshel, N. & Uchida, N. Neural Circuitry of Reward Prediction Error. *Annu. Rev. Neurosci.* **40,** 373–394 (2017).

25. Gadagkar, V., Puzerey, P. A., Chen, R., Baird-Daniel, E., Farhang, A. R. & Goldberg, J. H. Dopamine neurons encode performance error in singing birds. *Science* **354,** 1278–1282 (2016).

26. Joel, D., Niv, Y. & Ruppin, E. Actor–critic models of the basal ganglia: new anatomical and computational perspectives. *Neural Networks* **15,** 535–547 (2002).

27. Bromberg-Martin, E. S., Matsumoto, M. & Hikosaka, O. Dopamine in Motivational Control: Rewarding, Aversive, and Alerting. *Neuron* **68,** 815–834 (2010).

28. Cohen, J. Y., Haesler, S., Vong, L., Lowell, B. B. & Uchida, N. Neuron-type-specific signals for reward and punishment in the ventral tegmental area. *Nature* **482,** 85–8 (2012).

29. Lerner, T. N., Shilyansky, C., Davidson, T. J., Evans, K. E., Beier, K. T., Zalocusky, K. A., Crow, A. K., Malenka, R. C., Luo, L., Tomer, R. & Deisseroth, K. Intact-Brain Analyses Reveal Distinct Information Carried by SNc Dopamine Subcircuits. *Cell* **162,** 635–647 (2015).

30. Schultz, W. Multiple Dopamine Functions at Different Time Courses. *Annu. Rev. Neurosci.* **30,** 259–288 (2007).

31. Howe, M. W. & Dombeck, D. A. Rapid signalling in distinct dopaminergic axons during locomotion and reward. *Nature* **535,** 505–510 (2016).

32. Parker, N. F., Cameron, C. M., Taliaferro, J. P., Lee, J., Choi, J. Y., Davidson, T. J., Daw, N. D. & Witten, I. B. Reward and choice encoding in terminals of midbrain dopamine neurons depends on striatal target. *Nat. Neurosci.* **19,** 845–854 (2016).

33. da Silva, J. A., Tecuapetla, F., Paixão, V. & Costa, R. M. Dopamine neuron activity before action initiation gates and invigorates future movements. *Nature* (2018).

34. Coddington, L. T. & Dudman, J. T. Emergence of reward expectation signals in identified dopamine neurons. *bioRxiv* 238881 (2017).

35. Syed, E. C. J., Grima, L. L., Magill, P. J., Bogacz, R., Brown, P. & Walton, M. E. Action initiation shapes mesolimbic dopamine encoding of future rewards. *Nat. Neurosci.* **19,** 34–36 (2015).

36. Lammel, S., Lim, B. K. & Malenka, R. C. Reward and aversion in a heterogeneous midbrain dopamine system. *Neuropharmacology* **76,** 351–359 (2014).

37. Beier, K. T., Steinberg, E. E., Deloach, K. E., Xie, S., Miyamichi, K., Schwarz, L., Gao, X. J., Kremer, E. J., Malenka, R. C. & Luo, L. Circuit Architecture of VTA Dopamine Neurons Revealed by Systematic Input-Output Mapping. *Cell* **162,** 622–634 (2015).

38. Fiorillo, C. D., Song, M. R. & Yun, S. R. Multiphasic Temporal Dynamics in Responses of Midbrain Dopamine Neurons to Appetitive and Aversive Stimuli.

39. Rice, M. E., Patel, J. C. & Cragg, S. J. Dopamine release in the basal ganglia. *Neuroscience* **198,** 112–137 (2011).

40. Beaulieu, J.-M. & Gainetdinov, R. R. The Physiology, Signaling, and Pharmacology of Dopamine Receptors. *Pharmacol. Rev.* **63,** 182–217 (2011).

41. Surmeier, D. J., Ding, J., Day, M., Wang, Z. & Shen, W. D1 and D2 dopamine-receptor modulation of striatal glutamatergic signaling in striatal medium spiny neurons. *Trends Neurosci.* **30,** 228–235 (2007).

42. Dujardin, F. Mémoire sur le système nerveux des insectes. *Ann. Sci. Nat. Zool.* **14,** 195–206 (1850).

43. Strausfeld, N. J., Hansen, L., Li, Y., Gomez, R. S. & Ito, K. Evolution, Discovery, and Interpretations of Arthropod Mushroom Bodies. *Learn. Mem.* **5,** 11–37 (1998).

44. Mabuchi, I., Shimada, N., Sato, S., Ienaga, K., Inami, S. & Sakai, T. Mushroom body signaling is required for locomotor activity rhythms in Drosophila. *Neurosci. Res.* **111,** 25–33 (2016).

45. Martin, J. R., Ernst, R. & Heisenberg, M. Mushroom bodies suppress locomotor activity in Drosophila melanogaster. *Learn. Mem.* **5,** 179–191 (1998).

46. Tomita, J., Ban, G. & Kume, K. Genes and neural circuits for sleep of the fruit fly. *Neurosci. Res.* **118,** 82–91 (2017).

47. Artiushin, G. & Sehgal, A. The Drosophila circuitry of sleep–wake regulation. *Curr. Opin. Neurobiol.* **44,** 243–250 (2017).

48. Pitman, J. L., McGill, J. J., Keegan, K. P. & Allada, R. A dynamic role for the mushroom bodies in promoting sleep in Drosophila. *Nature* **441,** 753–756 (2006).

49. Joiner, W. J., Crocker, A., White, B. H. & Sehgal, A. Sleep in Drosophila is regulated by adult mushroom bodies. *Nature* **441,** 757–760 (2006).

50. Lin, C. & Strausfeld, N. J. Visual inputs to the mushroom body calyces of the whirligig beetle Dineutus sublineatus: Modality switching in an insect. *J. Comp. Neurol.* **520,** 2562–2574 (2012).

51. Chabaud, M. A., Devaud, J. M., Pham-Delègue, M. H., Preat, T. & Kaiser, L. Olfactory conditioning of proboscis activity in Drosophila melanogaster. *J. Comp. Physiol. A Neuroethol. Sensory, Neural, Behav. Physiol.* **192,** 1335–1348 (2006).

52. Zars, T. Behavioral functions of the insect mushroom bodies. *Curr. Opin. Neurobiol.* **10,** 790–795 (2000).

53. Heisenberg, M. What do the mushroom bodies do for the insect brain? an introduction. *Learn. Mem.* **5,** 1–10 (1998).

54. Laurent, G. & Naraghi, M. Odorant-induced oscillations in the mushroom bodies of

the locust. *J. Neurosci.* **14,** 2993–3004 (1994).

55. Perez-Orive, J., Mazor, O., Turner, G. C., Cassenaer, S., Wilson, R. I. & Laurent, G. Oscillations and sparsening of odor representations in the mushroom body. *Science (80-.).* **297,** 359–365 (2002).

56. Laurent, G. Olfactory network dynamics and the coding of multidimensional signals. *Nat. Rev. Neurosci.* **3,** 884–895 (2002).

57. Hammer, M. An identified neuron mediates the unconditioned stimulus in associative olfactory learning in honeybees. *Nature* **366,** 59–63 (1993).

58. Mauelshagen, J. Neural correlates of olfactory learning paradigms in an identified neuron in the honeybee brain. *J. Neurophysiol.* **69,** 609–625 (1993).

59. Strausfeld, N. J. Organization of the honey bee mushroom body: Representation of the calyx within the vertical and gamma lobes. *J. Comp. Neurol.* **450,** 4–33 (2002).

60. Strausfeld, N. J., Sinakevitch, I. & Vilinsky, I. The mushroom bodies of Drosophila melanogaster: An immunocytological and golgi study of Kenyon cell organization in the calyces and lobes. *Microsc. Res. Tech.* **62,** 151–169 (2003).

61. Farris, S. M. Evolution of insect mushroom bodies: Old clues, new insights. *Arthropod Struct. Dev.* **34,** 211–234 (2005).

62. Wolff, G. H., Thoen, H. H., Marshall, J., Sayre, M. E. & Strausfeld, N. J. An insect-like mushroom body in a crustacean brain. *Elife* **6,** e29889 (2017).

63. Maza, F. J., Sztarker, J., Shkedy, A., Peszano, V. N., Locatelli, F. F. & Delorenzi, A. Context-dependent memory traces in the crab's mushroom bodies: Functional support for a common origin of high-order memory centers. *Proc. Natl. Acad. Sci.* **113,** E7957–E7965 (2016).

64. Tomer, R., Denes, A. S., Tessmar-Raible, K. & Arendt, D. Profiling by Image Registration Reveals Common Origin of Annelid Mushroom Bodies and Vertebrate Pallium. *Cell* **142,** 800–809 (2010).

65. Farris, S. M. Are mushroom bodies cerebellum-like structures? *Arthropod Struct. Dev.* **40,** 368–379 (2011).

66. Quinn, W. G., Harris, W. A. & Benzer, S. Conditioned behavior in Drosophila melanogaster. *Proc. Natl. Acad. Sci. U. S. A.* **71,** 708–12 (1974).

67. Tempel, B. L., Bonini, N., Dawson, D. R. & Quinn, W. G. Reward learning in normal and mutant Drosophila. *Proc. Natl. Acad. Sci.* **80,** 1482–1486 (1983).

68. Tully, T. & Quinn, W. G. Classical conditioning and retention in normal and mutant Drosophila melanogaster. *J. Comp. Physiol. A* **157,** 263–277 (1985).

69. de Belle, J. & Heisenberg, M. Associative odor learning in Drosophila abolished by chemical ablation of mushroom bodies. *Science (80-.).* **263,** 692–695 (1994).

70. Heisenberg, M., Borst, A., Wagner, S. & Byers, D. Drosophila Mushroom Body Mutants are Deficient in Olfactory Learning. *J. Neurogenet.* **2,** 1–30 (1985).

71. McGuire, S. E., Deshazer, M. & Davis, R. L. Thirty years of olfactory learning and memory research in Drosophila melanogaster. *Prog. Neurobiol.* **76,** 328–347 (2005).

72. Davis, R. L. OLFACTORY MEMORY FORMATION IN DROSOPHILA : From Molecular to Systems Neuroscience. *Annu. Rev. Neurosci.* **28,** 275–302 (2005).

73. Roman, G. & Davis, R. L. Molecular biology and anatomy of Drosophila olfactory associative learning. *BioEssays* **23,** 571–581 (2001).

74. Kahsai, L. & Zars, T. Learning and memory in drosophila: Behavior, genetics, and neural systems. *Int. Rev. Neurobiol.* **99,** 139–167 (2011).

75. Levin, L. R., Han, P. L., Hwang, P. M., Feinstein, P. G., Davis, R. L. & Reed, R. R. The Drosophila learning and memory gene rutabaga encodes a Ca2+calmodulin-responsive adenylyl cyclase. *Cell* **68,** 479–489 (1992).

76. Waddell, S., Armstrong, J. D., Kitamoto, T., Kaiser, K. & Quinn, W. G. The amnesiac Gene Product Is Expressed in Two Neurons in the Drosophila Brain that Are Critical for Memory. *Cell* **103,** 805–813 (2000).

77. Kandel, E. R. The molecular biology of memory: cAMP, PKA, CRE, CREB-1, CREB-2, and CPEB. *Mol. Brain* **5,** 14 (2012).

78. Jay, T. M. Dopamine: a potential substrate for synaptic plasticity and memory mechanisms. *Prog. Neurobiol.* **69,** 375–90 (2003).

79. Yoshihara, M. & Ito, K. Acute genetic manipulation of neuronal activity for the functional dissection of neural circuits - A dream come true for the pioneers of behavioral genetics. *J. Neurogenet.* **26,** 43–52 (2012).

80. Olsen, S. R. & Wilson, R. I. Cracking neural circuits in a tiny brain: new approaches for understanding the neural circuitry of Drosophila. *Trends Neurosci.* **31,** 512–520 (2008).

81. Pascual, A. & Préat, T. Localization of long-term memory within the Drosophila mushroom body. *Science (80-.).* **294,** 1115–1117 (2001).

82. Isabel, G., Pascual, A. & Preat, T. Exclusive Consolidated Memory Phases in Drosophila. *Science (80-.).* **304,** 1024–1027 (2004).

83. Krashes, M. J., Keene, A. C., Leung, B., Armstrong, J. D. & Waddell, S. Sequential Use of Mushroom Body Neuron Subsets during Drosophila Odor Memory Processing. *Neuron* **53,** 103–115 (2007).

84. Krashes, M. J. & Waddell, S. Rapid Consolidation to a radish and Protein Synthesis-Dependent Long-Term Memory after Single-Session Appetitive Olfactory Conditioning in Drosophila. *J. Neurosci.* **28,** 3103–3113 (2008).

85. Colomb, J., Kaiser, L., Chabaud, M. A. & Preat, T. Parametric and genetic analysis of Drosophila appetitive long-term memory and sugar motivation. *Genes, Brain Behav.* **8,** 407–415 (2009).

86. Zhao, J., Lu, Y., Zhao, X., Yao, X., Shuai, Y., Huang, C., Wang, L., Jeong, S. H. & Zhong, Y. Dissociation of rugose-dependent short-term memory component from memory consolidation in Drosophila. *Genes, Brain Behav.* **12,** 626–632 (2013).

87. Cervantes-Sandoval, I., Martin-Pena, A., Berry, J. A. & Davis, R. L. System-Like Consolidation of Olfactory Memories in Drosophila. *J. Neurosci.* **33,** 9846–9854 (2013).

88. Yamagata, N., Ichinose, T., Aso, Y., Plaçais, P.-Y., Friedrich, A. B., Sima, R. J., Preat, T., Rubin, G. M. & Tanimoto, H. Distinct dopamine neurons mediate reward signals for short- and long-term memories. *Proc. Natl. Acad. Sci.* **112,** 578–583 (2015).

89. Ichinose, T., Aso, Y., Yamagata, N., Abe, A., Rubin, G. M. & Tanimoto, H. Reward signal in a recurrent circuit drives appetitive long-term memory formation. *Elife* **4,** 1–18 (2015).

90. Wu, J. K., Tai, C. Y., Feng, K. L., Chen, S. L., Chen, C. C. & Chiang, A. S. Long-term memory requires sequential protein synthesis in three subsets of mushroom body output neurons in Drosophila. *Sci. Rep.* **7,** 1–10 (2017).

91. Hirano, Y., Ihara, K., Masuda, T., Yamamoto, T., Iwata, I., Takahashi, A., Awata, H., Nakamura, N., Takakura, M., Suzuki, Y., Horiuchi, J., Okuno, H. & Saitoe, M. Shifting transcriptional machinery is required for long-term memory maintenance and modification in Drosophila mushroom bodies. *Nat. Commun.* **7,** 1–14 (2016).

92. Plaçais, P. Y., De Tredern, É., Scheunemann, L., Trannoy, S., Goguel, V., Han, K. A., Isabel, G. & Preat, T. Upregulated energy metabolism in the Drosophila mushroom body is the trigger for long-term memory. *Nat. Commun.* **8,** (2017).

93. Fischer, J. A., Giniger, E., Maniatis, T. & Ptashne, M. GAL4 activates transcription

in Drosophila. *Nature* **332,** 853–856 (1988).

94. Brand, A. H. & Perrimon, N. Targeted gene expression as a means of altering cell fates and generating dominant phenotypes. **118,** 401–415 (1993).

95. Yu, D., Keene, A. C., Srivatsan, A., Waddell, S. & Davis, R. L. Drosophila DPM neurons form a delayed and branch-specific memory trace after olfactory classical conditioning. *Cell* **123,** 945–957 (2005).

96. Yu, D., Akalal, D. B. G. & Davis, R. L. Drosophila α/β Mushroom Body Neurons Form a Branch-Specific, Long-Term Cellular Memory Trace after Spaced Olfactory Conditioning. *Neuron* **52,** 845–855 (2006).

97. Akalal, D.-B. G., Yu, D. & Davis, R. L. A Late-Phase, Long-Term Memory Trace Forms in the Neurons of Drosophila Mushroom Bodies after Olfactory Classical Conditioning. *J. Neurosci.* **30,** 16699–16708 (2010).

98. Davis, R. L. Traces of Drosophila Memory. *Neuron* **70,** 8–19 (2011).

99. Pitman, J. L., Huetteroth, W., Burke, C. J., Krashes, M. J., Lai, S. L., Lee, T. & Waddell, S. A pair of inhibitory neurons are required to sustain labile memory in the drosophila mushroom body. *Curr. Biol.* **21,** 855–861 (2011).

100. Plaçais, P. Y., Trannoy, S., Friedrich, A. B., Tanimoto, H. & Preat, T. Two pairs of mushroom body efferent neurons are required for appetitive long-term memory retrieval in drosophila. *Cell Rep.* **5,** 769–780 (2013).

101. Madalan, A., Yang, X., Ferris, J., Zhang, S. & Roman, G. G(o) activation is required for both appetitive and aversive memory acquisition in Drosophila. *Learn. Mem.* **19,** 26–34 (2011).

102. Keene, A. C., Stratmann, M., Keller, A., Perrat, P. N., Vosshall, L. B. & Waddell, S. Diverse odor-conditioned memories require uniquely timed dorsal paired medial neuron output. *Neuron* **44,** 521–533 (2004).

103. Yu, D., Akalal, D.-B. G. & Davis, R. L. Drosophila alpha/beta mushroom body neurons form a branch-specific, long-term cellular memory trace after spaced olfactory conditioning. *Neuron* **52,** 845–855 (2006).

104. Wang, Y., Mamiya, A., Chiang, A. -s. & Zhong, Y. Imaging of an Early Memory Trace in the Drosophila Mushroom Body. *J. Neurosci.* **28,** 4368–4376 (2008).

105. Akalal, D.-B. G., Yu, D. & Davis, R. L. The Long-Term Memory Trace Formed in the Drosophila / Mushroom Body Neurons Is Abolished in Long-Term Memory Mutants. *J. Neurosci.* **31,** 5643–5647 (2011).

106. Thompson, R. F. In Search of Memory Traces. *Annu. Rev. Psychol.* **56,** 1–23

(2005).

107. Gerber, B., Tanimoto, H. & Heisenberg, M. An engram found? Evaluating the evidence from fruit flies. *Curr. Opin. Neurobiol.* **14,** 737–744 (2004).

108. Masse, N. Y., Turner, G. C. & Jefferis, G. S. X. E. Olfactory Information Processing in Drosophila. *Curr. Biol.* **19,** R700--13 (2009).

109. Wilson, R. I. Early Olfactory Processing in *Drosophila*: Mechanisms and Principles. *Annu. Rev. Neurosci.* **36,** 217–241 (2013).

110. Caron, S. J. C., Ruta, V., Abbott, L. F. & Axel, R. Random convergence of olfactory inputs in the Drosophila mushroom body. *Nature* **497,** 113–117 (2013).

111. Murthy, M., Fiete, I. & Laurent, G. Testing Odor Response Stereotypy in the Drosophila Mushroom Body. *Neuron* **59,** 1009–1023 (2008).

112. Litwin-Kumar, A., Harris, K. D., Axel, R., Sompolinsky, H. & Abbott, L. F. Optimal Degrees of Synaptic Connectivity. *Neuron* **93,** 1153–1164.e7 (2017).

113. Olshausen, B. A. & Field, D. J. Sparse coding of sensory inputs. *Curr. Opin. Neurobiol.* **14,** 481–487 (2004).

114. Aso, Y., Hattori, D., Yu, Y., Johnston, R. M., Iyer, N. A., Ngo, T. T. B., Dionne, H., Abbott, L. F., Axel, R., Tanimoto, H. & Rubin, G. M. The neuronal architecture of the mushroom body provides a logic for associative learning. *Elife* **3,** e04577 (2014).

115. Tanaka, N. K., Tanimoto, H. & Ito, K. Neuronal assemblies of the Drosophila mushroom body. *J. Comp. Neurol.* **508,** 711–755 (2008).

116. Waddell, S. Reinforcement signalling in Drosophila; dopamine does it all after all. *Current Opinion in Neurobiology* **23,** 324–329 (2013).

117. Séjourn, J., Plaçais, P. Y., Aso, Y., Siwanowicz, I., Trannoy, S., Thoma, V., Tedjakumala, S. R., Rubin, G. M., Tchénio, P., Ito, K., Isabel, G., Tanimoto, H. & Preat, T. Mushroom body efferent neurons responsible for aversive olfactory memory retrieval in Drosophila. *Nat. Neurosci.* **14,** 903–910 (2011).

118. Aso, Y. *et al.* Mushroom body output neurons encode valence and guide memory-based action selection in Drosophila. *Elife* **3,** e04580 (2014).

119. Owald, D., Felsenberg, J., Talbot, C. B., Das, G., Perisse, E., Huetteroth, W. & Waddell, S. Activity of defined mushroom body output neurons underlies learned olfactory behavior in Drosophila. *Neuron* **86,** 417–427 (2015).

120. Zhang, K., Guo, J. Z., Peng, Y., Xi, W. & Guo, A. Dopamine-mushroom body

circuit regulates saliency-based decision-making in Drosophila. *Science (80-.).* **316,** 1901–1904 (2007).

121. Bang, S., Hyun, S., Hong, S. T., Kang, J., Jeong, K., Park, J. J., Choe, J. & Chung, J. Dopamine signalling in mushroom bodies regulates temperature-preference behaviour in Drosophila. *PLoS Genet.* **7,** e1001346 (2011).

122. van Swinderen, B., McCartney, A., Kauffman, S., Flores, K., Agrawal, K., Wagner, J. & Paulk, A. Shared visual attention and memory systems in the Drosophila brain. *PLoS One* **4,** e5989 (2009).

123. Hattori, D., Aso, Y., Swartz, K. J., Rubin, G. M., Abbott, L. F. & Axel, R. Representations of Novelty and Familiarity in a Mushroom Body Compartment. *Cell* **169,** 956–969.e17 (2017).

124. Sitaraman, D., Aso, Y., Jin, X., Chen, N., Felix, M., Rubin, G. M. & Nitabach, M. N. Propagation of Homeostatic Sleep Signals by Segregated Synaptic Microcircuits of the Drosophila Mushroom Body. *Curr. Biol.* **25,** 2915–2927 (2015).

125. Lewis, L. P. C., Siju, K. P., Aso, Y., Friedrich, A. B., Bulteel, A. J. B., Rubin, G. M. & Grunwald Kadow, I. C. A Higher Brain Circuit for Immediate Integration of Conflicting Sensory Information in Drosophila. *Curr. Biol.* **25,** 2203–2214 (2015).

126. Azanchi, R., Kaun, K. R. & Heberlein, U. Competing dopamine neurons drive oviposition choice for ethanol in Drosophila. *Proc. Natl. Acad. Sci.* **110,** 21153–21158 (2013).

127. Bräcker, L. B., Siju, K. P., Arela, N., So, Y., Hang, M., Hein, I., Vasconcelos, M. L. & Grunwald Kadow, I. C. Essential role of the mushroom body in context-dependent CO2 avoidance in drosophila. *Curr. Biol.* **23,** 1228–1234 (2013).

128. Siju, K. P., Bräcker, L. B. & Grunwald Kadow, I. C. Neural mechanisms of context-dependent processing of CO2 avoidance behavior in fruit flies. *Fly (Austin).* **8,** 68–74 (2014).

129. Cassenaer, S. & Laurent, G. Conditional modulation of spike-timing-dependent plasticity for olfactory learning. *Nature* **482,** 47–51 (2012).

130. Frémaux, N. & Gerstner, W. Neuromodulated Spike-Timing-Dependent Plasticity, and Theory of Three-Factor Learning Rules. *Front. Neural Circuits* **9,** 85 (2016).

131. Malenka, R. C. & Bear, M. F. LTP and LTD: an embarrassment of riches. *Neuron* **44,** 5–21 (2004).

132. Feldman, D. E. The Spike-Timing Dependence of Plasticity. *Neuron* **75,** 556–571 (2012).

133. Keene, A. C. & Waddell, S. Drosophila olfactory memory: Single genes to complex neural circuits. *Nat. Rev. Neurosci.* **8,** 341–354 (2007).

134. Tomchik, S. M. & Davis, R. L. Drosophila Memory Research through Four Eras. Genetic, Molecular Biology, Neuroanatomy, and Systems Neuroscience. *Handb. Behav. Neurosci.* **22,** 359–377 (2013).

135. Tsao, C., Chen, C., Lin, C. & Yang, H. Drosophila mushroom bodies integrate hunger and satiety signals to control innate food-seeking behavior.

136. Sayin, S., De Backer, J.-F., Wosniack, M. E., Lewis, L., Siju, K. P., Frisch, L.-M., Gjorgjieva, J. & Grunwald Kadow, I. Specific octopaminergic neurons arbitrate between perseverance and reward in hungry Drosophila. *bioRxiv* (2018).

137. Turner, G. C., Bazhenov, M. & Laurent, G. Olfactory Representations by Drosophila Mushroom Body Neurons. *J. Neurophysiol.* **99,** 734–746 (2008).

138. Larsson, M. C., Domingos, A. I., Jones, W. D., Chiappe, M. E., Amrein, H. & Vosshall, L. B. Or83b encodes a broadly expressed odorant receptor essential for Drosophila olfaction. *Neuron* **43,** 703–714 (2004).

139. Benton, R., Sachse, S., Michnick, S. W. & Vosshall, L. B. Atypical membrane topology and heteromeric function of Drosophila odorant receptors in vivo. *PLoS Biol.* **4,** 240–257 (2006).

140. Vosshall, L. B., Wong, A. M. & Axel, R. An olfactory sensory map in the fly brain. *Cell* **102,** 147–159 (2000).

141. Sato, K., Pellegrino, M., Nakagawa, T., Nakagawa, T., Vosshall, L. B. & Touhara, K. Insect olfactory receptors are heteromeric ligand-gated ion channels. *Nature* **452,** 1002–1006 (2008).

142. Degennaro, M., McBride, C. S., Seeholzer, L., Nakagawa, T., Dennis, E. J., Goldman, C., Jasinskiene, N., James, A. A. & Vosshall, L. B. Orco mutant mosquitoes lose strong preference for humans and are not repelled by volatile DEET. *Nature* **498,** 487–491 (2013).

143. Yan, H. *et al.* An Engineered orco Mutation Produces Aberrant Social Behavior and Defective Neural Development in Ants. *Cell* **170,** 736–747.e9 (2017).

144. Trible, W., Olivos-Cisneros, L., McKenzie, S. K., Saragosti, J., Chang, N. C., Matthews, B. J., Oxley, P. R. & Kronauer, D. J. C. orco Mutagenesis Causes Loss of Antennal Lobe Glomeruli and Impaired Social Behavior in Ants. *Cell* **170,** 727–735.e10 (2017).

145. Rimal, S. & Lee, Y. The multidimensional ionotropic receptors of *Drosophila*

melanogaster. *Insect Mol. Biol.* **27,** 1–7 (2018).

146. Benton, R., Vannice, K. S., Gomez-Diaz, C. & Vosshall, L. B. Variant Ionotropic Glutamate Receptors as Chemosensory Receptors in Drosophila. *Cell* **136,** 149–162 (2009).

147. Scott, K. Gustatory Processing in *Drosophila melanogaster*. *Annu. Rev. Entomol.* **63,** 15–30 (2018).

148. Silbering, A. F., Rytz, R., Grosjean, Y., Abuin, L., Ramdya, P., Jefferis, G. S. X. E. & Benton, R. Complementary Function and Integrated Wiring of the Evolutionarily Distinct Drosophila Olfactory Subsystems. *J. Neurosci.* **31,** 13357–13375 (2011).

149. Olsen, S. R., Bhandawat, V. & Wilson, R. I. Divisive normalization in olfactory population codes. *Neuron* **66,** 287–299 (2010).

150. Su, C.-Y., Martelli, C., Emonet, T. & Carlson, J. R. Temporal coding of odor mixtures in an olfactory receptor neuron. *Proc. Natl. Acad. Sci.* **108,** 5075–5080 (2011).

151. Su, C. Y., Menuz, K., Reisert, J. & Carlson, J. R. Non-synaptic inhibition between grouped neurons in an olfactory circuit. *Nature* **492,** 66–71 (2012).

152. Ng, M., Roorda, R. D., Lima, S. Q., Zemelman, B. V., Morcillo, P. & Miesenböck, G. Transmission of olfactory information between three populations of neurons in the antennal lobe of the fly. *Neuron* **36,** 463–474 (2002).

153. Wilson, R. I., Turner, G. C. & Laurent, G. Transformation of Olfactory Representations in the Drosophila Antennal Lobe. *Science (80-.).* **303,** 366–370 (2004).

154. Kazama, H. & Wilson, R. I. Homeostatic Matching and Nonlinear Amplification at Identified Central Synapses. *Neuron* **58,** 401–413 (2008).

155. Silbering, A. F., Okada, R., Ito, K. & Galizia, C. G. Olfactory Information Processing in the Drosophila Antennal Lobe: Anything Goes? *J. Neurosci.* **28,** 13075–13087 (2008).

156. Wang, J. W., Wong, A. M., Flores, J., Vosshall, L. B. & Axel, R. Two-photon calcium imaging reveals an odor-evoked map of activity in the fly brain. *Cell* **112,** 271–282 (2003).

157. Yu, D., Ponomarev, A. & Davis, R. L. Altered representation of the spatial code for odors after olfactory classical conditioning: Memory trace formation by synaptic recruitment. *Neuron* **42,** 437–449 (2004).

158. Sachse, S., Rueckert, E., Keller, A., Okada, R., Tanaka, N. K., Ito, K. & Vosshall,

L. B. Activity-Dependent Plasticity in an Olfactory Circuit. *Neuron* **56,** 838–850 (2007).

159. Kremer, M. C., Christiansen, F., Leiss, F., Paehler, M., Knapek, S., Andlauer, T. F. M., Förstner, F., Kloppenburg, P., Sigrist, S. J. & Tavosanis, G. Structural long-term changes at mushroom body input synapses. *Curr. Biol.* **20,** 1938–1944 (2010).

160. Faber, T., Joerges, J. & Menzel, R. Associative learning modifies neural representations of odors in the insect brain. *Nat. Neurosci.* **2,** 74–78 (1999).

161. Hallem, E. A., Ho, M. G. & Carlson, J. R. The Molecular Basis of Odor Coding in the Drosophila Antenna. *Cell* **117,** 965–979 (2004).

162. Schultzhaus, J. N., Saleem, S., Iftikhar, H. & Carney, G. E. The role of the Drosophila lateral horn in olfactory information processing and behavioral response. *J. Insect Physiol.* **98,** 29–37 (2017).

163. Jefferis, G. S. X. E., Potter, C. J., Chan, A. M., Marin, E. C., Rohlfing, T., Maurer, C. R. & Luo, L. Comprehensive Maps of Drosophila Higher Olfactory Centers: Spatially Segregated Fruit and Pheromone Representation. *Cell* **128,** 1187–1203 (2007).

164. Ruta, V., Datta, S. R., Vasconcelos, M. L., Freeland, J., Looger, L. L. & Axel, R. A dimorphic pheromone circuit in Drosophila from sensory input to descending output. *Nature* **468,** 686–690 (2010).

165. Dolan, M.-J., Belliart-Guerin, G., Bates, A. S., Aso, Y., Frechter, S., Roberts, R. J. V, Schlegel, P., Wong, A., Hammad, A., Bock, D., Rubin, G. M., Preat, T., Placais, P.-Y. & Jefferis, G. S. X. E. Communication from learned to innate olfactory processing centers is required for memory retrieval in Drosophila. *bioRxiv* (2017).

166. Wong, A. M., Wang, J. W. & Axel, R. Spatial representation of the glomerular map in the Drosophila protocerebrum. *Cell* **109,** 229–241 (2002).

167. Marin, E. C., Jefferis, G. S. X. E., Komiyama, T., Zhu, H. & Luo, L. Representation of the glomerular olfactory map in the Drosophila brain. *Cell* **109,** 243–255 (2002).

168. Parnas, M., Lin, A. C., Huetteroth, W. & Miesenb??ck, G. Odor Discrimination in Drosophila: From Neural Population Codes to Behavior. *Neuron* **79,** 932–944 (2013).

169. Liang, L., Li, Y., Potter, C. J., Yizhar, O., Deisseroth, K., Tsien, R. W. & Luo, L. GABAergic Projection Neurons Route Selective Olfactory Inputs to Specific Higher-Order Neurons. *Neuron* **79,** 917–931 (2013).

170. Fişek, M. & Wilson, R. I. Stereotyped connectivity and computations in higher-order olfactory neurons. *Nat. Neurosci.* **17,** 280–288 (2014).

171. Wang, K., Gong, J., Wang, Q., Li, H., Cheng, Q., Liu, Y., Zeng, S. & Wang, Z. Parallel pathways convey olfactory information with opposite polarities in Drosophila. *Proc. Natl. Acad. Sci.* **111,** 3164–3169 (2014).

172. Strutz, A., Soelter, J., Baschwitz, A., Farhan, A., Grabe, V., Rybak, J., Knaden, M., Schmuker, M., Hansson, B. S. & Sachse, S. Decoding odor quality and intensity in the Drosophila brain. *Elife* **3,** e04147 (2014).

173. Yusuyama, K., Meinertzhagen, I. A. & Schürmann, F. W. Synaptic organization of the mushroom body calyx in Drosophila melanogaster. *J. Comp. Neurol.* **445,** 211–226 (2002).

174. Leiss, F., Groh, C., Butcher, N. J., Meinertzhagen, I. A. & Tavosanis, G. Synaptic organization in the adult Drosophila mushroom body calyx. *J. Comp. Neurol.* **517,** 808–824 (2009).

175. Butcher, N. J., Friedrich, A. B., Lu, Z., Tanimoto, H. & Meinertzhagen, I. A. Different classes of input and output neurons reveal new features in microglomeruli of the adult Drosophila mushroom body calyx. *J. Comp. Neurol.* **520,** 2185–2201 (2012).

176. Li, H., Li, Y., Lei, Z., Wang, K. & Guo, A. Transformation of odor selectivity from projection neurons to single mushroom body neurons mapped with dual-color calcium imaging. *Proc. Natl. Acad. Sci.* **110,** 12084–12089 (2013).

177. Gruntman, E. & Turner, G. C. Integration of the olfactory code across dendritic claws of single mushroom body neurons. *Nat. Neurosci.* **16,** 1821–1829 (2013).

178. Assisi, C., Stopfer, M., Laurent, G. & Bazhenov, M. Adaptive regulation of sparseness by feedforward inhibition. *Nat. Neurosci.* **10,** 1176–1184 (2007).

179. Liu, X., Krause, W. C. & Davis, R. L. GABAAReceptor RDL Inhibits Drosophila Olfactory Associative Learning. *Neuron* **56,** 1090–1102 (2007).

180. Lin, A. C., Bygrave, A. M., De Calignon, A., Lee, T. & Miesenböck, G. Sparse, decorrelated odor coding in the mushroom body enhances learned odor discrimination. *Nat. Neurosci.* **17,** 559–568 (2014).

181. Papadopoulou, M., Cassenaer, S., Nowotny, T. & Laurent, G. Normalization for Sparse Encoding of Odors by a Wide-Field Interneuron. *Science (80-.).* **332,** 721–725 (2011).

182. Gupta, N. & Stopfer, M. Olfactory coding: giant inhibitory neuron governs sparse

odor codes. *Curr. Biol.* **21,** R504-6 (2011).

183. Lei, Z., Chen, K., Li, H., Liu, H. & Guo, A. The GABA system regulates the sparse coding of odors in the mushroom bodies of Drosophila. *Biochem. Biophys. Res. Commun.* **436,** 35–40 (2013).

184. Jortner, R. A., Farivar, S. S. & Laurent, G. A Simple Connectivity Scheme for Sparse Coding in an Olfactory System. *J. Neurosci.* **27,** 1659–1669 (2007).

185. Wang, Y. Stereotyped Odor-Evoked Activity in the Mushroom Body of Drosophila Revealed by Green Fluorescent Protein-Based Ca2+ Imaging. *J. Neurosci.* **24,** 6507–6514 (2004).

186. Honegger, K. S., Campbell, R. A. A. & Turner, G. C. Cellular-Resolution Population Imaging Reveals Robust Sparse Coding in the Drosophila Mushroom Body. *J. Neurosci.* **31,** 11772–11785 (2011).

187. Campbell, R. A. A., Honegger, K. S., Qin, H., Li, W., Demir, E. & Turner, G. C. Imaging a Population Code for Odor Identity in the Drosophila Mushroom Body. *J. Neurosci.* **33,** 10568–10581 (2013).

188. Itskov, V. & Abbott, L. F. Pattern capacity of a perceptron for sparse discrimination. *Phys. Rev. Lett.* **101,** 18101 (2008).

189. Arena, P., Patané, L., Stornanti, V., Termini, P. S., Zäpf, B. & Strauss, R. Modeling the insect mushroom bodies: Application to a delayed match-to-sample task. *Neural Networks* **41,** 202–211 (2013).

190. Zhang, D., Li, Y., Wu, S. & Rasch, M. J. Design principles of the sparse coding network and the role of 'sister cells' in the olfactory system of Drosophila. *Front. Comput. Neurosci.* **7,** 141 (2013).

191. Chacron, M. J., Longtin, A. & Maler, L. Efficient computation via sparse coding in electrosensory neural networks. *Curr. Opin. Neurobiol.* **21,** 752–760 (2011).

192. Kirkhart, C. & Scott, K. Gustatory Learning and Processing in the Drosophila Mushroom Bodies. *J. Neurosci.* **35,** 5950–5958 (2015).

193. Vogt, K., Aso, Y., Hige, T., Knapek, S., Ichinose, T., Friedrich, A. B., Turner, G. C., Rubin, G. M. & Tanimoto, H. Direct neural pathways convey distinct visual information to drosophila mushroom bodies. *Elife* **5,** 1–13 (2016).

194. Yagi, R., Mabuchi, Y., Mizunami, M. & Tanaka, N. K. Convergence of multimodal sensory pathways to the mushroom body calyx in Drosophila melanogaster. *Sci. Rep.* **6,** 1–8 (2016).

195. Ardin, P., Peng, F., Mangan, M., Lagogiannis, K. & Webb, B. Using an Insect

Mushroom Body Circuit to Encode Route Memory in Complex Natural Environments. *PLOS Comput. Biol.* **12,** e1004683 (2016).

196. Wessnitzer, J., Young, J. M., Armstrong, J. D. & Webb, B. A model of non-elemental olfactory learning in Drosophila. *J. Comput. Neurosci.* **32,** 197–212 (2012).

197. Su, C.-Y., Menuz, K. & Carlson, J. R. Olfactory perception: receptors, cells, and circuits. *Cell* **139,** 45–59 (2009).

198. Root, C. M., Denny, C. A., Hen, R. & Axel, R. The participation of cortical amygdala in innate, odour-driven behaviour. *Nature* **515,** 269–273 (2014).

199. Stettler, D. D. & Axel, R. Representations of Odor in the Piriform Cortex. *Neuron* **63,** 854–864 (2009).

200. Apicella, A., Yuan, Q., Scanziani, M. & Isaacson, J. S. Pyramidal Cells in Piriform Cortex Receive Convergent Input from Distinct Olfactory Bulb Glomeruli. *J. Neurosci.* **30,** 14255–14260 (2010).

201. Sosulski, D. L., Lissitsyna Bloom, M., Cutforth, T., Axel, R. & Datta, S. R. Distinct representations of olfactory information in different cortical centres. *Nature* **472,** 213–219 (2011).

202. Linster, C. & Cleland, T. A. Neuromodulation of olfactory transformations. *Curr. Opin. Neurobiol.* **40,** 170–177 (2016).

203. Strauch, C. & Manahan-Vaughan, D. In the Piriform Cortex, the Primary Impetus for Information Encoding through Synaptic Plasticity Is Provided by Descending Rather than Ascending Olfactory Inputs. *Cereb. Cortex* **28,** 764–776 (2018).

204. Korsching, S. I. Odor maps in the brain: Spatial aspects of odor representation in sensory surface and olfactory bulb. *Cell. Mol. Life Sci.* **58,** 520–530 (2001).

205. Inada, K., Tsuchimoto, Y. & Kazama, H. Origins of Cell-Type-Specific Olfactory Processing in the Drosophila Mushroom Body Circuit. *Neuron* **95,** 357–367.e4 (2017).

206. Qin, H., Cressy, M., Li, W., Coravos, J. S., Izzi, S. A. & Dubnau, J. Gamma neurons mediate dopaminergic input during aversive olfactory memory formation in drosophila. *Curr. Biol.* **22,** 608–614 (2012).

207. Xie, Z., Huang, C., Ci, B., Wang, L. & Zhong, Y. Requirement of the combination of mushroom body γ lobe and α/β lobes for the retrieval of both aversive and appetitive early memories in Drosophila. *Learn. Mem.* **20,** 474–81 (2013).

208. Zhang, S. & Roman, G. Presynaptic inhibition of gamma lobe neurons is required

for olfactory learning in Drosophila. *Curr. Biol.* **23,** 2519–2527 (2013).

209. Aso, Y., Herb, A., Ogueta, M., Siwanowicz, I., Templier, T., Friedrich, A. B., Ito, K., Scholz, H. & Tanimoto, H. Three Dopamine pathways induce aversive odor memories with different stability. *PLoS Genet.* **8,** (2012).

210. Liu, C., Plaçais, P.-Y., Yamagata, N., Pfeiffer, B. D., Aso, Y., Friedrich, A. B., Siwanowicz, I., Rubin, G. M., Preat, T. & Tanimoto, H. A subset of dopamine neurons signals reward for odour memory in Drosophila. *Nature* **488,** 512–516 (2012).

211. Aso, Y. & Rubin, G. M. Dopaminergic neurons write and update memories with cell-type-specific rules. *Elife* **5,** 1–15 (2016).

212. Hige, T., Aso, Y., Rubin, G. M. & Turner, G. C. Plasticity-driven individualization of olfactory coding in mushroom body output neurons. *Nature* **526,** 258–262 (2015).

213. Barnstedt, O., Owald, D., Felsenberg, J., Brain, R., Moszynski, J. P., Talbot, C. B., Perrat, P. N. & Waddell, S. Memory-Relevant Mushroom Body Output Synapses Are Cholinergic. *Neuron* **89,** 1237–1247 (2016).

214. Knapek, S., Kahsai, L., Winther, Å. M. E., Tanimoto, H. & Nässel, D. R. Short neuropeptide F acts as a functional neuromodulator for olfactory memory in kenyon cells of Drosophila mushroom bodies. *Ann. Intern. Med.* **158,** 5340–5345 (2013).

215. Johard, H. A. D., Enell, L. E., Gustafsson, E., Trifilieff, P., Veenstra, J. A. & Nässel, D. R. Intrinsic neurons of Drosophila mushroom bodies express short neuropeptide F: Relations to extrinsic neurons expressing different neurotransmitters. *J. Comp. Neurol.* **507,** 1479–1496 (2008).

216. Owald, D. & Waddell, S. Olfactory learning skews mushroom body output pathways to steer behavioral choice in Drosophila. *Curr. Opin. Neurobiol.* **35,** 178–184 (2015).

217. Mao, Z. Eight different types of dopaminergic neurons innervate the Drosophila mushroom body neuropil: anatomical and physiological heterogeneity. *Front. Neural Circuits* **3,** 1–17 (2009).

218. Aso, Y., Siwanowicz, I., Bräcker, L., Ito, K., Kitamoto, T. & Tanimoto, H. Specific dopaminergic neurons for the formation of labile aversive memory. *Curr. Biol.* **20,** 1445–1451 (2010).

219. Burke, C. J., Huetteroth, W., Owald, D., Perisse, E., Krashes, M. J., Das, G., Gohl, D., Silies, M., Certel, S. & Waddell, S. Layered reward signalling through octopamine and dopamine in Drosophila. *Nature* **492,** 433–437 (2012).

220. Claridge-Chang, A., Roorda, R. D., Vrontou, E., Sjulson, L., Li, H., Hirsh, J. & Miesenböck, G. Writing Memories with Light-Addressable Reinforcement Circuitry. *Cell* **139,** 405–415 (2009).

221. Huetteroth, W., Perisse, E., Lin, S., Klappenbach, M., Burke, C. & Waddell, S. Sweet taste and nutrient value subdivide rewarding dopaminergic neurons in drosophila. *Curr. Biol.* **25,** 751–758 (2015).

222. Kim, Y.-C., Lee, H.-G. & Han, K.-A. D1 Dopamine Receptor dDA1 Is Required in the Mushroom Body Neurons for Aversive and Appetitive Learning in Drosophila. *J. Neurosci.* **27,** 7640–7647 (2007).

223. Himmelreich, S., Masuho, I., Berry, J. A., MacMullen, C., Skamangas, N. K., Martemyanov, K. A. & Davis, R. L. Dopamine Receptor DAMB Signals via Gq to Mediate Forgetting in Drosophila. *Cell Rep.* **21,** 2074–2081 (2017).

224. Greengard, P. The neurobiology of dopamine signaling. *Biosci. Rep.* **21,** 247–269 (2001).

225. Girault, J.-A. & Greengard, P. The Neurobiology of Dopamine Signaling. *Arch. Neurol.* **61,** 641 (2004).

226. Hige, T., Aso, Y., Modi, M. N., Rubin, G. M. & Turner, G. C. Heterosynaptic Plasticity Underlies Aversive Olfactory Learning in Drosophila. *Neuron* **88,** 985–998 (2015).

227. Tomchik, S. M. & Davis, R. L. Dynamics of Learning-Related cAMP Signaling and Stimulus Integration in the Drosophila Olfactory Pathway. *Neuron* **64,** 510–521 (2009).

228. Gervasi, N., Tchénio, P. & Preat, T. PKA Dynamics in a Drosophila Learning Center: Coincidence Detection by Rutabaga Adenylyl Cyclase and Spatial Regulation by Dunce Phosphodiesterase. *Neuron* **65,** 516–529 (2010).

229. Boto, T., Louis, T., Jindachomthong, K., Jalink, K. & Tomchik, S. M. Dopaminergic modulation of cAMP drives nonlinear plasticity across the Drosophila mushroom body lobes. *Curr. Biol.* **24,** 822–831 (2014).

230. De Schutter, E. & Bjaalie, J. G. Coding in the granular layer of the cerebellum. *Prog. Brain Res.* **130,** 279–296 (2001).

231. Chadderton, P., Margie, T. W. & Häusser, M. Integration of quanta in cerebellar granule cells during sensory processing. *Nature* **428,** 856–860 (2004).

232. Ekerot, C.-F. & Jörntell, H. Synaptic Integration in Cerebellar Granule Cells. *The Cerebellum* **7,** 539–541 (2008).

233. Kanichay, R. T. & Silver, R. A. Synaptic and Cellular Properties of the Feedforward Inhibitory Circuit within the Input Layer of the Cerebellar Cortex. *J. Neurosci.* **28,** 8955–8967 (2008).

234. Shomrat, T., Turchetti-Maia, A. L., Stern-Mentch, N., Basil, J. A. & Hochner, B. The vertical lobe of cephalopods: an attractive brain structure for understanding the evolution of advanced learning and memory systems. *J. Comp. Physiol. A Neuroethol. Sensory, Neural, Behav. Physiol.* **201,** 947–956 (2015).

235. Roth, G. Convergent evolution of complex brains and high intelligence. *Philos. Trans. R. Soc. B Biol. Sci.* **370,** 20150049–20150049 (2015).

236. Le Guen, M. C. & De Zeeuw, C. I. Presynaptic plasticity at cerebellar parallel fiber terminals. *Funct. Neurol.* **25,** 141–151 (2010).

237. Bengtsson, F. & Hesslow, G. Cerebellar control of the inferior olive. *Cerebellum* **5,** 7–14 (2006).

238. Farris, S. M. Evolution of brain elaboration. *Philos. Trans. R. Soc. B Biol. Sci.* **370,** 20150054–20150054 (2015).

239. Cohen, J. Y., Haesler, S., Vong, L., Lowell, B. B. & Uchida, N. Neuron-type-specific signals for reward and punishment in the ventral tegmental area. *Nature* **482,** 85–88 (2012).

240. Wise, R. A. Dopamine, learning and motivation. *Nat. Rev. Neurosci.* **5,** 483–494 (2004).

241. Yamamoto, S. & Seto, E. S. Dopamine Dynamics and Signaling in Drosophila: An Overview of Genes, Drugs and Behavioral Paradigms. *Exp. Anim.* **63,** 107–119 (2014).

242. Van Swinderen, B. & Andretic, R. Dopamine in Drosophila: setting arousal thresholds in a miniature brain. *Proc. R. Soc. B Biol. Sci.* **278,** 906–913 (2011).

243. Beninger, R. J. The role of dopamine in locomotor activity and learning. *Brain Res. Rev.* **6,** 173–196 (1983).

244. Howe, M. W., Tierney, P. L., Sandberg, S. G., Phillips, P. E. M. & Graybiel, A. M. Prolonged dopamine signalling in striatum signals proximity and value of distant rewards. *Nature* **500,** 575–579 (2013).

245. Bloem, B., Huda, R., Sur, M. & Graybiel, A. M. Two-photon imaging in mice shows striosomes and matrix have overlapping but differential reinforcement-related responses. *Elife* **6,** (2017).

246. Chen, T. W., Wardill, T. J., Sun, Y., Pulver, S. R., Renninger, S. L., Baohan, A.,

Schreiter, E. R., Kerr, R. A., Orger, M. B., Jayaraman, V., Looger, L. L., Svoboda, K. & Kim, D. S. Ultrasensitive fluorescent proteins for imaging neuronal activity. *Nature* **499,** 295–300 (2013).

247. Dreosti, E. & Lagnado, L. Optical reporters of synaptic activity in neural circuits. *Exp. Physiol.* **96,** 4–12 (2010).

248. Catterall, W. A. & Few, A. P. Calcium Channel Regulation and Presynaptic Plasticity. *Neuron* **59,** 882–901 (2008).

249. Catterall, W. A., Leal, K. & Nanou, E. Calcium channels and short-term synaptic plasticity. *J. Biol. Chem.* **288,** 10742–10749 (2013).

250. Regehr, W. G. Short-term presynaptic plasticity. *Cold Spring Harb. Perspect. Biol.* **4,** 1–19 (2012).

251. Peled, E. S., Newman, Z. L. & Isacoff, E. Y. Evoked and spontaneous transmission favored by distinct sets of synapses. *Curr. Biol.* **24,** 484–493 (2014).

252. Peled, E. S. & Isacoff, E. Y. Optical quantal analysis of synaptic transmission in wild-type and rab3-mutant Drosophila motor axons. *Nat. Neurosci.* **14,** 519–526 (2011).

253. Zhang, Y. Q., Rodesch, C. K. & Broadie, K. Living synaptic vesicle marker: Synaptotagmin-GFP. *Genesis* **34,** 142–145 (2002).

254. Dreosti, E., Odermatt, B., Dorostkar, M. M. & Lagnado, L. A genetically encoded reporter of synaptic activity in vivo. *Nat. Methods* **6,** 883–889 (2009).

255. Ventimiglia, D. & Bargmann, C. I. Diverse modes of synaptic signaling, regulation, and plasticity distinguish two classes of C. elegans glutamatergic neurons. *Elife* **6,** e31234 (2017).

256. Stevens, R. J., Akbergenova, Y., Jorquera, R. A. & Littleton, J. T. Abnormal Synaptic Vesicle Biogenesis in Drosophila Synaptogyrin Mutants. *J. Neurosci.* **32,** 18054–18067 (2012).

257. Petrenko, A. G., Perin, M. S., Davletov, B. A., Ushkaryov, Y. A., Geppert, M. & Sudhof, T. C. Binding of synaptotagmin to the alpha-latrotoxin receptor implicates both in synaptic vesicle exocytosis. *Nature* **353,** 65–68 (1991).

258. Connolly, J. B., Roberts, I. J. H., Armstrong, J. D., Kaiser, K., Forte, M., Tully, T. & O'Kane, C. J. Associative Learning Disrupted by Impaired Gs Signaling in Drosophila Mushroom Bodies. *Science (80-.).* **274,** 2104–2107 (1996).

259. Ito, K., Suzuki, K., Estes, P., Ramaswami, M., Yamamoto, D. & Strausfeld, N. J. The Organization of Extrinsic Neurons and Their Implications in the Functional

Roles of the Mushroom Bodies in Drosophila melanogaster Meigen. *Learn. Mem.* **5,** 52–77 (1998).

260. Goda, Y. & Davis, G. W. Mechanisms of synapse assembly and disassembly. *Neuron* **40,** 243–64 (2003).

261. Han, K. A., Millar, N. S., Grotewiel, M. S. & Davis, R. L. DAMB, a novel dopamine receptor expressed specifically in Drosophila mushroom bodies. *Neuron* **16,** 1127–1135 (1996).

262. Kim, Y. C., Lee, H. G., Seong, C. S. & Han, K. A. Expression of a D1 dopamine receptor dDA1/DmDOP1 in the central nervous system of Drosophila melanogaster. *Gene Expr. Patterns* **3,** 237–245 (2003).

263. Schwaerzel, M., Monastirioti, M., Scholz, H., Friggi-Grelin, F., Birman, S. & Heisenberg, M. Dopamine and octopamine differentiate between aversive and appetitive olfactory memories in Drosophila. *J. Neurosci.* **23,** 10495–502 (2003).

264. Friggi-Grelin, F., Coulom, H., Meller, M., Gomez, D., Hirsh, J. & Birman, S. Targeted gene expression in Drosophila dopaminergic cells using regulatory sequences from tyrosine hydroxylase. *J. Neurobiol.* **54,** 618–627 (2003).

265. Lin, S., Owald, D., Chandra, V., Talbot, C., Huetteroth, W. & Waddell, S. Neural correlates of water reward in thirsty Drosophila. *Nat. Neurosci.* **17,** 1536–1542 (2014).

266. Tomchik, S. M. Dopaminergic neurons encode a distributed, asymmetric representation of temperature in Drosophila. *J. Neurosci.* **33,** 2166--76a (2013).

267. Das, G., Klappenbach, M., Vrontou, E., Perisse, E., Clark, C. M., Burke, C. J. & Waddell, S. Drosophila learn opposing components of a compound food stimulus. *Curr. Biol.* **24,** 1723–1730 (2014).

268. Galili, D. S., Dylla, K. V., Lüdke, A., Friedrich, A. B., Yamagata, N., Wong, J. Y. H., Ho, C. H., Szyszka, P. & Tanimoto, H. Converging circuits mediate temperature and shock aversive olfactory conditioning in Drosophila. *Curr. Biol.* **24,** 1712–1722 (2014).

269. Matsumoto, M. & Hikosaka, O. Two types of dopamine neuron distinctly convey positive and negative motivational signals. *Nature* **459,** 837–41 (2009).

270. Mann, K., Gordon, M. & Scott, K. A pair of interneurons influences the choice between feeding and locomotion in Drosophila. *Neuron* **79,** 754–765 (2013).

271. Marella, S., Mann, K. & Scott, K. Dopaminergic Modulation of Sucrose Acceptance Behavior in Drosophila. *Neuron* **73,** 941–950 (2012).

272. Plaçais, P.-Y., Trannoy, S., Isabel, G., Aso, Y., Siwanowicz, I., Belliart-Guérin, G., Vernier, P., Birman, S., Tanimoto, H. & Preat, T. Slow oscillations in two pairs of dopaminergic neurons gate long-term memory formation in Drosophila. *Nat. Neurosci.* **15,** 592–599 (2012).

273. Shuai, Y., Hirokawa, A., Ai, Y., Zhang, M., Li, W. & Zhong, Y. Dissecting neural pathways for forgetting in *Drosophila* olfactory aversive memory. *Proc. Natl. Acad. Sci.* **112,** E6663–E6672 (2015).

274. Berry, J. A., Cervantes-Sandoval, I., Chakraborty, M. & Davis, R. L. Sleep Facilitates Memory by Blocking Dopamine Neuron-Mediated Forgetting. *Cell* **161,** 1656–1667 (2015).

275. Ichinose, T., Tanimoto, H. & Yamagata, N. Behavioral Modulation by Spontaneous Activity of Dopamine Neurons. *Front. Syst. Neurosci.* **11,** 1–12 (2017).

276. Yttri, E. A. & Dudman, J. T. Opponent and bidirectional control of movement velocity in the basal ganglia. *Nature* **533,** 402–406 (2016).

277. Grace, A. A., Floresco, S. B., Goto, Y. & Lodge, D. J. Regulation of firing of dopaminergic neurons and control of goal-directed behaviors. *Trends Neurosci.* **30,** 220–227 (2007).

278. Cervantes-Sandoval, I., Phan, A., Chakraborty, M. & Davis, R. L. Reciprocal synapses between mushroom body and dopamine neurons form a positive feedback loop required for learning. *Elife* **6,** 1–16 (2017).

279. Jenett, A. *et al.* A GAL4-Driver Line Resource for Drosophila Neurobiology. *Cell Rep.* **2,** 991–1001 (2012).

280. Yao, Z., Macara, A. M., Lelito, K. R., Minosyan, T. Y. & Shafer, O. T. Analysis of functional neuronal connectivity in the Drosophila brain. *Journal of Neurophysiology* **108,** 684–696 (2012).

281. Yamagata, N., Hiroi, M., Kondo, S., Abe, A. & Tanimoto, H. Suppression of Dopamine Neurons Mediates Reward. *PLoS Biol.* **14,** 1–16 (2016).

282. Ueoka, Y., Hiroi, M., Abe, T. & Tabata, T. Suppression of a single pair of mushroom body output neurons in Drosophila triggers aversive associations. *FEBS Open Bio* **7,** 562–576 (2017).

283. Zhao, X., Lenek, D., Dag, U., Dickson, B. J. & Keleman, K. Persistent activity in a recurrent circuit underlies courtship memory in Drosophila. *Elife* **7,** e31425 (2018).

284. Perisse, E., Owald, D., Barnstedt, O., Talbot, C. B. B., Huetteroth, W. & Waddell,

S. Aversive Learning and Appetitive Motivation Toggle Feed-Forward Inhibition in the Drosophila Mushroom Body. *Neuron* **90,** 1086–1099 (2016).

285. Felsenberg, J., Barnstedt, O., Cognigni, P., Lin, S. & Waddell, S. Re-evaluation of learned information in Drosophila. *Nature* **544,** 240–244 (2017).

286. Schultz, W. Updating dopamine reward signals. *Curr. Opin. Neurobiol.* **23,** 229–238 (2013).

287. Eshel, N., Bukwich, M., Rao, V., Hemmelder, V., Tian, J. & Uchida, N. Arithmetic and local circuitry underlying dopamine prediction errors. *Nature* **525,** 243–246 (2015).

288. Tian, J., Huang, R., Cohen, J. Y., Osakada, F., Kobak, D., Machens, C. K., Callaway, E. M., Uchida, N. & Watabe-Uchida, M. Distributed and Mixed Information in Monosynaptic Inputs to Dopamine Neurons. *Neuron* **91,** 1374–1389 (2016).

289. Barter, J. W., Li, S., Lu, D., Bartholomew, R. A., Rossi, M. A., Shoemaker, C. T., Salas-Meza, D., Gaidis, E. & Yin, H. H. Beyond reward prediction errors: the role of dopamine in movement kinematics. *Front. Integr. Neurosci.* **9,** 1–22 (2015).

290. Berridge, K. C. & Robinson, T. E. What is the role of dopamine in reward: hedonic impact, reward learning, or incentive salience? *Brain Res. Brain Res. Rev.* **28,** 309–69 (1998).

291. Montague, P. R., Hyman, S. E. & Cohen, J. D. Computational roles for dopamine in behavioural control. *Nature* **431,** 760–767 (2004).

292. da Silva, J. A., Tecuapetla, F., Paixão, V. & Costa, R. M. Dopamine neuron activity before action initiation gates and invigorates future movements. *Nature* **554,** 244–248 (2018).

293. Panigrahi, B., Martin, K. A., Li, Y., Graves, A. R., Vollmer, A., Olson, L., Mensh, B. D., Karpova, A. Y. & Dudman, J. T. Dopamine Is Required for the Neural Representation and Control of Movement Vigor. *Cell* **162,** 1418–1430 (2015).

294. Sasaki, T., Matsuki, N. & Ikegaya, Y. Heterogeneity and independency of unitary synaptic outputs from hippocampal CA3 pyramidal cells. *J. Physiol.* **590,** 4869–4880 (2012).

295. Guerrero, G., Rieff, D. F., Agarwal, G., Ball, R. W., Borst, A., Goodman, C. S. & Isacoff, E. Y. Heterogeneity in synaptic transmission along a Drosophila larval motor axon. *Nat. Neurosci.* **8,** 1188–1196 (2005).

296. Alle, H. & Geiger, J. R. Analog signalling in mammalian cortical axons. *Curr. Opin.*

Neurobiol. **18,** 314–320 (2008).

297. Pelkey, K. A. & McBain, C. J. Differential regulation at functionally divergent release sites along a common axon. *Curr. Opin. Neurobiol.* **17,** 366–373 (2007).

298. Markram, H., Wang, Y. & Tsodyks, M. Differential signaling via the same axon of neocortical pyramidal neurons. *Proc. Natl. Acad. Sci.* **95,** 5323–5328 (1998).

299. Hendricks, M. Compartmentalized calcium dynamics in a C. elegans interneuron encode head movement. *Nature* **487,** 99–103 (2012).

300. Chen, Y., Akin, O., Nern, A., Tsui, C. Y. K., Pecot, M. Y. & Zipursky, S. L. Cell-type-specific labeling of synapses in vivo through synaptic tagging with recombination. *Neuron* **81,** 280–293 (2014).

301. Lee, T. & Luo, L. Mosaic Analysis with a Repressible Cell Marker for Studies of Gene Function in Neuronal Morphogenesis. *Neuron* **22,** 451–461 (1999).

302. Krashes, M. J., DasGupta, S., Vreede, A., White, B., Armstrong, J. D. & Waddell, S. A Neural Circuit Mechanism Integrating Motivational State with Memory Expression in Drosophila. *Cell* **139,** 416–427 (2009).

303. Sulzer, D., Joyce, M. P., Lin, L., Geldwert, D., Haber, S. N., Hattori, T. & Rayport, S. Dopamine neurons make glutamatergic synapses in vitro. *J Neurosci* **18,** 4588–4602 (1998).

304. Tritsch, N. X., Ding, J. B. & Sabatini, B. L. Dopaminergic neurons inhibit striatal output through non-canonical release of GABA. *Nature* **490,** 262–266 (2012).

305. Takemura, S. *et al.* A connectome of a learning and memory center in the adult Drosophila brain. *Elife* **6,** e26975 (2017).

306. Berry, J. A., Cervantes-Sandoval, I., Nicholas, E. P. & Davis, R. L. Dopamine Is Required for Learning and Forgetting in Drosophila. *Neuron* **74,** 530–542 (2012).

307. Keleman, K., Vrontou, E., Kruttner, S., Yu, J. Y., Kurtovic-Kozaric, A. & Dickson, B. J. Dopamine neurons modulate pheromone responses in Drosophila courtship learning. *Nature* **489,** 145–149 (2012).

308. Pech, U., Pooryasin, A., Birman, S. & Fiala, A. Localization of the Contacts Between Kenyon Cells and Aminergic Neurons in the Drosophila melanogaster Brain Using SplitGFP Reconstitution. *J. Comp. Neurol.* **521,** 3992–4026 (2013).

309. Ueno, T. & Kume, K. Functional characterization of dopamine transporter in vivo using Drosophila melanogaster behavioral assays. *Front. Behav. Neurosci.* **8,** 303 (2014).

310. Kume, K. Dopamine Is a Regulator of Arousal in the Fruit Fly. *J. Neurosci.* **25,** 7377–7384 (2005).

311. Cragg, S. J. & Rice, M. E. DAncing past the DAT at a DA synapse. *Trends Neurosci.* **27,** 270–277 (2004).

312. Bzdok, D., Krzywinski, M. & Altman, N. Points of Significance: Machine learning: a primer. *Nat. Methods* **14,** 1119–1120 (2017).

313. Koester, H. J. & Sakmann, B. Calcium dynamics associated with action potentials in single nerve terminals of pyramidal cells in layer 2/3 of the young rat neocortex. *J. Physiol.* **529 Pt 3,** 625–46 (2000).

314. Cassenaer, S. & Laurent, G. Hebbian STDP in mushroom bodies facilitates the synchronous flow of olfactory information in locusts. *Nature* **448,** 709–713 (2007).

315. Préat, T. Decreased odor avoidance after electric shock in Drosophila mutants biases learning and memory tests. *J. Neurosci.* **18,** 8534–8 (1998).

316. Sayin, S., Boehm, A. C., Kobler, J. M., De Backer, J.-F. & Grunwald Kadow, I. C. Internal State Dependent Odor Processing and Perception-The Role of Neuromodulation in the Fly Olfactory System. *Front. Cell. Neurosci.* **12,** 11 (2018).

317. Beshel, J. & Zhong, Y. Graded encoding of food odor value in the Drosophila brain. *J. Neurosci.* **33,** 15693–704 (2013).

318. Formenti, a, Martina, M., Plebani, A. & Mancia, M. Multiple modulatory effects of dopamine on calcium channel kinetics in adult rat sensory neurons. *J. Physiol.* **509 (Pt 2,** 395–409 (1998).

319. Huang, Y.-Y., Simpson, E., Kellendonk, C. & Kandel, E. R. Genetic evidence for the bidirectional modulation of synaptic plasticity in the prefrontal cortex by D1 receptors. *Proc. Natl. Acad. Sci. U. S. A.* **101,** 3236–3241 (2004).

320. Calabresi, P., Picconi, B., Tozzi, A. & Di Filippo, M. Dopamine-mediated regulation of corticostriatal synaptic plasticity. *Trends in Neurosciences* **30,** 211–219 (2007).

321. Shen, W., Flajolet, M., Greengard, P. & Surmeier, D. J. Dichotomous dopaminergic control of striatal synaptic plasticity. *Science (80-.).* **321,** 848–851 (2008).

322. Yarali, A., Nehrkorn, J., Tanimoto, H. & Herz, A. V. M. Event timing in associative learning: From biochemical reaction dynamics to behavioural observations. *PLoS One* **7,** e32885 (2012).

323. Tanimoto, H., Heisenberg, M. & Gerber, B. Experimental psychology: Event timing

turns punishment to reward. *Nature* **430,** 983–983 (2004).

324. Louis, T., Stahl, A., Boto, T. & Tomchik, S. M. Cyclic AMP-dependent plasticity underlies rapid changes in odor coding associated with reward learning. *Proc. Natl. Acad. Sci.* 201709037 (2017).

325. Evans, G. J. O. & Morgan, A. Regulation of the exocytotic machinery by cAMP-dependent protein kinase: implications for presynaptic plasticity. *Biochem. Soc. Trans.* **31,** 824–827 (2003).

326. Waltereit, R. & Weller, M. Signaling from cAMP/PKA to MAPK and synaptic plasticity. *Mol. Neurobiol.* **27,** 99–106 (2003).

327. Mons, N., Guillou, J. L. & Jaffard, R. The role of Ca2+/calmodulin-stimulable adenylyl cyclases as molecular coincidence detectors in memory formation. *Cell. Mol. Life Sci.* **55,** 525–533 (1999).

328. Zars, T., Fischer, M., Schulz, R. & Heisenberg, M. Localization of a short-term memory in Drosophila. *Science (80-.).* **288,** 672–675 (2000).

329. Vogt, K., Yarali, A. & Tanimoto, H. Reversing Stimulus Timing in Visual Conditioning Leads to Memories with Opposite Valence in Drosophila. *PLoS One* **10,** e0139797 (2015).

330. Hansson, B. S., Knaden, M., Sachse, S., Stensmyr, M. C. & Wicher, D. Towards plant-odor-related olfactory neuroethology in Drosophila. *Chemoecology* **20,** 51–61 (2010).

331. Gaudry, Q., Hong, E. J., Kain, J., De Bivort, B. L. & Wilson, R. I. Asymmetric neurotransmitter release enables rapid odour lateralization in Drosophila. *Nature* **493,** 424–428 (2013).

332. Cardé, R. T. Odour plumes and odour-mediated flight in insects. *Ciba Found. Symp.* **200,** 54-66-70 (1996).

333. Wolf, H. & Wehner, R. Pinpointing food sources: olfactory and anemotactic orientation in desert ants, Cataglyphis fortis. *J. Exp. Biol.* **203,** 857–868 (2000).

334. Togunov, R. R., Derocher, A. E. & Lunn, N. J. Windscapes and olfactory foraging in a large carnivore. *Sci. Rep.* **7,** 46332 (2017).

335. Yu, Y. S. W., Graff, M. M., Bresee, C. S., Man, Y. B. & Hartmann, M. J. Z. Whiskers aid anemotaxis in rats. *Sci. Adv.* **2,** e1600716–e1600716 (2016).

336. Bell, J. S. & Wilson, R. I. Behavior Reveals Selective Summation and Max Pooling among Olfactory Processing Channels. *Neuron* **91,** 425–438 (2016).

337. Flügge, C. Geruchliche Raumorientierung von Drosophila melanogaster. *Z. Vgl. Physiol.* **20,** 463–500 (1934).

338. Kennedy, J. S. & Marsh, D. Pheromone-regulated anemotaxis in flying moths. *Science* **184,** 999–1001 (1974).

339. Steck, K., Veit, D., Grandy, R., Badia, S. B. I., Mathews, Z., Verschure, P., Hansson, B. S. & Knaden, M. A high-throughput behavioral paradigm for Drosophila olfaction - The Flywalk. *Sci. Rep.* **2,** 1–9 (2012).

340. Buckley, C. L. & Toyoizumi, T. A theory of how active behavior stabilises neural activity: Neural gain modulation by closed-loop environmental feedback. *PLOS Comput. Biol.* **14,** e1005926 (2018).

341. Dombeck, D. A. & Reiser, M. B. Real neuroscience in virtual worlds. *Curr. Opin. Neurobiol.* **22,** 3–10 (2012).

342. Green, J., Adachi, A., Shah, K. K., Hirokawa, J. D., Magani, P. S. & Maimon, G. A neural circuit architecture for angular integration in Drosophila. *Nature* **546,** 101–106 (2017).

343. Seelig, J. D., Chiappe, M. E., Lott, G. K., Dutta, A., Osborne, J. E., Reiser, M. B. & Jayaraman, V. Two-photon calcium imaging from head-fixed Drosophila during optomotor walking behavior. *Nat. Methods* **7,** 535–540 (2010).

344. Moore, R. J. D., Taylor, G. J., Paulk, A. C., Pearson, T., van Swinderen, B. & Srinivasan, M. V. FicTrac: A visual method for tracking spherical motion and generating fictive animal paths. *J. Neurosci. Methods* **225,** 106–119 (2014).

345. Yorozu, S., Wong, A., Fischer, B. J., Dankert, H., Kernan, M. J., Kamikouchi, A., Ito, K. & Anderson, D. J. Distinct sensory representations of wind and near-field sound in the Drosophila brain. *Nature* **458,** 201–205 (2009).

346. Seelig, J. D. & Jayaraman, V. Neural dynamics for landmark orientation and angular path integration. *Nature* **521,** 186–191 (2015).

347. Kim, I. S. & Dickinson, M. H. Idiothetic Path Integration in the Fruit Fly Drosophila melanogaster. *Curr. Biol.* **27,** 2227–2238.e3 (2017).

348. Talay, M., Richman, E. B., Snell, N. J., Hartmann, G. G., Fisher, J. D., Sorkaç, A., Santoyo, J. F., Chou-Freed, C., Nair, N., Johnson, M., Szymanski, J. R. & Barnea, G. Transsynaptic Mapping of Second-Order Taste Neurons in Flies by trans-Tango. *Neuron* **96,** 783–795.e4 (2017).

349. Strauss, R. The central complex and the genetic dissection of locomotor behaviour. *Curr. Opin. Neurobiol.* **12,** 633–638 (2002).

350. Seelig, J. D. & Jayaraman, V. Feature detection and orientation tuning in the Drosophila central complex. *Nature* **503,** 262–266 (2013).

351. Weir, P. T., Schnell, B. & Dickinson, M. H. Central complex neurons exhibit behaviorally gated responses to visual motion in Drosophila. *J. Neurophysiol.* **111,** 62–71 (2014).

352. Pfeiffer, K. & Homberg, U. Organization and Functional Roles of the Central Complex in the Insect Brain. *Annu. Rev. Entomol.* **59,** 165–184 (2014).

353. Guo, P. & Ritzmann, R. E. Neural activity in the central complex of the cockroach brain is linked to turning behaviors. *J. Exp. Biol.* **216,** 992–1002 (2013).

354. Kim, S. S., Rouault, H., Druckmann, S. & Jayaraman, V. Ring attractor dynamics in the *Drosophila* central brain. *Science (80-.).* **356,** 849–853 (2017).

355. Turner-Evans, D. B. & Jayaraman, V. The insect central complex. *Curr. Biol.* **26,** R453–R457 (2016).

356. Wolff, T., Iyer, N. A. & Rubin, G. M. Neuroarchitecture and neuroanatomy of the Drosophila central complex: A GAL4-based dissection of protocerebral bridge neurons and circuits. *J. Comp. Neurol.* **523,** 997 (2015).

357. Turner-Evans, D., Wegener, S., Rouault, H., Franconville, R., Wolff, T., Seelig, J. D., Druckmann, S. & Jayaraman, V. Angular velocity integration in a fly heading circuit. *Elife* **6,** (2017).

358. Hsu, C. T. & Bhandawat, V. Organization of descending neurons in Drosophila melanogaster. *Sci. Rep.* **6,** 20259 (2016).

359. Namiki, S., Dickinson, M. H., Wong, A. M., Korff, W. & Card, G. M. The functional organization of descending sensory-motor pathways in Drosophila. *bioRxiv* (2017).

360. Mamiya, A., Beshel, J., Xu, C. & Zhong, Y. Neural representations of airflow in Drosophila mushroom body. *PLoS One* **3,** e4063 (2008).

361. Tecuapetla, F., Jin, X., Lima, S. Q. & Costa, R. M. Complementary Contributions of Striatal Projection Pathways to Action Initiation and Execution. *Cell* **166,** 703–715 (2016).

362. Vicente, A. M., Galvão-Ferreira, P., Tecuapetla, F. & Costa, R. M. Direct and indirect dorsolateral striatum pathways reinforce different action strategies. *Curr. Biol.* **26,** R267–R269 (2016).

363. Jin, X. & Costa, R. M. Shaping action sequences in basal ganglia circuits. *Curr. Opin. Neurobiol.* **33,** 188–196 (2015).

364. Akhlaghpour, H., Wiskerke, J., Choi, J. Y., Taliaferro, J. P., Au, J. & Witten, I. B. Dissociated sequential activity and stimulus encoding in the dorsomedial striatum during spatial working memory. *Elife* **5,** e19507 (2016).

365. Howe, M. W. & Dombeck, D. A. Rapid signalling in distinct dopaminergic axons during locomotion and reward. *Nature* **535,** 505–510 (2016).

366. Bloem, B., Huda, R., Sur, M. & Graybiel, A. M. Two-photon imaging in mice shows striosomes and matrix have overlapping but differential reinforcement-related responses. *Elife* **6,** (2017).

367. Tsao, C.-H., Chen, C.-C., Lin, C.-H., Yang, H.-Y. & Lin, S. Drosophila mushroom bodies integrate hunger and satiety signals to control innate food-seeking behavior. *Elife* **7,** e35264 (2018).

368. Graybiel, A., Aosaki, T., Flaherty, A. & Kimura, M. The basal ganglia and adaptive motor control. *Science (80-.).* **265,** 1826–1831 (1994).

369. Andermann, M. L. & Lowell, B. B. Toward a Wiring Diagram Understanding of Appetite Control. *Neuron* **95,** 757–778 (2017).

370. Aponte, Y., Atasoy, D. & Sternson, S. M. AGRP neurons are sufficient to orchestrate feeding behavior rapidly and without training. *Nat. Neurosci.* **14,** 351–355 (2011).

371. Betley, J. N., Xu, S., Cao, Z. F. H., Gong, R., Magnus, C. J., Yu, Y. & Sternson, S. M. Neurons for hunger and thirst transmit a negative-valence teaching signal. *Nature* **521,** 180–185 (2015).

372. Burgess, C. R., Ramesh, R. N., Sugden, A. U., Levandowski, K. M., Minnig, M. A., Fenselau, H., Lowell, B. B. & Andermann, M. L. Hunger-Dependent Enhancement of Food Cue Responses in Mouse Postrhinal Cortex and Lateral Amygdala. *Neuron* **91,** 1154–1169 (2016).

373. Aitken, T. J., Greenfield, V. Y. & Wassum, K. M. Nucleus accumbens core dopamine signaling tracks the need-based motivational value of food-paired cues. *J. Neurochem.* **136,** 1026–1036 (2016).

374. Plaçais, P. Y. & Preat, T. To favor survival under food shortage, the brain disables costly memory. *Science (80-.).* **339,** 440–442 (2013).

375. Hirano, Y., Masuda, T., Naganos, S., Matsuno, M., Ueno, K., Miyashita, T., Horiuchi, J. & Saitoe, M. Fasting launches CRTC to facilitate long-term memory formation in Drosophila. *Science (80-.).* **339,** 443–446 (2013).

376. Yapici, N., Cohn, R., Schusterreiter, C., Ruta, V. & Vosshall, L. B. A Taste Circuit

that Regulates Ingestion by Integrating Food and Hunger Signals. *Cell* **165,** 715–729 (2016).

377. Cohn, R., Morantte, I. & Ruta, V. Coordinated and Compartmentalized Neuromodulation Shapes Sensory Processing in Drosophila. *Cell* **163,** 1742–1755 (2015).

378. Calabresi, P., Picconi, B., Tozzi, A., Ghiglieri, V. & Di Filippo, M. Direct and indirect pathways of basal ganglia: a critical reappraisal. *Nat. Neurosci.* **17,** 1022–1030 (2014).

379. Ramdya, P., Lichocki, P., Cruchet, S., Frisch, L., Tse, W., Floreano, D. & Benton, R. Mechanosensory interactions drive collective behaviour in Drosophila. *Nature* **519,** 233–6 (2015).

380. Dhawale, A. K., Smith, M. A. & Ölveczky, B. P. The Role of Variability in Motor Learning. *Annu. Rev. Neurosci.* **40,** 479–498 (2017).

381. Dhawale, A. K., Poddar, R., Wolff, S. B., Normand, V. A., Kopelowitz, E. & Ölveczky, B. P. Automated long-term recording and analysis of neural activity in behaving animals. *Elife* **6,** (2017).

382. Klaus, A., Martins, G. J., Paixao, V. B., Zhou, P., Paninski, L. & Costa, R. M. The Spatiotemporal Organization of the Striatum Encodes Action Space. *Neuron* **95,** 1171–1180.e7 (2017).

383. Venkatraman, S., Jin, X., Costa, R. M. & Carmena, J. M. Investigating neural correlates of behavior in freely behaving rodents using inertial sensors. *J. Neurophysiol.* **104,** 569–75 (2010).

384. Berman, G. J., Bialek, W. & Shaevitz, J. W. Predictability and hierarchy in Drosophila behavior. *Proc. Natl. Acad. Sci. U. S. A.* **113,** 11943–11948 (2016).

385. Wiltschko, A. B., Johnson, M. J., Iurilli, G., Peterson, R. E., Katon, J. M., Pashkovski, S. L., Abraira, V. E., Adams, R. P. & Datta, S. R. Mapping Sub-Second Structure in Mouse Behavior. *Neuron* **88,** 1121–1135 (2015).

386. Kabra, M., Robie, A. A., Rivera-Alba, M., Branson, S. & Branson, K. JAABA: interactive machine learning for automatic annotation of animal behavior. *Nat. Methods* **10,** 64–67 (2013).

387. Stern, S., Kirst, C. & Bargmann, C. I. Neuromodulatory Control of Long-Term Behavioral Patterns and Individuality across Development. *Cell* **171,** 1649–1662.e10 (2017).

388. Ouellette, M.-H., Desrochers, M., Gheta, I., Ramos, R. & Hendricks, M. A gate-

and-switch model for head orientation behaviors in C. elegans. *bioRxiv* (2018).

389. DasGupta, S., Ferreira, C. H. & Miesenbock, G. FoxP influences the speed and accuracy of a perceptual decision in Drosophila. *Science (80-.).* **344,** 901–904 (2014).

390. Jung, S.-H., Hueston, C. & Bhandawat, V. Odor-identity dependent motor programs underlie behavioral responses to odors. *Elife* **4,** e11092 (2015).

391. Ghosh, K. K., Burns, L. D., Cocker, E. D., Nimmerjahn, A., Ziv, Y., Gamal, A. El & Schnitzer, M. J. Miniaturized integration of a fluorescence microscope. *Nat. Methods* **8,** 871–878 (2011).

392. Helmchen, F., Fee, M. S., Tank, D. W. & Denk, W. A miniature head-mounted two-photon microscope. high-resolution brain imaging in freely moving animals. *Neuron* **31,** 903–12 (2001).

393. Grover, D., Katsuki, T. & Greenspan, R. J. Flyception: imaging brain activity in freely walking fruit flies. *Nat. Methods* **13,** 569–572 (2016).

394. Aronov, D. & Tank, D. W. Engagement of Neural Circuits Underlying 2D Spatial Navigation in a Rodent Virtual Reality System. *Neuron* **84,** 442–456 (2014).

395. Harvey, C. D., Collman, F., Dombeck, D. A. & Tank, D. W. Intracellular dynamics of hippocampal place cells during virtual navigation. *Nature* **461,** 941–946 (2009).

396. Rajasethupathy, P., Sankaran, S., Marshel, J. H., Kim, C. K., Ferenczi, E., Lee, S. Y., Berndt, A., Ramakrishnan, C., Jaffe, A., Lo, M., Liston, C. & Deisseroth, K. Projections from neocortex mediate top-down control of memory retrieval. *Nature* **526,** 653–659 (2015).

397. Maimon, G., Straw, A. D. & Dickinson, M. H. A Simple Vision-Based Algorithm for Decision Making in Flying Drosophila. *Curr. Biol.* **18,** 464–470 (2008).

398. Albergaria, C., Silva, N. T., Pritchett, D. & Carey, M. R. Locomotor activity modulates associative learning in mouse cerebellum. *bioRxiv* (2017).

399. Brembs, B. *Operant Behavior in Model Systems*. *Learning and Memory: A Comprehensive Reference* (Elsevier, 2017).

400. Perisse, E., Yin, Y., Lin, A. C., Lin, S., Huetteroth, W. & Waddell, S. Different Kenyon Cell Populations Drive Learned Approach and Avoidance in Drosophila. *Neuron* **79,** 945–956 (2013).

401. Lammel, S., Lim, B. K., Ran, C., Huang, K. W., Betley, M. J., Tye, K. M., Deisseroth, K. & Malenka, R. C. Input-specific control of reward and aversion in the ventral tegmental area. *Nature* **491,** 212–217 (2012).

402. Durstewitz, D., Seamans, J. K. & Sejnowski, T. J. Neurocomputational Models of Working Memory. *Nat. Neurosci.* **3,** 1184–1191 (2000).

403. Eichenbaum, H. Hippocampus. *Neuron* **44,** 109–120 (2004).

404. Kim, H., Kirkhart, C. & Scott, K. Long-range projection neurons in the taste circuit of Drosophila. *Elife* **6,** 1–24 (2017).

405. Dolan, M.-J., Belliart-Guerin, G., Bates, A. S., Aso, Y., Frechter, S., Roberts, R. J. V., Schlegel, P., Wong, A., Hammad, A., Bock, D., Rubin, G. M., Preat, T., Placais, P.-Y. & Jefferis, G. S. X. E. Communication from learned to innate olfactory processing centers is required for memory retrieval in Drosophila. *bioRxiv* 167312 (2017).

406. Eichler, K., Li, F., Litwin-Kumar, A., Park, Y., Andrade, I., Schneider-Mizell, C. M., Saumweber, T., Huser, A., Eschbach, C., Gerber, B., Fetter, R. D., Truman, J. W., Priebe, C. E., Abbott, L. F., Thum, A. S., Zlatic, M. & Cardona, A. The complete connectome of a learning and memory centre in an insect brain. *Nature* **548,** 175–182 (2017).

407. Nichols, T. R. Reflex Circuits. in *Encyclopedia of Neuroscience* 73–79 (Elsevier, 2009).

408. Flavell, S. W., Pokala, N., Macosko, E. Z., Albrecht, D. R., Larsch, J. & Bargmann, C. I. Serotonin and the neuropeptide PDF initiate and extend opposing behavioral states in C. Elegans. *Cell* **154,** 1023–1035 (2013).

409. Clowney, E. J., Iguchi, S., Bussell, J. J., Scheer, E. & Ruta, V. Multimodal Chemosensory Circuits Controlling Male Courtship in Drosophila. *Neuron* **87,** 1036–1049 (2015).

410. Klapoetke, N. C., Nern, A., Peek, M. Y., Rogers, E. M., Breads, P., Rubin, G. M., Reiser, M. B. & Card, G. M. Ultra-selective looming detection from radial motion opponency. *Nature* **551,** 237–241 (2017).

411. von Reyn, C. R., Breads, P., Peek, M. Y., Zheng, G. Z., Williamson, W. R., Yee, A. L., Leonardo, A. & Card, G. M. A spike-timing mechanism for action selection. *Nat. Neurosci.* **17,** 962–970 (2014).

412. Gibson, D. G. Synthesis of DNA fragments in yeast by one-step assembly of overlapping oligonucleotides. *Nucleic Acids Res.* **37,** 6984–6990 (2009).

413. Inagaki, H. K., Jung, Y., Hoopfer, E. D., Wong, A. M., Mishra, N., Lin, J. Y., Tsien, R. Y. & Anderson, D. J. Optogenetic control of Drosophila using a red-shifted channelrhodopsin reveals experience-dependent influences on courtship. *Nat. Methods* **11,** 325–332 (2014).

414. Riemensperger, T., Völler, T., Stock, P., Buchner, E. & Fiala, A. Punishment prediction by dopaminergic neurons in Drosophila. *Curr. Biol.* **15,** 1953–1960 (2005).

415. Li, H., Chaney, S., Forte, M. & Hirsh, J. Ectopic G-protein expression in dopamine and serotonin neurons blocks cocaine sensitization in Drosophila melanogaster. *Curr. Biol.* **10,** 211–214 (2000).

416. Gordon, M. D. & Scott, K. Motor Control in a Drosophila Taste Circuit. *Neuron* **61,** 373–384 (2009).

417. Murthy, M. & Turner, G. Dissection of the head cuticle and sheath of living flies for whole-cell patch-clamp recordings in the brain. *Cold Spring Harb. Protoc.* **8,** 134–139 (2013).

418. Luo, L. & Wu, J. S. A protocol for mosaic analysis with a repressible cell marker (Marcm) in drosophila. *Nat. Protoc.* **1,** 2583–2589 (2007).

419. Ishikawa, D., Takahashi, N., Sasaki, T., Usami, A., Matsuki, N. & Ikegaya, Y. Fluorescent pipettes for optically targeted patch-clamp recordings. *Neural Networks* **23,** 669–672 (2010).

420. Kohatsu, S. & Yamamoto, D. Visually induced initiation of Drosophila innate courtship-like following pursuit is mediated by central excitatory state. *Nat. Commun.* **6,** 6457 (2015).

421. Murthy, M. & Turner, G. Whole-cell in vivo patch-clamp recordings in the drosophila brain. *Cold Spring Harb. Protoc.* **8,** 140–148 (2013).